

Novel Imaging Biomarkers for the Diagnosis and Study of Neuromyelitis Optica

Lucy Matthews

Nuffield Department of Clinical Neurosciences

Trinity College

Hilary Term 2013

--ABSTRACT--

Novel Imaging Biomarkers for the Diagnosis and Study of Neuromyelitis Optica

Lucy Matthews, Trinity College
Hilary Term 2013

Neuromyelitis optica spectrum disorder (NMOSD) is a relapsing demyelinating neurological condition that requires prompt diagnosis and treatment to prevent the accrual of significant disability, such as blindness and immobility. It is caused by antibodies to the aquaporin-4 water channel, which can be detected within the serum of patients and are therefore a highly specific biomarker for the condition. However NMOSD can have overlapping clinical features with the more prevalent demyelinating disease relapsing remitting multiple sclerosis (RRMS). Thus in the situation of a negative aquaporin-4 antibody assay result diagnostic distinction can be difficult to achieve. This in turn leads to a treatment dilemma as NMOSD requires long term immunosuppression, and disease modifying therapies used in RRMS can worsen disease activity in NMOSD.

The work presented in this thesis aimed to find further biomarkers of NMOSD, focusing on conventional and quantitative magnetic resonance imaging, and markers of neurodegeneration. The principle findings are:

- Lesion probability mapping analysis revealed that T2 lesion distribution and morphology can distinguish RRMS from NMO with a 92% sensitivity and 96% specificity. Radiological criteria to aid diagnosis have been proposed.
- Quantitative imaging methods that provide complementary micro-structural measures within CNS tissue have shown that RRMS is associated with widespread neurodegenerative changes in the normal appearing tissue, where as NMO is lesion focused.
- NMO is not associated with diffuse global neurodegeneration in the non-lesioned CNS tissue over a one-year period as determined by serial MRI.
- Normalised thalamic and whole brain volume can be used in a function to help discriminate NMOSD and RRMS

This thesis therefore contributes the knowledge that conventional and quantitative imaging can distinguish NMOSD and RRMS, and provides practical methods in which to apply this to patient management. It is the first longitudinal quantitative imaging study of NMOSD and lends further proof that global or diffuse neurodegeneration of the normal appearing brain or spinal cord tissue is not a feature of this condition.

--CONTENTS--

Abstract 2

1:0 The Clinical and Pathological Features of Neuromyelitis Optica 11
1.1 The Clinical Definition of Neuromyelitis Optica: 11
1.2 The Natural History of Neuromyelitis Optica 12
1.3 The Pathophysiology of NMO 13
1.3.1 Evidence for Autoimmunity against Aquaporin-4 13
1.3.2 Aquaporin-4 15
1.3.3 The Distribution of Aquaporin-4 16
1.3.4 The Mechanism of NMO Lesion Formation 17
1.4 Testing for Aquaporin-4 Antibodies 19
1.5 The Emergence of the NMO Spectrum and Antibody Negative NMO 20
1.6 Differences between NMO and MS on Pathological Examination: 22
1.7 The Requirement for the Early Identification of NMO 23
1.8 An NMO/MS Borderline Case History 23
1.9 Summary 25

2.0 Conventional MRI Findings in Neuromyelitis Optica 26
2.1 Spinal Cord 26
2.2 Brain 29
2.3 Summary 32

3.0 Quantitative Imaging in Neuromyelitis Optica 33
3.1 Existing Literature 33
3.1.1 Diffusion Tensor and Magnetisation Transfer Imaging 33
3.1.2 Magnetic Resonance Spectroscopy: 36
3.1.3 Volumetric Imaging: 36
3.1.4 Functional MRI: 37
3.2 Candidate Quantitative MRI Methods to Study NMO: 37
3.2.1 Myelin Water Imaging 38
3.2.2 Magnetization Transfer Imaging of the Spinal Cord 39
3.3 Summary 40

4.0 Objectives 42
4.1 Research Questions 42
4.2 Research Aims 42

5.0 Study Overview 43
5.1 Study Design 43
5.2 Considerations for Powering the Study 44
5.3 Study Participants 44
5.4 Clinical Assessment 46
5.5 Serum Collection 47
5.6 Aqauporin-4 Antibody Assay 47
5.7 MRI Acquisition Protocol 47
5.8 Wider Cohort Data Collection 49

6.0 Experimental Chapter: The Utility of Conventional Brain MRI to Distinguish Neuromyelitis Optica Spectrum Disorder and Relapsing Multiple Sclerosis 50
6.1 Introduction 50
6.2 Objectives 51
6.3 Methods 51
6.3.1 NMOSD Cohort 51
6.3.2 RRMS Cohort 52
6.3.3 Imaging Sequences 52
6.3.4 Lesion Probability Maps 53
6.3.5 Description of Lesion Distribution in NMOSD Cohort 53
6.4 Results 54
6.4.1 T2 Lesion Volume and Number 54
6.4.2 Lesion Distribution 54
6.4.3 Lesion Characteristics 55
6.4.4 Formulation of Criteria for the Separation of RRMS and NMOSD 58
6.5 Discussion 59

7.0 Experimental Chapter: The Application of Quantitative Brain MRI to Differentiate Neuromyelitis Optica Spectrum Disorder and Multiple Sclerosis 61
7.1 Introduction 61
7.2 Objectives 62
7.3 Methods 63
7.3.1 Study Participants 63
7.3.2 Study Examinations 63
7.3.3 MRI Acquisition Protocol 63
7.3.4 MRI Data Analysis and Statistical Testing 64
7.3.4.1 Whole Brain Volume 64
7.3.4.2 Thalamic and Caudate Volumes 65
7.3.4.3 Voxel-Based Morphometry 66
7.3.4.4 Diffusion Tensor Imaging of the Normal Appearing White Matter 67
7.3.4.5 Myelin Water Imaging of the Normal Appearing White Matter 68
7.4 Results 68
7.4.1 Whole brain, thalamus and caudate volumes 68
7.4.2 Voxel Based Morphometry 71
7.4.3 Diffusion Tensor Imaging of the Normal Appearing White Matter 71
7.4.4 Myelin Water Imaging of the Normal Appearing White Matter 74
7.4.5 Correlation of thalamic volume with FA and myelin water fraction 76
7.4.6 Individualised Measures 76
7.5 Discussion 79
7.6 Conclusions 80

8.0 Experimental Chapter: Differentiating between NMOSD and RRMS with Quantitative Imaging of the Spinal Cord 81
8.1 Introduction 81
8.2 Objectives 83
8.3 Methods 83
8.2.1 Subject Characteristics 83
8.2.2 Acquisition Protocol 84
8.2.3 Analysis 84
8.4 Results 87
8.4.1 Spinal Cord Atrophy 87
8.4.2 Comparison of lesion magnetization transfer in NMOSD and RRMS 89
8.4.3 Comparison of NAWM and NAGM magnetization transfer values in NMOSD, RRMS and healthy controls. 90
8.5 Discussion 92
8.6 Conclusion 93

9.0 Experimental Chapter: Comparison of NMOSD and RRMS with Longitudinal MRI Measures of Neurodegeneration 94
9.1 Introduction 94
9.2 Objectives 95
9.3 Methods 96
9.3.1 Subject Details 96
9.3.2 MRI Acquisition 96
9.3.2 Data Analysis 97
9.4 Results 99
9.4.1 Whole Brain Atrophy (SIENA analysis) 99
9.4.2 Thalamic Volume 102
9.4.3 Diffusion Tensor Imaging 103
9.4.4 Myelin Water Imaging 103
9.5 Discussion 105
9.6 Conclusion 107

10.0 Experimental Chapter: Serum N-Acetylaspartate Measurement and Formulation of A Function to Discriminate Between NMOSD and RRMS 108
10.1 Introduction 108
10.2 Objectives 110
10.3 Methods 110
10.3.1 Subject Cohort 110
10.3.2 Serum Collection 111
10.3.3 NAA Analysis 111
10.3.4 Statistical Testing 111
10.3.5 Discriminant Analysis 112
10.4 Results 112
10.4.1 NAA 112
10.4.2 Correlation of NAA with MRI measures of Neurodegeneration 114
10.4.3 Discriminant Analysis 115
10.5 Discussion 121
10.6 Conclusions 122

11.0 Discussion 123
11.1 Summary of Key Findings 123
11.2 Interpretation of Key Findings 125
11.3 Implications to Clinical Practice 133
11.4 Implications to MRI Research 134
11.5 Recommendations for Future Work 134
11.6 Overall Conclusion 135

References 136

Appendix I: Patient Details 149

Appendix II. Full MRI Protocol used in the core study 152

--TABLES AND FIGURES--

Chapter 1

Table 1.1 Evidence for the pathogenic role of aquaporin-4 autoantibodies in NMO
Table 1.2 The NMO Spectrum

Figure 1.1 The Location of Aquaporin-4 Water Channels on Astrocytes
Figure 1.2 The Distribution of Aqauporin-4

Chapter 2

Figure 2.1 Longitudinally Extensive Transverse Myelitis
Figure 2.2 Brain lesions in NMOSD

Chapter 3

Figure 3.1 Qualitative *Post mortem* Myelin Water Imaging Correlation with Myelin Staining
Figure 3.2 Comparison of MTCSF and Conventional Images

Chapter 5

Table 5.1 Subjects Recruited and Followed-up
Table 5.2 Baseline Characteristics Summary Table
Table 5.3 Summary of MRI Protocol Selected

Figure 5.1 Flow Diagram Outlining Study Design

Chapter 6

Table 6.1 Subject Characteristics
Table 6.2 Lesion Volume and Number
Table 6.3 Lesions Location for 26 Aquaporin-4 Antibody Positive NMOSD Patients
Table 6.4 Proposed Criteria for the Separation of RRMS and NMOSD

Figure 6.1 Lesion Probability Maps

Chapter 7

Table 7.1 Brain volume ANCOVA
Table 7.2 Thalamic volume ANCOVA
Table 7.3 Thalamic volume pairwise comparison
Table 7.4 Caudate volume ANCOVA
Table 7.5 Caudate volume pairwise comparison

Figure 7.1 Example of the segmentation of the thalamus using the FSL FIRST tool
Figure 7.2 Bar Charts showing the differences in volumetric measures between subject groups
Figure 7.3 Voxel-based morphology comparing RRMS and Controls
Figure 7.4 Diffusion tensor imaging of the normal appearing white matter
Figure 7.5 Bar graph showing the average FA within the non-lesioned voxels of the optic radiations
Figure 7.6 Myelin water imaging of the normal appearing white matter
Figure 7.7 Partial correlation between thalamic volume and measures of normal appearing white matter integrity controlling for age for the multiple sclerosis cohort
Figure 7.8 Box plots indicating the median, 25th and 75th centiles and range of the data

Chapter 8
Table 8.1 ANCOVA analysis comparing spinal cord volume in subject groups
Table 8.2 Pairwise comparison of spinal cord volume
Table 8.3 ANOVA analysis comparing MTCSF grey:white matter ratio
Table 8.4 Pairwise comparison of MTCSF grey:white matter ratio

Figure 8.1 Location of slice placement for spinal cord measures
Figure 8.2 Automated outline of the spinal cord as derived by the 'Cord Finder' tool of Jim 6.0
Figure 8.3 The region of interests sampled in the analysis of the MTCSF data
Figure 8.4 Bar graph showing the mean spinal cord volume in the subject groups
Figure 8.5 a. Example of NMO and MS lesions seen with MT contrast
b. Bar graph showing mean lesion MTCSF
Figure 8.6 Examples of where MTCSF can reveal abnormalities not seen on T2
Figure 8.7 Average MTCSF white to grey matter contrast ratio in the subject groups

Chapter 9
Table 9.1 Demographic features of the patients attending follow-up
Table 9.2 ANCOVA results for the comparison between percentage brain volume change in one year between the subject groups

Figure 9.1 Bar graph showing the average percentage brain volume change over 1 year
Figure 9.2 Results of a voxelwise SIENA analysis showing a significant cluster of brain atrophy
Figure 9.3 Scatter graph with line of best fit showing the partial correlation, corrected for age, between baseline left/right average thalamic volume and percentage brain volume change in one year for the multiple sclerosis group.
Figure 9.4 Correlation between individual subject's baseline and follow-up thalamic volumes
Figure 9.5 Change in estimated marginal means of thalamic volume corrected for age and time between scans
Figure 9.6 Significant areas of reduction in FA over one year follow-up period in RRMS cohort
Figure 9.7 Significant reduction in MWF over a one year follow-up period in RRMS cohort

Chapter 10
Table 10.1 Subject characteristics
Table 10.2 ANCOVA results for comparison of serum NAA levels between subject groups
Table 10.3 Partial correlations from regression model of NAA with quantitative MRI measures, corrected for age and multiple comparisons
Table 10.4 Group centroids and standard deviations for function to discriminate NMOSD and RRMS
Table 10.5 Cross-validation of function for the separation of NMOSD and RRMS

Figure 10.1 Box plot showing range of serum NAA values in each subject group
Figure 10.2 Statistically significant partial correlations of NAA with quantitative MRI outcomes for MS cohort
Figure 10.3 Plot showing the separation of the NMOSD, RRMS and control groups using the derived canonical discriminant functions
Figure 10.4 a. Box plot showing the grouping of the data when the simplified function for the separation of RRMS and NMO
b. Histogram demonstrating the discriminant function's separation of NMOSD and RRMS

--PUBLICATIONS--

Paper:

- **Matthews L**, Marasco R, Jenkinson M, Kuker W, Luppe S, Leite MI, Giorgio A, De Stefano N, Robertson N, Johansen-Berg H, Evangelou N, Palace J. Distinction of Seropositive NMO Spectrum Disorder and MS Brain Lesion Distribution. Neurology. 2013 Apr 2;80(14):1330-7.

Published Abstracts:

- **Matthews L**, Marasco R, Jenkinson M, Kuker W, Leite M, Giorgio A, De Stefano N, Luppe S, Robertson N, Johansen-Berg H, Evangelou N, Palace J: Neuromyelitis optica can be distinguished on the basis of MRI brain lesion characteristics. Multiple Sclerosis Journal 2012;18: S4: 9. Presented at ECTRIMS 2012.

- **Matthews L,** Brazier A, Kolind SH, Leite MI, Johansen-Berg H, Palace JA: Can MRI be used as a diagnostic tool in neuromyelitis optica spectrum disorder? J Neurol Neurosurg Psychiatry 2012;83:e1: 141. Presented at Association British Neurologists Annual Meeting 2011.

- **Matthews L**, Kolind S, Jenkinson M, Leite, M, Johansen-Berg H, Palace J: Distinction of aquaporin-4 antibody positive neuromyelitis optica from multiple sclerosis using diffusion tensor and myelin water imaging. Multiple Sclerosis Journal 2011: 17: S165: P402. Presented at ECTRIMS 2011.

--ACKNOWELDGEMENTS--

I thank my supervisors Dr Jacqueline Palace and Prof Heidi Johansen-Berg for their guidance and training throughout my doctoral studies, and for their help in the preparation of this thesis.

My work would not have been possible without the funding of the Medical Research Council and the dedication of the volunteers who gave up their time for this research.

I also thank my colleagues and collaborators in particular Dr Shannon Kolind, Dr Jonathan Brooks, Dr Mark Jenkinson, Dr Charlotte Teunissen, Prof Nikos Evangelou and the FMRIB support staff.

Last but not least thank you to my husband Rob for his tireless proof reading.

1.0 The Clinical and Pathological Features of Neuromyelitis Optica

Neuromyelitis optica (NMO) is a severe inflammatory demyelinating condition of the central nervous system associated with significant morbidity and mortality. The purpose of this chapter is to review our current understanding of NMO, to highlight where advanced MRI techniques could improve diagnosis and clinical management.

1.1 The Clinical Definition of Neuromyelitis Optica (NMO)

NMO is an acquired neurological disorder characterized by its predilection for the optic nerves and spinal cord (Wingerchuk *et al.* 2007). It is a chronic relapsing condition that causes inflammatory and demyelinating lesions. It affects both sexes with a female:male ratio of 6:1 as estimated in a UK cohort by Cossburn *et al.* (2012) and has been documented to be present at all ages - children appear more likely to develop brain lesions, young adults optic neuritis, and older adults myelitis (Kitley *et al.* 2012). Eugine Devic is commonly attributed with the first description of the condition in 1894, hence the disease is still eponymously termed Devic's disease by many.

For most of the 20th century NMO was regarded as a variant of multiple sclerosis (MS) due to similarities in clinical presentation particularly early in the disease course. However a humoral autoimmune mechanism was implicated by two important observations. Firstly, patients with NMO commonly had coincidental non-organ specific antibody mediated conditions (such as systemic lupus erythematosus and the antiphospholipid syndrome as described by Hutchinson *et al.* 2000) and secondly, *post mortem* examination of the demyelinating lesions revealed vasculocentric immunoglobulin deposition and activation of the complement pathway (Lucchinetti *et al.* 2002). The discovery of NMO-IgG in 2004 (Lennon *et*

al. 2004), and later that its antigenic target appeared to be aquaporin-4 water channels (Lennon *et al.* 2005), was a critical step in firmly establishing NMO as a distinct clinical entity.

In Western countries NMO is considered a rare condition, but because it has only relatively recently been defined it is likely to be more common than initially thought. The most recent estimate of the prevalence amongst the UK population is 19.6 per million (Cossburn *et al.* 2012). It is more common in people who originate from Africa, the Caribbean, the Indian sub-continent, China or Japan (Matiello *et al.* 2007). Despite this, and rare reports of familial aggregation of NMO (Matiello *et al.* 2010), the role of genetic factors is unknown.

The first diagnostic criteria for NMO were proposed in 1999 by Dean Wingerchuk and colleagues from the Mayo Clinic and updated in 2006 in light of the discovery of aquaporin-4 antibodies. Patients must have both optic neuritis and acute myelitis and at least two of three supportive criteria: (1) A contiguous spinal cord MRI lesion extending over >3 vertebral segments (2) Brain MRI not meeting diagnostic criteria for MS and (3) NMO-IgG seropositive status. In reality patients can have aquaporin-4 antibodies (which are highly specific for NMO) and not fulfil the diagnostic criteria. These patients are usually classed as suffering from NMO spectrum disorder (NMOSD) and are discussed below.

1.2 The Natural History of NMO

People with NMO accumulate disability during relapses, which can be fulminant, and unlike MS a progressive phase has not been observed clinically (Wingerchuk *et al.* 2007). Kitley *et al*. (2012) reported that in a cohort of 106 antibody positive NMO patients from the UK and Japan, 18% had developed permanent bilateral visual

disability, 34% permanent motor disability and 9% had died after a median of 75 months. However as NMO becomes increasingly recognized and diagnosed more quickly, the early use of immunosuppressive agents to treat this condition should improve the prognosis.

1.3 The Pathophysiology of NMO

1.3.1 Evidence for Autoimmunity against Aquaporin-4

Immunological, *post mortem* and clinical findings provide indirect evidence that the aetiology of NMO is pathogenic antibodies targeted against aquaporin-4 water channels. These are summarised in Table 1.1. To date no animal model for the condition has resulted from attempts to induce aquaporin-4 antibodies alone, although direct injection of NMO-IgG and human complement into the brain of a live mouse model has resulted in NMO-like lesions (Saadoun *et al.* 2010).

Table 1.1: Evidence for the pathogenic role of aquaporin-4 autoantibodies in NMO:

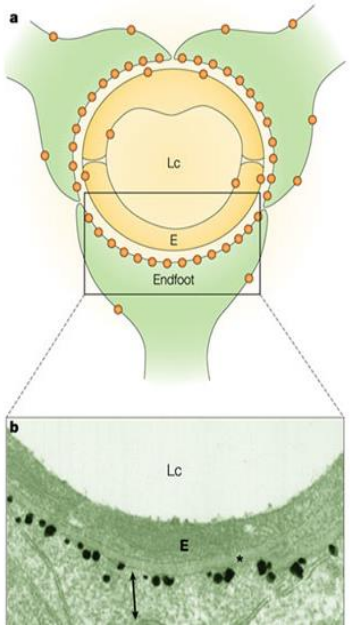
References	**Finding**	**Interpretation**
Hutchinson *et al.* 2000; Pittock *et al.* 2008	Patients with NMO frequently have other autoimmune conditions such as myasthenia gravis and Graves' thyroid disease.	It is well-documented that patients with antibody-mediated conditions are at greater risk of developing other autoimmune conditions. The same has been noted for NMO.
Wingerchuk 2007	Patients with NMO respond to high dose steroid and other immunomodulatory treatments such as plasma exchange.	Intuitively suppressing the immune system is the most effective therapy for autoimmune conditions, but does not have the same level of efficacy on polygenic conditions such as MS.
Lucchinetti *et al.* 2002	NMO lesions show vasculocentric 'rim and rosette' immunoglobulin and complement deposition	This is consistent with other autoimmune diseases.
Sinclair *et al.* 2007	Absence of aquaporin-4 in lesions	In inflammatory lesions due to MS aquaporin-4 is upregulated. In NMO lesions there is selective loss of aquaporin-4 immunoreactivity.
Lennon *et al.* 2005	NMO patient serum binding patterns	NMO-IgG binds selectively to membranes of AQP4 transfected cells but not to CNS tissue from AQP4 null mice.

1.3.2 Aquaporin-4

Water can diffuse across cell membranes through osmosis, however the rapid need for water within cells led to the search for other means of trans-cellular transport. The aquaporins are a family of integral membrane proteins that selectively conduct water in and out of cells and were first described by Peter Agre in 1988, who was later awarded a Nobel Prize for his discovery. Aquaporin-4 are the only aquaporins found in the central nervous system (Jung *et al.* 1994; Nagelhus *et al.* 2004). As shown in Figure 1.1 they are situated in close proximity to the blood brain barrier on the abluminal foot processes of astrocytes. What is interesting is that aquaporin-4 is not expressed on myelin or oligodendrocytes that produce myelin, and the method by which immune attack of these channels causes demyelinating lesions is yet to be elucidated.

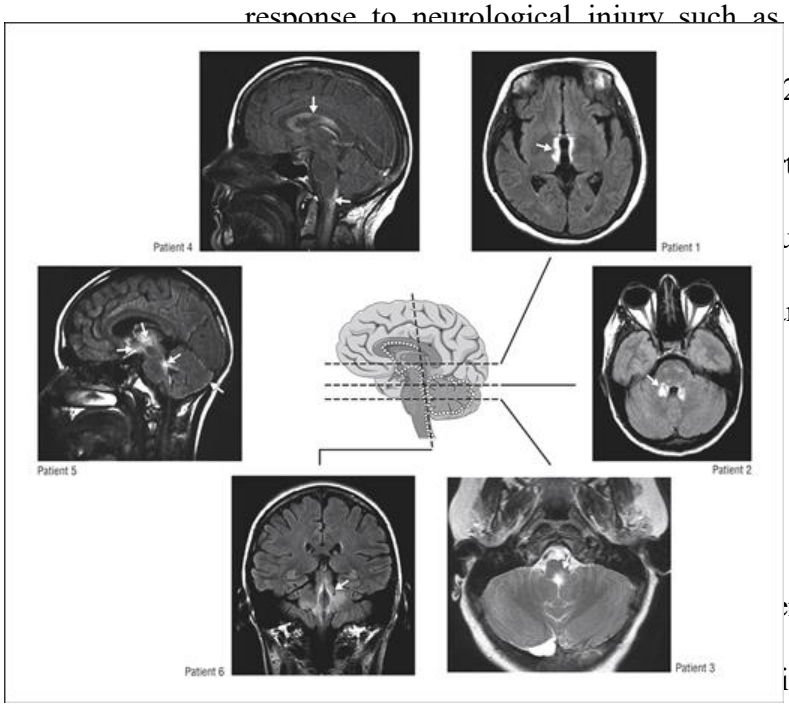
Figure 1.1: The location of aquaporin-4 water channels (shown in red) on the foot processes of astrocytes (green), surrounding the microvasculature of the brain (yellow). Aquaporin-4 is the most abundant water channel in the CNS and is involved in osmoregulation. Endothelial cells (E) are also thought to express aquaporin-4 at their ad and ab luminal membranes.

Diagram taken from Amiry-Moghaddam and Ole P. Ottersen, Nature Reviews Neuroscience, December 2003.



Aquaporin-4 is thought to have an important role in the maintenance of water homeostasis in the brain, and has been shown to mediate cerebral oedema in

response to neurological injury such as stroke or trauma (Nagelhus *et al.* 2004; 2008). Aquaporin-4 is also expressed in the tion of gastric parietal cells, however an unction has not been reported. This may be nnels that perform a similar function to



ntial involvement of the optic nerves and igh aquaporin-4 expression (Li *et al.* 2009). These regions also include the periependymal areas lining the lateral, third and fourth ventricles, the hypothalamus and the periaqueductal grey matter (Figure 1.2).

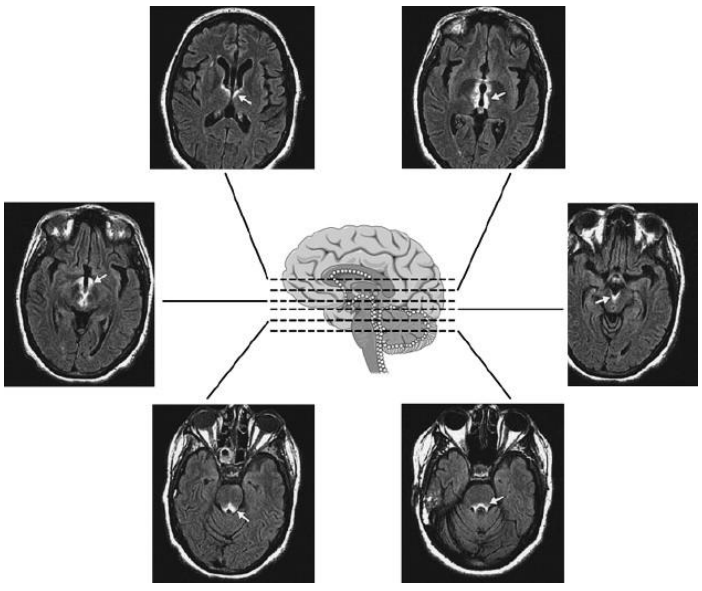


Figure 1.2: The distribution of AQP4. This diagram taken from Pittock et al, 2006, shows with a white beaded line the areas of high AQP4 concentration within the brain. NMO 'typical' lesions can occur in this region as displayed.

Brain lesions that occur in this region are generally regarded as consistent with NMO however they only occur in a small percentage of patients (Pittock *et al.* 2006). The majority of NMO patients have non-specific deep white matter lesions (Pittock *et al.* 2006; Cabrera-Gomez and Kister 2012), and lesions do not typically occur in other aquaporin-4 rich regions such as cerebral cortex and retinal Müller cells. This suggests that the distribution of aquaporin-4 is clearly not the only determinant of lesion location in NMO. The capillary wall endothelium of the blood brain barrier (BBB) should prevent antibodies gaining access to the astrocytic foot processes where the majority of aquaporin-4 is located, therefore relatively heightened permeability of the BBB must occur prior to the formation of a lesion, and perhaps this better explains the distribution of the disease. Portions of the brain with no BBB include the pineal gland, subforniceal organ, subcommissural organ, organum vasculosum of the lamina terminalis (hypothalamic output), median eminence of hypothalamus (hypothalamic output), posterior pituitary and area postrema, and lesions thought to be unique to NMO have been described in some of these locations (Viegas *et al.* 2009; Popescu *et al.* 2011). The optic nerve head is also known to have a relatively higher BBB permeability (Tso *et al.* 1975), and this may be the reason for the common occurrence of optic neuritis in NMO. However BBB differences still do not explain the high prevalence of non-specific deep white matter and subcortical lesions in NMOSD: The MRI features of NMO in contrast to MS are discussed in detail in chapters 2 and 3.

1.3.4 The Mechanism of NMO Lesion Formation

As eluded to in the above sections, the mechanism by which CNS tissue destruction is mediated in NMO is currently unclear. Lucchinetti *et al.* (2002) postulate that

binding of aquaporin-4 antibody causes aquaporin-4 to endocytose and cross-linkage of the antibody-antigen complex activates a damaging lytic complement cascade evidenced by the deposition of a complement complex (C9neo antigen) in lesions and the presence of activated macrophages. They propose that there is also disruption of glutamate homeostasis leading to oligodendrocyte injury and subsequent demyelination (Hu *et al.* 2009). This latter proposition is supported by the fact that a glutamate transporter EAAT2 co-localises with aquaporin-4 which also appears to be endocytosed by aquaporin-4 antibodies (Hinson *et al.* 2007). High levels of glutamate are known to cause neuronal damage in a phenomenon coined "excitotoxicity" (Manev *et al*. 1989).

In contrast, Matsuoka and colleagues (2011) have more recently published a case series of NMO versus MS lesions showing significant heterogeneity in aquaporin-4 expression between lesions. There did not appear to be a clear relationship between the loss of aquaporin-4 and the level of complement and immunoglobulin deposition suggesting that endocytosis of aquaporin-4 and EAAT2 is not the only mechanism by which NMO lesions are formed.

The blood brain barrier has to be disrupted to allow the passage of NMO-IgG into the brain or spinal cord tissue. Bradl *et al.* (2009) have shown that the infusion of IgG from NMO patients into healthy rats fails to either produce the clinical or pathological features of NMO. However NMO-like lesions have been observed by Kinoshita *et al.* 2009 after the passive transfer of NMO patient IgG into rats with pre-existing experimental autoimmune encephalitis (induced with an encephalolitogenic mixture of bovine myelin basic protein and *Mycobacterium tuberculosis)* to create a reduction in the integrity of the BBB and heightened permeability to NMO-IgG. There are also clinical observations to support this -

NMO-IgG has been reported in the serum of a patient taken many years before the first clinical symptoms of the condition (Nishiyama *et al.* 2009).

NMO-like lesions have also been formed through the direct injection of IgG from aquaporin-4 antibody positive patients together with human complement into the brain parenchyma of mice (Saadoun *et al.* 2010), however we are yet to find an animal model that truly mirrors the clinical and pathological features of NMO.

Once an NMO lesion is formed it is characterized by extensive demyelination, necrosis, cavitation and axonal loss as described by Lucchinetti *et al*. in 2002. In this paper it was also reported that NMO lesions affect both the grey and white matter. In active lesions, oedema and leukocyte infiltration are prominent. Immune complexes are observed around the blood vessels in a 'ring and rosette' pattern.

Popescu *et al.* (2011) communicated that AQP4 loss without demyelination and necrosis can be found in the area postrema. Reversible MRI lesions have also been reported in this region (Apiwattanakul *et al.* 2010). In MS, aquaporin-4 loss only occurs in destructive end-stage lesions (Roemer *et al*. 2007).

1:4 Testing for Aquaporin-4 Antibodies:

Immunoglobulin targeted against aquaporin-4 can be detected in the sera of patients with NMO and is a powerfully sensitive and specific diagnostic tool. However there is not currently any international standardisation for the methods used to detect these antibodies across diagnostic units, and hence the true sensitivity of the assay has been unclear. In a recent multicentre study by Waters *et al.* (2012) serum samples from 35 patients who fulfilled the 2006 diagnostic criteria for NMO, 25 who were diagnosed with NMOSD and 86 controls (22 healthy controls and 64 with

miscellaneous diseases including MS) were tested using six different assay techniques, both in-house and commercial. These assays were run at the Mayo Clinic, where NMO was first described by Lennon *et al.* (2004) as an autoimmune condition and who use an indirect immunofluorescence assay detection method (Lennon *et al.*, 2005), and at the University of Oxford where the aquaporin-4 antibody cell based assay was developed (Waters *et al.* 2008). The highest sensitivity found in the study was with the latter Waters *et al.* method that uses IgG binding to cells expressing recombinant AQP4 with quantitative flow cytometry (77%; 46 of 60) or visual observation (73%; 44 of 60).

A further difficulty with demonstrating the true sensitivity of the AQP4 antibody assay is that the phenotypic limits of NMO are not yet known, as discussed below.

1:5 The Emergence of the NMOSD Spectrum and Antibody Negative NMOSD

Aquaporin-4 antibodies are highly specific for NMO (Lennon *et al.* 2004; Waters *et al.* 2008). As a result of the widespread availability of aquaporin-4 antibody and NMO-IgG assays the NMO spectrum of clinical phenotypes has expanded considerably (Table 1.2). There are recent reports of patients with aquaporin-4 antibodies who present atypically with brain symptoms prior to any optic nerve or spinal cord involvement (McKeon *et al.* 2008; Apiwattanakul *et al.* 2010; Kim *et al.* 2011; Nagaishi *et al.* 2011) and limited forms of the disease such as recurrent severe optic neuritis and transverse myelitis (Waters *et al.* 2008; Matthews *et al.* 2009). We therefore commonly use the term NMO spectrum disorder (NMOSD) to encompass all of these phenotypes.

Table 1.2: The NMO Spectrum:

Typical NMO Phenotype	**Rarer or less common Clinical Features Reported in Association with Aquaporin-4 Antibodies or NMO-IgG**
Relapsing course, with attacks of: • Longitudinally extensive transverse myelitis, extending over more than three vertebral segments (Wingerchuk *et al.* 1999; Wingerchuk *et al.* 2006; Waters *et al.* 2008) • Optic neuritis, often bilateral and resulting in severe residual visual loss (Wingerchuk *et al.* 1999; Wingerchuk *et al.* 2006; Merle *et al.* 2007) • Brainstem symptoms such as intractable hiccups, nausea and vomiting (Wingerchuk and Weinshenker 2003; Misu *et al.* 2005; McKeon *et al.* 2008; Kim *et al.* 2011)	• Cerebral symptoms arising from hemispheric lesions (Isose *et al.* 2011; Kim *et al.* 2011) • Transverse myelitis extending over less than 3 vertebral segments,(Krampla *et al.* 2009) in patients who presented with longitudinally extensive lesions during other relapses • Endocrine manifestations and hyper-somnolence due to hypothalamic involvement (Pittock *et al.* 2006; McKeon *et al.* 2008; Kanbayashi *et al.* 2009; Viegas *et al.* 2009) • Encephalopathy, which can cause seizures and headache (McKeon *et al.* 2008; Magana *et al.* 2009; Kim *et al.* 2011)

With the variability in disease presentation it can be difficult to define the boundaries of antibody negative NMOSD and in particular to differentiate it from the more prevalent demyelinating condition MS. There is clinical need for other differentiating biomarkers, not only to identify seronegative NMOSD but also to assess the sensitivity of aquaporin-4 antibody assays and to enable us to monitor the

effectiveness of treatments in clinical practice and trials. This thesis explores the scope of both conventional and non-conventional MRI to provide such a surrogate marker.

1.6 Differences between NMO and MS on Pathological Examination

NMO has distinct pathological and immunological features that have enabled its differentiation from MS, and have been summarised above. However without the benefit of histological examination of tissue the features of NMO can overlap with the more prevalent demyelinating disease MS. MS pathology remains incompletely understood but summarised here are key features that could be important to consider in the search of diagnostic biomarkers that distinguish it from NMO:

- The hallmark of MS on *post mortem* examination is demyelination with multifocal plaques scattered throughout the CNS particularly the perventricular tissue, optic nerves, brainstem, cerebellum and spinal cord (Lassmann *et al.* 2007). NMO lesions are also commonly seen in these regions with the exception of the cerebellum (Pittock *et al.* 2006).
- MS lesions are reported to be associated with both oligodendrocyte damage and primary demyelination (Lucchinetti *et al.* 2000). In acute lesions macrophages phagocytose myelin debris. The myelin damage in NMO is associated with less selective tissue destruction and necrotic changes (Lucchinetti *et al.* 2002)
- NMO lesions are characteristically perivascular (Lucchinetti *et al.* 2002) whereas MS lesions can be perivenular or parenchymal (Lassmann *et al.* 2007).

- For both NMO and MS lesions the inflammatory reaction is associated with microglia and macrophage activation, complement and IgG deposition however in MS there is a predominance of T cells, and in NMO B cells and eosinophils (Lucchinetti *et al.* 2002; Lassmann *et al.* 2007; Matsuoka *et al.* 2011).
- NMO lesions are often associated with a loss of astrocytes, whereas astrocyte activation is a common finding in an acute MS lesion (Matsuoka *et al.* 2011).
- Grey matter atrophy and a reduction in axonal density within the normal appearing tissue is a feature of RRMS (Evangelou *et al.* 2000) that has not been reported in NMO.

1.7 The Requirement for the Early Identification of NMO

The early identification of NMOSD is imperative to allow the implementation of long-term relapse preventing immunosuppressive therapies such as azathioprine or methotrexate (Wingerchuk 2007). Beta-interferon and Natalizumab commonly used as disease modifying therapies in MS have been reported to worsen NMOSD (Palace *et al.* 2010; Kleiter *et al.* 2012). In addition mild MS relapses are commonly not treated, but in the case of NMOSD relapses must be treated early and aggressively with intravenous steroid or plasma exchange to prevent the resulting permanent disability.

1.8 An NMO/MS Borderline Case History

A 31 year old women who was usually fit and well presented with a myelitis causing lower limb parasthesia and right leg weakness. Two weeks afterwards she developed a severe optic neuritis. MRI showed high T2 signal within both the thoracic cord and

right optic nerve typical of demyelinating lesions. She made a good recovery from the myelitis but remained partially sighted in the right eye. Three months later she developed a severe transverse myelitis and was unable to walk. MRI showed a longitudinally extensive transverse myelitis in the thoracic spinal cord. Treated with prednisolone and azathioprine she made a reasonable recovery over a six month period.

After a further six months she had a relapse manifesting as an expressive dysphasia with a new lesion visible on MRI in the left frontal lobe. Despite an increase in steroid therapy she developed a transverse myelitis at T10. Unlike typical NMO this was again a short lesion. After several further relapses, including a severe right optic neuritis which reduced her vision to 'hand movements only', she was treated with natalizumab therapy. This resulted in a severe brain relapse with clinical signs of encephalopathy and multiple confluent lesions on MRI.

There were features of both NMO (LETM and severe optic neuritis) and MS (short transverse myelitis and brain lesions) in this case. The patient was aquaporin-4 antibody negative on repeated assay, and it was therefore decided to treat her with natalizumab, a treatment licensed for the management of severe MS. This resulted in a detrimental brain relapse. Worsening of NMO has been described with natalizumab in the literature and therefore would not have been the treatment of choice if the diagnosis of NMO had been confirmed.

This case highlights that seronegative patients, who have an MS/NMO borderline phenotype, can be difficult to manage where the diagnosis is not definite.

1.9 Summary

The evidence is clear that NMO is a disease distinct from MS that requires different and more aggressive treatment in order to prevent devastating relapses and the accrual of disability. The clinical presentation of NMO and MS can however be very similar, particularly early in the disease course - in keeping with this historically NMO was considered a variant of MS for most of the 20th century.

As discussed in the next chapter imaging already provides clues to the diagnosis of NMO. Quantitative MRI may have the potential to provide a second biomarker for the condition that would be invaluable in diagnosing patients with antibody negative disease.

There are still many unanswered questions about the pathophysiology of NMO: MRI could be particularly useful in identifying whether this demyelinating inflammatory disease is associated with progressive sub-clinical neurodegeneration as is typical of MS.

2:0 Conventional MRI Findings in Neuromyelitis Optica

Conventional MRI refers to the sequences used commonly in clinical practice namely T1 weighting, T2 weighting, fluid attenuated T2 weighting (FLAIR) and proton density weighted. These sequences provide complimentary anatomical information that is reconstructed into images allowing abnormalities in structure or contrast (such as the high T2 contrast of an inflammatory lesion) to be observed.

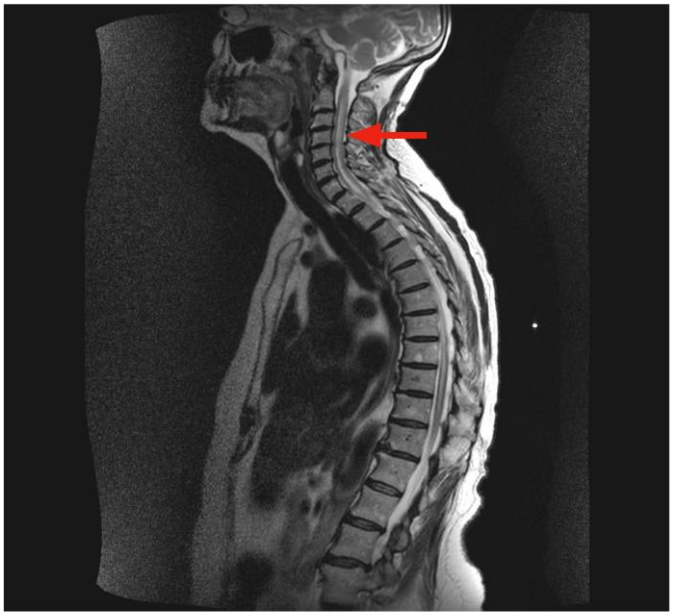
2.1 Spinal Cord

The conventional MRI appearances for a patient presenting with an MS-like illness provide a strong clue that they may have NMOSD. Longitudinally extensive spinal cord lesions (LETM; defined as greater than three vertebral segments in length), which can be visualised as high signal on T2 weighted spin-echo MRI, form part of the 2006 revised diagnostic criteria for NMO (Figure 2.1; Wingerchuk *et al.* 2006). They have high sensitivity and specificity. In the acute stage these lesions may be associated with gadolinium contrast enhancement and probable cord swelling (Wingerchuk *et al.* 1999; de Seze *et al.* 2002). Shorter lesions can be seen either early in a relapse (in the first days) or in patients who have had other attacks with longitudinally extensive lesions as shown by Krampla *et al.* 2009.

Longitudinally extensive transverse myelitis (LETM) is currently the most important MRI marker used in clinical practice for NMOSD and should prompt testing for serum AQP4 antibodies. MS is characterised by short and often multiple spinal cord lesions, or diffuse changes particularly in the later stages (Bot *et al.* 2004). Long spinal cord lesions are rare in western type MS and when present they may be explained by the confluence of several smaller spinal cord lesions (Bot *et al.* 2004). In large cross-sectional Dutch and Australian studies of MS spinal cord

imaging the prevalence of longitudinally extensive T2 signal change is estimated at 2.9% and 2.3% respectively (Bot *et al.* 2004; Qiu *et al.* 2010) and is very exceptionally a presenting feature (4/574 patients in the Qiu *et al.* study). T1 hypointensity has been reported during the acute phase of NMO transverse myelitis but is not usually seen in MS (Miller *et al.* 2008; Downer *et al.* 2011).

Figure 2.1: Longitudinally extensive transverse myelitis (LETM) affecting the cervical spinal cord in an NMO patient.



NMOSD spinal lesions, like those found in MS, are most often located in the cervical cord (Wingerchuk *et al.* 1999; de Seze *et al.* 2002; Pittock *et al.* 2006; Wingerchuk *et al.* 2006). Extension of these lesions superiorly into the medulla is also a feature of NMOSD (de Seze *et al.* 2002; Wingerchuk *et al.* 2006) and has been found to be highly predictive of AQP4 positivity (Lu *et al.* 2010). Axial T2 weighted MRI commonly, but not invariably, reveals NMOSD lesions to be centrally located (Wingerchuk *et al.* 1999; de Seze *et al.* 2002; Nakamura *et al.* 2008; Krampla *et al.* 2009). This is in contrast to MS where lesions are more often found in the lateral white matter (Nakamura *et al.* 2008). The central location of NMOSD lesions corresponds to sites of high aquaporin-4 water channel concentration i.e. in the spinal grey matter (as shown in immunopathological studies; Roemer *et al.* 2007). Nakamura *et al.* (2008) demonstrated that over 60% of NMO spinal lesions occupied the central grey matter in the acute stage, compared to less than 20% of MS lesions on conventional cervical and thoracic spinal imaging.

On long term follow up, T1 imaging of the spinal cord can display hypointensities (or "black holes") and spinal cord atrophy at the site of previous lesions (de Seze *et al.* 2002; Nakamura *et al.* 2008; Krampla *et al.* 2009). T1 black holes can also be commonly found in MS and have been shown in histopathological studies to relate to areas of axonal loss (Bruck *et al.* 1997; Bitsch *et al.* 2001).

The use of the term 'Asian opticospinal MS' is confusing and controversial. In this form of MS, LETM is reported to be common, for example 65% in a large cohort of Japanese patients (Matsuoka *et al.* 2007). However, over a quarter of such patients in this study were aquaporin-4 antibody positive, indicating that they had been misclassified, and there is a current debate over whether this MS phenotype is actually NMOSD (Weinshenker *et al.* 2006).

LETM has also been reported in systemic lupus erythematous (SLE), Sjögren's syndrome and in infectious myelitis and para-infectious idiopathic tranverse myelitis (Kitley *et al.* 2011). However the observed coexistence of other autoantibodies and antibody mediated conditions in patients with NMO may explain LETM in Sjögren's syndrome and SLE (Pittock *et al.* 2008). Hence all patients with LETM should be tested for serum aquaporin-4 antibodies; where negative the differential becomes wider, and without biopsy and pathological examination, differentiating an MS phenotype with LETM from aquaporin-4 antibody negative NMOSD presents a dilemma.

2.2 Brain

NMOSD includes patients with serum aquaporin-4 antibodies, and the discovery of this biomarker has revealed the true frequency and nature of brain lesions associated with the condition. It has now been widely published that over time the prevalence of NMO patients (who fulfil the Mayo clinic 2006 criteria) with lesions on brain MRI is greater than 50% (Pittock *et al.* 2006; Li *et al.* 2008; McKeon *et al.* 2008; Downer *et al.* 2011; Kim *et al.* 2011).

A normal brain MRI at onset is unusual for MS (Miller *et al.* 2008; Polman *et al.* 2011). In NMO, brain MRI is more likely to be normal the closer it is performed to onset of the initial symptoms (Wingerchuk *et al.* 1999; Pittock *et al.* 2006). However Pittock and colleagues (2006) documented that 48% of 27 patients with NMO who were imaged within six months of their first symptoms had an abnormal brain MRI. NMO typical lesions have been described in approximately 7% of patients (Pittock *et al.* 2006). These include signal change in areas of high aquaporin-4 expression, namely the brainstem, hypothalamus and in the periependymal tissue bordering the lateral, third and fourth ventricles, and the Sylvian aqueduct (Figure 2.2; O'Riordan *et al.* 1996; Poppe *et al.* 2005;

Pittock *et al.* 2006; Pittock *et al.* 2006; Downer *et al.* 2011). Lesions in the area postrema are indicative of NMO (Downer *et al.* 2011; Popescu *et al.* 2011). The commonest brain abnormality however is non-specific deep or subcortical white matter lesions, which are found in 55-82% of patients on long-term follow-up (Figure 2.2; Pittock *et al.* 2006; Cabrera-Gomez *et al.* 2008).

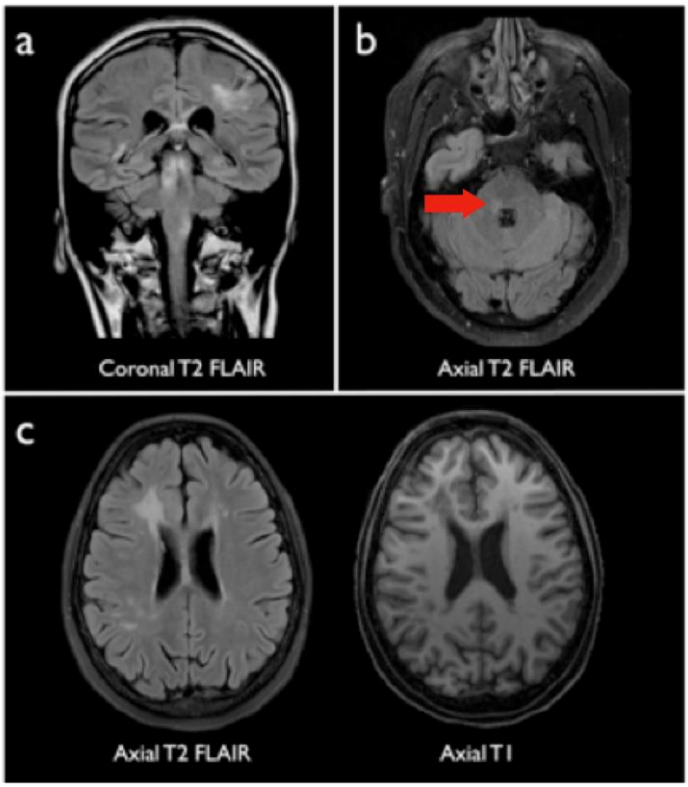


Figure 2.2 Brain lesions in NMOSD: a. a seropositive patient with lesions in a periventricular distribution and a large hemispheric lesion that had been biopsied. b. a lesion adjacent to the forth ventricle and c. non specific deep white matter lesions.

MS-like lesions have been reported in 5-6% of NMOSD patients on initial imaging (Pittock *et al.* 2006; Downer *et al.* 2011) and 10% on the last available scan (Pittock *et al.* 2006). Several studies have investigated whether brain lesion distribution can distinguish NMO from MS (Pittock *et al.* 2006; Li *et al.* 2008; Matsushita *et al.* 2010; Downer *et al.* 2011). Pittock found that 66% of NMO patients (4 of 6 patients) with MS-like brain lesions fulfilled Barkhof's MRI criteria for MS (Barkhof *et al.* 1997; Pittock *et*

al. 2006). Difficulty arises with antibody negative patients, as the current NMO diagnostic criteria would favour against the diagnosis if they fulfil such criteria at onset (Wingerchuk *et al.* 2006)

As in MS, NMO lesions can show gadolinium contrast enhancement, especially during relapse (Cabrera-Gomez *et al.* 2008; Ito *et al.* 2009; Kim *et al.* 2011). A particular "cloud-like" pattern of enhancement has been described as well as accompanying oedema (Ito *et al.* 2009). Tumefactive, enhancing and symptomatic brain lesions are particularly prevalent in the paediatric population (McKeon *et al.* 2008). Relapse related periventricular and posterior reversible encephalopathy-like NMO lesions have also been observed to disappear completely on follow up imaging (Cabrera-Gomez *et al.* 2008; Magana *et al.* 2009).

Calabrese *et al.* (2012) reported that cortical lesions could be identified in 66.7% of patients with RRMS (n=30) but no patients with NMOSD (n=30) using double inversion recovery MR imaging of the cortex.

The literature on optic nerve MRI features specific to NMOSD is limited. During an inflammatory optic neuritis of any cause there can be high signal within the optic nerve on a fat-suppressed T2 weighted scan, gadolinium contrast enhancement and in the long-term atrophy of the affected optic nerve occurs (Rizzo *et al.* 2002; Kidd *et al.* 2003; Wang *et al.* 2011). Contrast enhancement post optic neuritis can last for at least thirty days (Hickman *et al.* 2004). Li *et al. (2008)* reported optic nerve sheath thickening in NMOSD patients with previous recurrent optic neuritis and advised that bilateral optic nerve enhancement with extension to the optic chiasm should alert the clinician to the possibility of NMOSD.

2.3 Summary

Conventional MRI has greatly advanced neurological science and can provide strong clues that a patient has NMO, particularly in the case of longitudinally extensive transverse myelitis that is highly suggestive of the diagnosis. However such lesions result in significant disability and thus a means of identifying and treating NMO before this point would greatly improve the long-term prognosis.

Because of the relatively unique nature of the *post mortem* findings in NMO there is the potential to find a specific MRI biomarker using methods that can measure neuronal and microstructural qualities. This could also provide a way of monitoring disease activity, which would be useful to guide treatment regimes and clinical trials of new candidate therapies for the condition. The next section overviews the existing research in the field of quantitative MRI and NMO.

3.0 Quantitative Imaging in Neuromyelitis Optica

This chapter reviews the existing findings of researchers who have applied quantitative imaging to the study of NMO, and identifies areas for further exploration.

3.1 Existing Literature

3.1.1 Diffusion Tensor and Magnetization Transfer Imaging

Diffusion MRI and Magnetization Transfer Imaging (MTI) provide *in vivo* quantitative measurements of tissue structure not detected on standard imaging. Diffusion imaging is a well-established method first described 27 years ago by Le Bihan and Breton (1985). Diffusion tensor imaging (DTI) acquires diffusion weighted imaging in six or more orthogonal diffusion directions (Basser *et al.* 1994a; Basser *et al.* 1994b) to form the diffusion tensor, and non-invasively measures the degree and directionality of the movement of water molecules in tissue (Le Bihan and Johansen-Berg 2012). Water molecules diffuse with random Brownian motion, but in human tissue restriction of water diffusion can be caused by cell membranes and macromolecules. By quantifying the degree of this restriction in three dimensions, the structural integrity of white mater tracts influenced by demyelination and axonal damage can be assessed (Ciccarelli *et al.* 2008).

Magnetization transfer imaging (MTI) gives an *in vivo* surrogate measure of hydrogen bound macromolecules, such as myelin and axonal membranes, and is commonly normalised as a ratio with the MR signal from the free protons (magnetization transfer ratio (MTR); Wolff and Balaban 1989; Wolff and Balaban 1994). It therefore reflects tissue integrity and has been shown to be a sensitive marker of neurodegeneration (Bozzali *et al.* 2001; Dehmeshki *et al.* 2003). Conventional MR cannot detect protons associated with macromolecules because the T2 relaxation times are less than 1ms. MTI applies an off-resonance radio frequency pulse to the macromolecular protons and the

saturation of these protons is then transferred to the bulk water protons. This causes a decrease in signal – the greater the macromolecular pool (e.g. in areas of high myelination) the greater the reduction in signal.

MRI research investigating whether there are occult abnormalities in the normal appearing brain tissue of NMO patients, using DTI and MTI, has shown variable results. The first quantitative imaging study by Filippi *et al*. in 1999 demonstrated no group differences in the normal appearing brain tissue MTR between eight NMO patients compared to healthy controls whereas they did find a difference when comparing MS patients to controls. Later the same research group was able to identify reduced MTR and increased mean diffusivity (MD) within the grey matter when compared to controls, but no significant difference in the white matter (Rocca *et al.* 2004). Yu *et al.* (2006) also found abnormalities within the normal appearing brain tissue but in contrast reported changes in the white matter with low fractional anisotropy (FA), and elevated MD within the region of the optic and corticospinal tracts. Conversely in the region of the corpus callosum they showed no significant difference between NMO and control DTI indices, and in a subsequent publication suggested that NMO and relapsing remitting MS (RRMS) could be differentiated using these corpus callosum values, as they were significantly lower in the RRMS group (Yu *et al.* 2007). Further work showed correlation between disability scores measuring visual and pyramidal function, and the optic and corticospinal tract diffusion measures respectively (Yu *et al.* 2008). The authors postulated this was due to Wallerian degeneration secondary to a lack of sensory input. It is important to note that the aquaporin-4 antibody status is unavailable for the five studies discussed in this paragraph.

A more recent study by Pichiecchio *et al.* (2012) that utilized a method known as Tract-Based Spatial Statistics (TBSS; Smith *et al.* 2006) aimed at improving the

sensitivity and reliability of multi-subject DTI studies, found localised reductions in FA in the optic radiations. In this study 4 of 7 patients were aquaporin-4 antibody seropositive. Using the same method of DTI analysis (TBSS) Liu *et al.* published a study in the same year (2012) that reported a widespread significant increase in the diffusion indices MD, λ 1 and λ 23 in the white matter of patients with clinically defined NMO when compared to controls. Although a relatively large group of NMO patients was recruited (n=27), neither aquaporin-4 antibody nor NMO-Ig testing was available to the authors. The authors do not specify how they excluded brain lesions from the analysis and do not correct for multiple comparisons of voxelwise measures across space.

Spinal Cord:

The spinal cord has to date been relatively poorly studied with quantitative imaging techniques due to the challenges presented by its size and acute sensitivity to motion such as cardiac pulsation and respiration. However, when seeking an imaging biomarker for NMO the spinal cord is an important pathological site.

Limited spinal cord studies in NMO have been published to date: Disruption of white matter tracts on DTI was noted in one patient (Vargas *et al.* 2008). FA was reduced in the dorsal and lateral white matter of the NMO cervical spinal cord in 10 antibody positive patients, which correlated with disability (Qian *et al.* 2011). Filippi *et al.* also studied the MTR of the upper cervical cord in their 1999 study (Filippi *et al.* 1999) and found reduction within lesioned spinal cord that was indistinguishable from the changes found in lesioned MS spinal cord.

3.1.2 Magnetic Resonance Spectroscopy

Proton or magnetic resonance spectroscopy (MRS) measures the MR signal from hydrogen-bound neural metabolites and quantifies the biochemical constitution of tissues (Soares and Law 2009). In support of the hypothesis that NMOSD is lesion focused and spares the normal appearing brain tissue, the metabolite n-acetyl aspartate (NAA; a surrogate marker of neural integrity) as a ratio to creatine was at normal levels when measured over multiple voxels positioned in the normal appearing deep white matter in a group of eight seropositive NMOSD patients (Aboul-Enein *et al.* 2010). The research also demonstrated normal choline:creatine ratios. This result was reproduced in a larger study of 24 patient which also showed normal myoinositol:creatine ratio (de Seze *et al.* 2010). Conversely NAA has been found to be consistently low in the normal appearing brain tissue of MS patients (e.g. Davie *et al.* 1997; Chard *et al.* 2002). Thus normal NAA levels in the normal appearing white matter may be in favour of NMO versus MS.

3.1.3 Volumetric Imaging

Structural MRI, particularly if acquired with a three dimensional sequence, can be analysed in such a way to quantify and compare the volumes of whole brains, sub-cortical structures and tissue types. Filippi (1999) reported in his MTI paper that there was no significant difference between the whole brain volumes of NMO patients when compared to the healthy control group (Filippi, Rocca *et al.* 1999). In contrast to this significant atrophy of MS brains and subcortical structures has been widely reported, even at the earliest stage (e.g. Dalton *et al.* 2004).

A voxel-based morphometry study looking at differences in grey matter volume between NMO patients, RRMS patients and controls showed no significant differences between NMO patients when compared to the healthy volunteers, when corrected for

multiple comparisons (Duan *et al.* 2011) but widespread significant reductions in grey matter volume in RRMS compared with both controls and NMO patients.

An analysis of cortical thickness in NMO using the Freesurfer tool (Fischl *et al.* 2000) found mild thinning in some cortical areas (the postcentral, precentral and calcarine gyri) and the thalamus when compared to controls (Calabrese *et al.* 2012).

3.1.4 Functional MRI

Two studies from the same research group in Beijing have found disruption in the amplitude and homogeneity in the resting state functional networks of NMO patients with normal brain MRIs, when compared to controls (Liang, Liu *et al.* 2011; Liu, Liang *et al.* 2011). The abnormalities were localised to areas of the frontal, cingulate and temporal cortex as well as the thalamus and caudate. The serological status of these patients is not known. Disruption to the resting state networks of MS patients has also been demonstrated (Bonavita *et al.* 2011).

Rocca (2004) measured the hand movement related activation of the cortex in NMO patients with spinal cord lesions, finding increased recruitment of sensorimotor, temporal and occipital cortical areas when compared to controls (Rocca *et al.* 2004). The increased activation in these regions correlated with MTR measures of spinal cord damage. Functional cortical reorganisation in MS patients with spinal cord disease has also been reported (Filippi *et al.* 2002).

3.2 Candidate Quantitative MRI Methods to Study NMO

Outlined here are two more recently described MRI methods that have been selected as potentially useful in the study of NMOSD, and that have been included as part of the investigation of the condition.

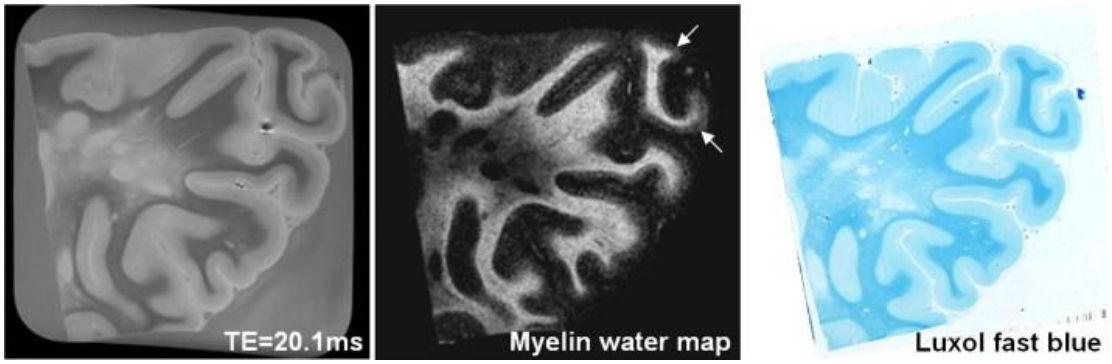
3.2.1 Myelin Water Imaging

Progress continues to be made in the development of quantitative MRI. Multicomponent Relaxometry (Deoni *et al.* 2008) is a method that has not previously been applied to the study of NMO. It currently gives the most direct representation of the integrity of central nervous system myelin *in vivo*. Although DTI metrics are influenced by myelination they are also likely to be affected by the density of axonal packing, the orientation of fibres and the number and nature of the neuroglia. MTI signal is also affected by the density of myelin however is very sensitive to inflammation and other factors that may influence the macromolecular pool resulting in the measure being relatively non-specific.

The basis of myelin water imaging is the observation that water trapped between the myelin bilayers relaxes faster than water in the intra and extra cellular space. Using this principle multicomponent relaxometry aims to separate the MRI signal into contributions from these water pools. Myelin Water Fraction (MWF) is the signal from the myelin bound water pool divided by the total water signal (MacKay *et al.* 1994). MWF has been shown to correlate both visually (as shown in Figure 3.1) and quantitatively with histopathological *post mortem* measures of myelin integrity (Laule *et al.* 2006; Laule *et al.* 2008). A multicomponent technique that utilises rapid gradients to acquire high resolution in clinically feasible times has been developed by Deoni *et al*. (2008) and is known as Multicomponent Driven Equilibrium Single Pulse Observation of T1 and T2 (mcDESPOT).

Applied to primary progressive MS this technique has revealed widespread myelin loss *in vivo* in the both lesions and the normal appearing brain tissue (Kolind, Matthews *et al*. 2012), and has shown anatomical correlation with disability measures.

Figure 3.1: Qualitative post-mortem myelin water imaging correlation with myelin staining with Luxol fast blue (Laule et al. 2008)



The pathogenesis of MS lesions involves primary myelin loss (Lassmann *et al.* 2007) whereas the evidence suggests that astrocytes are the primary target in NMO (Jacob *et al.* 2012). A specific *in vivo* MRI measure of residual myelin density within lesions and in the normal appearing brain tissue has the potential to be very useful in differentiating between NMO and MS.

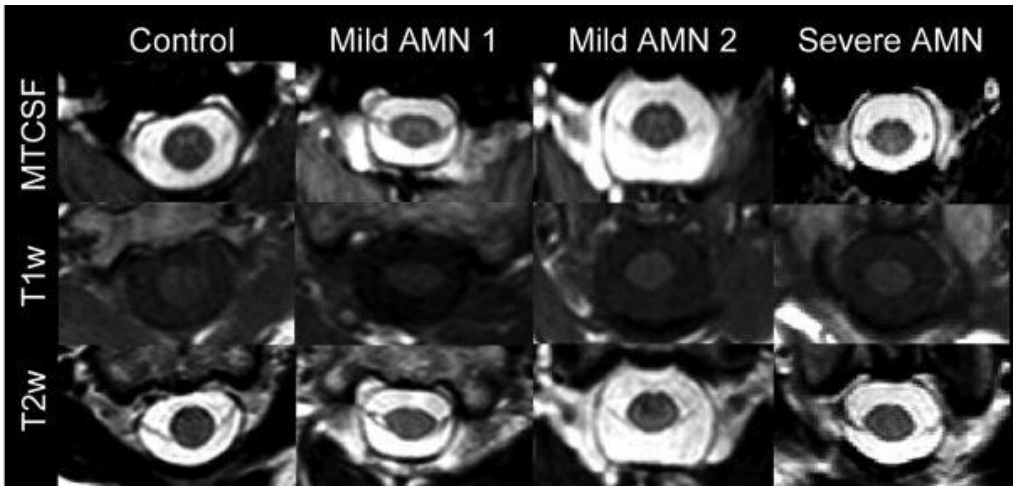
3.2.2 Magnetization Transfer Imaging of the Spinal Cord

Magnetisation transfer imaging (MTI) requires the calculation of a ratio between two consecutively acquired scans, one with and one without radiofrequency saturation of the macromolecular spins in the tissue (Wolff and Balaban 1989; Wolff and Balaban 1994). Due to spinal cord movement it is extremely difficult to reliably co-register these two scans, and a suggested alternative method by Seth Smith *et al.* (2005) is to use a motion insensitive internal standard – in this case the cerebrospinal fluid, and hence this technique has been coined MTCSF. The method has been applied to five patients with

adrenomyeloneuropathy (AMN; Smith *et al.* 2005), a spinal cord white matter disease, comparing them with six healthy controls showing loss of grey/white matter distinction and hyperintensity within the lateral and dorsal white matter (suggesting white matter damage) only detectable on the MTCSF and not seen on the conventional axial T2 scan (Figure 3.2).

This technique has not yet been applied to the study of NMOSD but could reveal important information as to the nature and severity of spinal cord tissue damage not appreciated on a conventional spinal cord protocol, and therefore was chosen as one of the quantitative MRI modalities with which to investigate NMO in this thesis.

Figure 3.2: Comparison of MTCSF and conventional Images for a healthy volunteer and three AMN patients (taken from Smith et al. 2005)



3.3 Summary

The literature presented above has some contradictory findings. Nearly all of the studies discussed have NMO cohorts with relatively low proportions of antibody positive patients risking the inclusion of MS or other mimicking inflammatory disorders. This may explain some of the contradictory results. To truly characterise NMO it is necessary to study a

group of NMO patients who all are seropositive for aquaporin-4 antibodies. The work presented in this thesis takes this approach to the problem.

To date there are no published longitudinal studies of NMO characterising changes between relapses, and measuring whether lesions cause subsequent neurodegeneration. In this thesis NMO and MS have been studied over a one year period with quantitative MRI techniques.

4:0 Objectives

4:1 Research Questions

This thesis aims to explore the following questions:

- Can MRI, either conventional or quantitative, provide an additional biomarker for NMO to allow prompt and accurate diagnosis?
- Is neurodegeneration a feature of neuromyelitis optica spectrum disorder?
- Can serum N-acetylaspartate levels be used as adjunctive information to allow the distinction of NMO and RRMS?

4:2 Research Aims

The objective of each presented experimental chapter is as follows:

- *Chapter 6:* To explore the utility of conventional MRI brain in the distinction of NMOSD and RRMS
- *Chapter 7:* To investigate whether NMO is associated with widespread neurodegeneration as found in RRMS, and whether quantitative measures can provide a biomarker for the diagnosis of NMOSD.
- *Chapter 8:* To investigate the utility of quantitative spinal cord imaging in the study of NMO
- *Chapter 9:* To investigate whether NMO is associated with longitudinal changes in quantitative imaging indices consistent with neurodegeneration
- *Chapter 10:* To investigate whether the serum metabolite N-acetylaspartate (a neural marker) can distinguish NMO and RRMS. To further explore whether a combination of quantitative imaging and serum measures can provide a biomarker for NMOSD.

5:0 Study Overview

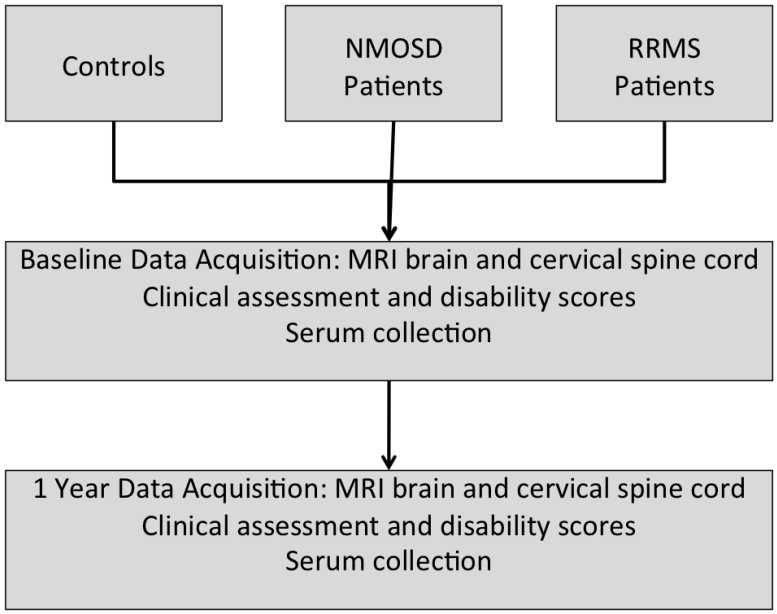
A clinical imaging study was designed to answer the research questions posed in the previous section. The data in this thesis is taken predominantly from this core study, but an additional dataset is used in chapter 6. This is detailed in section 5.8.

5.1 Study Design

The core study was designed to compare conventional and quantitative imaging in three subject groups: Controls, neuromyelitis optica spectrum disorder (NMOSD) patients and relapsing remitting multiple sclerosis patients (RRMS).

Figure 5.1 outlines the study design.

Figure 5.1: Flow-diagram outlining study design:



In adherence to ethical regulations from U.K. National Research Ethics Service, all research participants were fully informed of the techniques and the potential risks in the study (REC reference number 09/H0501/55). Each subject underwent a baseline brain and spinal cord MRI with collection of clinical disability data and serum, and asked to return at one year for a repeat study, clinical assessment and serum collection.

5.2 Considerations for Powering the Study

The cross-sectional component of the study was designed to have the power to detect significant differences in anatomical volumes and diffusion indices between patients with relapsing MS and healthy controls based on previously published investigations of this type (e.g. Coombs *et al.* 2004, Filippi *et al.* 1998).

5.3 Study Participants

Healthy controls and RRMS patients were aged matched where possible for the NMOSD patients recruited. The inclusion criteria were as follows:

NMOSD:

- Clinical syndrome consistent with NMO or NMOSD as diagnosed by an expert neurologist
- Aquaporin-4 antibody positivity
- Age over 18 years

RRMS:

- Clinically defined RRMS using MacDonald's revised criteria (Polman, Reingold et al. 2011)
- Aquaporin-4 antibody negative
- Age over 18 years

Healthy Controls:

- Age over 18 years

Exclusion criteria for all groups were as follows:

- Had any of the commonly accepted contraindications to MRI scanning, for example severe claustrophobia, presence of metallic implants, a pacemaker etc.
- Pregnancy.
- Did not have adequate understanding of verbal and written information in English, sufficient to complete an MRI safety screening questionnaire.
- Unable to give informed consent.
- Had any other significant disease or disorder that could put the participant at risk, compromise their ability to participate or influence the results of the study.
- Was within four weeks of the onset of a clinical relapse

Table 5.1 summarises the number of subjects recruited and those who attended follow-up.

Table 5.1: Subjects recruited and followed-up

Subject Group	Number undergoing baseline assessment	Number attending follow-up	Percentage attrition
NMOSD	18	16	11.1%
RRMS	15	13	13.3%
Control	17	16	5.9%
Total	**50**	**45**	**10%**

The baseline characteristics of the subjects included in this study are shown Appendix I and summarised in Table 5.2.

Table 5.2: Baseline characteristics summary table

Subject Group	Number	Age, range (median)	Sex	Aquaporin-4 antibody positive	EDSS, range (median)	Disease Duration, range (median)
NMOSD	18	20-76 (46)	15F 3M	18 (100%)	2-6 (4)	12-186 (57.5)
RRMS	15	22-62 (38)	11F 4M	0 (0%)	0-5 (2)	24-240 (72)
Control	17	21-77 (47)	13F 4M	0 (0%)	-	-

5.4 Clinical Assessment

Patients were assessed at baseline and at 1 year with the following disability scores.

- Expanded Disability Status Scale (EDSS) (Kurtzke 1983)
- 25ft timed walk
- 9 hole peg test

- Corrected visual acuity (Snellen chart)

5.5 Serum Collection

Blood was collected in a Vacutainer™ SST Tube with Silica Clot Activator, Polymer Gel and Silicone-Coated Interior for AQP4-ab assay and N-acetylaspartate analysis. The blood was centrifuged for 10 minutes within 4 hours of collection, and the separated serum frozen and stored at -80°C.

5.6 Aquaporin-4 Antibody Assay

AQP4-ab assay was run on each subject's serum using a cell-based assay as described by Waters *et al*. 2012. The samples were independently blinded so that the diagnosis was unknown. Table 5.2 shows that all NMO subjects had a positive assay, and none of the MS or control subjects.

5.7 MRI Acquisition Protocol

Multiparametric MRI of the brain and cervical spinal cord were performed separately within two weeks of each other. All imaging was performed at 3T (Siemens Magnetom® Verio, Erlangen, Germany) using a 32 channel receive head coil for the brain imaging and 12 channel head and 4 channel neck array receive coils for the cervical spinal imaging.

An MRI protocol was selected in order to answer the research questions posed in section 4:0 and is summarised below in Table 5:3. The full MRI protocol is given in the relevant chapters and recorded in full in Appendix II.

Table 5.3: Summary of the MRI protocol selected

Imaging Measure Required	**MRI Sequence**	**Reason for Selection**	**References**
White Matter Integrity	Brain Diffusion Tensor Imaging	Shown to be able to detect abnormalities in the normal appearing brain tissue in MS and other conditions. Good 'within scanner' coefficient of variation (0.8-3.0% for fractional anisotropy). Tested and published analysis pipelines.	Douaud, Smith *et al.* 2007; Bakshi, Thompson *et al.* 2008; Filippini, MacIntosh *et al.* 2009; Douaud, Filippini *et al.* 2011; Filippi, Rocca *et al.* 2012; Volmar *et al.* 2012; Smith *et al.* 2006
	Brain Myelin Water Imaging (MWI)	Complementary data providing myelin specific information.	(Kolind, Matthews *et al.* 2012)
	Spinal Magnetisation Transfer Ratio	Registration not required. Much less susceptible than DTI to movement artefact.	(Smith, Golay *et al.* 2005)
Brain, spinal cord and regional atrophy	3-dimensional high resolution T1 weighted image	Optimal protocol to utilise SIENA method of measuring brain volume and atrophy.	(Smith, Zhang *et al*. 2002; Bakshi, Thompson *et al.* 2008)
Brain lesion volume and location	Brain axial T2 weighted images included fluid attenuated T2	Standard protocols for identifying and segmenting lesions	
Spinal lesion volume and location	Spinal sagittal and axial T2 and Proton density	Standard protocols for identifying and segmenting lesions	

5.8 Wider Cohort Data Collection:

Participants in the core study were recruited from the national NMO clinic run in Oxford and funded by NHS Specialised Services (http://www.specialisedservices.nhs.uk).

In addition to this data, chapter 6.0 also includes data collected from collaborators and scans that were acquired with the same protocol as the core study using a Siemens 3T Verio MR scanner of the same make, model and age. This is detailed in the methods section.

6.0 The Utility of Conventional Brain MRI to Distinguish Neuromyelitis Optica Spectrum Disorder and Relapsing MS

In this chapter quantitative analysis techniques are applied to conventional MRI to identify differences in the brain lesion distributions of NMOSD and RRMS, which are then used to direct the formulation of criteria to aid the differentiation of the two conditions.

6.1 Introduction

Lesion probability mapping is a technique first used by Narayanan *et al.* (1997) to describe the lesion distribution of patients with MS. Lesion probability maps provide a voxel-wise, quantitative description of the topographic distribution of brain lesions and are essentially a group average lesion map which is usually represented with a scale from 0-100% where 0% indicates that no patients had a lesion in that spatial location, and 100% means they all had a lesion at that location.

A normal MRI brain scan at presentation is more indicative of NMOSD than MS (Wingerchuk *et al.* 1999). However it is has been reported that 48% of patients who fulfil the 2006 diagnostic criteria for NMOSD will have brain lesions at presentation, and 60% on long term follow up (Pittock *et al.* 2006). Previous case series however show that the majority of patients have non-specific lesions in the deep and subcortical white matter, and some have lesions that would fulfil Barkhof criteria for the dissemination of brain lesions in space (i.e. diagnostic criteria for MS; Pittock *et al.* 2006; Downer *et al.* 2011). Therefore as well as comparing the distribution of brain lesions in the two conditions, the morphology of the lesions is closely considered.

Patients with antibody negative NMOSD are more likely than those with aquaporin-4 antibodies to have brain lesions that fulfill the diagnosis for MS (Downer *et al.* 2011),

therefore to truly characterise the lesion distribution of patients with NMOSD only seropositive patients have been included to avoid any doubt about the diagnosis.

6.2 Objectives

- To investigate whether quantitative T2 lesion mapping can identify differences in lesion distribution between NMO and MS.
- To determine whether there are differences in the morphology of lesions in NMO and MS.
- To determine whether patients with antibody positive NMOSD can fulfil well-established diagnostic criteria for MS.
- To develop MRI criteria for the diagnostic distinction of MS and NMOSD.

6.3 **Methods**

The data included in this experiment is from the wider cohort described in section 5.8. The dataset represents a cross-sectional sample of patients with clinically defined RRMS and aquaporin-4 antibody positive NMOSD. The characteristics of the patients are summarised in Table 6.1.

***6.3.1 NMOSD cohort*:** All NMOSD patients included were aquaporin-4 antibody positive. Patient data was collected from Oxford and Cardiff University Hospitals. All aquaporin-4 antibody assays were performed in Oxford using the cell-based method as described by Waters *et al.* (2012). Of 44 patients, 29 were identified to have T2 hyperintense lesions on brain MRI. Three of these patients had a vascular–like lesion distribution. When un-blinded it was apparent that these patients were older than the remaining NMOSD cohort (with ages 72, 76 and 77 years), in keeping with the likelihood

of finding incidental vascular lesions. These subjects were excluded from the group used to create the lesion probability distribution.

6.3.2 RRMS cohort: 50 subjects with the diagnosis RRMS who fulfilled McDonald's revised criteria were included as a comparator cohort (Polman *et al.* 2005).

6.3.3 Imaging Sequences: Each subject had a T1, T2 and FLAIR image of variable sequence acquisition protocol depending on the source of the data but established high quality.

Table 6.1: Subject characteristics

	Diagnosis	
	NMOSD AQP4ab +ve	RRMS
Number of Subjects	44	50
Age Range (median)	19-77 (47)	26 -65 (42)
Gender	5M, 39F	16M, 34F
Mean disease duration at time of MRI/ years (SD)	8.44 (6.4)	12.3 (6.8)
Mean EDSS (SD)	4.9 (2.1)	1.83 (1.3)
Number with abnormal brain MRI	29	50
Number with vascular-like appearance	3	0
Number included in lesion probability maps	26	50

Abbreviations: AQP4= aquaporin-4; EDSS = Expanded Disability Status Scale, F= Female; M = Male; NMOSD = Neuromyelitis Optica Spectrum Disorder, RRMS = Relapsing Remitting MS

6.3.4 Lesion Probability Maps: Imaging data were analyzed using the FMRIB software library of tools (FSL; Smith *et al.* 2004; Woolrich *et al.* 2009). For each subject hyperintense T2 lesions were segmented manually on an axial FLAIR image, in native space, with simultaneous reference to the T2 scan. This process was conducted independently on every scan by myself and one neuroradiologist (Dr Rita Marasco). The FLAIR images were then registered to the Montreal Neurological Institute (MNI) 2mm standard space template using a non-linear transformation method (FNIRT; Jenkinson *et al.* 2002) The non-linear transformation matrix was then applied to the respective lesion segmentation masks to transform them into the space of the standard template. After transformation the lesion masks were thresholded at 50% and binarised again to avoid the volume increase caused by the trilinear interpolation. They were then summed and averaged for each subject group to create lesion probability maps. A group level comparison of lesion distribution was conducted using the non-parametric permutation testing tool *Randomise* with cluster-based thresholding and corrected for multiple comparisons (Smith *et al.* 2004).

6.3.5 Description of Lesion Distribution in NMOSD cohort: T2 lesions were counted, and the lesion location and characteristics were documented. Barkhof criteria (Barkhof *et al.* 1997) for the dissemination of MS lesions in space were applied to the unenhanced brain scans alone (spinal cord scans were not available in all patients of both groups). Barkhof criteria are (a) at least nine lesions on T2-weighted images (b) at least three periventricular lesions, (c) at least one juxtacortical lesion, and (d) at least one infratentorial lesion. The cutoff for positivity is three out of four criteria. The NMOSD scans were also examined for lesion morphology typical of MS, namely juxtacortical

lesions in the U-fibre (with a curved/ s-shaped morphology) and ovoid perpendicular lesions adjacent to the body of the lateral ventricles often described as Dawson's fingers.

6.4 Results

6.4.1 T2 Lesion Volume and Number:

Table 6.2 shows the number of patients with T2 lesions and the relative lesion loads in each group. There was a greater number and volume of lesions in the MS group, which was not significantly different to the NMO group due to the high variability.

Table 6.2: Lesion Volume and Number

Diagnosis	Number of Subjects	Number included in lesion probability mapping	Mean T2 lesion volume (SD)/mm3	Number of T2 lesions, range (median)
NMOSD	44	26	4045 (3082)	1-27 (13)
RRMS	50	50	11870 (9328)	4-54 (20)

6.4.2 Lesion Distribution:

The lesion probability distributions for the RRMS and NMOSD patient groups are shown in Figure 6.1A and B. The majority of lesions in the NMOSD patients were smaller in size, and fewer in number compared to MS. The distribution throughout the brain tissue was also widely variable: This is reflected in the low probability of lesions occurring in the same spatial location in more than two patients. The area of highest probability of a lesion occurring in the NMOSD group was within the frontal deep white matter (MNI coordinate -24 mm, 8 mm, 20 mm at a probability of 20%). Conversely the most likely place for an RRMS lesion to occur was adjacent to the posterior of the body of the lateral ventricle in the parietal white matter (MNI coordinate 30 mm, -50 mm, 14 mm), at a high

probability of 54% indicating greater lesion load and coherence of lesion location amongst the RRMS group. Figure 6.1C shows a subtraction map where the average NMOSD lesion map has been subtracted from the average RRMS lesion map to allow direct comparison of the distributions. Lesions in NMOSD and RRMS were found throughout the supra and infratentorial white and grey matter. However distinguishing features of note were more NMOSD lesions in the medulla oblongata, whereas in the RRMS group more lesions were noted within the cerebellum, bordering the lateral aspect of the body of the lateral ventricles (including within the periventricular grey matter) and in the temporal lobes. Both conditions were associated with lesions in the corpus callosum. Figure 6.1D shows the voxel-wise permutation-testing comparison of the lesion distributions in each group. RRMS lesions are significantly more likely than NMOSD lesions adjacent to the body of the lateral ventricle (corrected $p<0.05$). The lesional region with the greatest likelihood to be within the NMOSD and not RRMS group was adjacent to the 4th ventricle within the pons. This did not reach statistical significance (corrected $p=0.35$) due to the lower lesion load in NMOSD.

The proportion of NMOSD T2 lesions occurring in specific spatial locations within the brain is shown in Table 6.3. Of note the commonest distribution for the NMOSD patients is supratentorial deep white matter lesions.

6.4.3 Lesion Characteristics:

7/26 NMOSD patients with brain lesions, or 15.9 % of all antibody positive NMOSD patients, fulfilled Barkhof criteria for the dissemination of RRMS lesions in space (Barkhof *et al.* 1997) based on unenhanced brain MRI alone. There are important differences however in the morphology of the lesions. None of the NMOSD patients had juxta-cortical T2 hyperintensities with morphology suggestive of location in the U-fibre

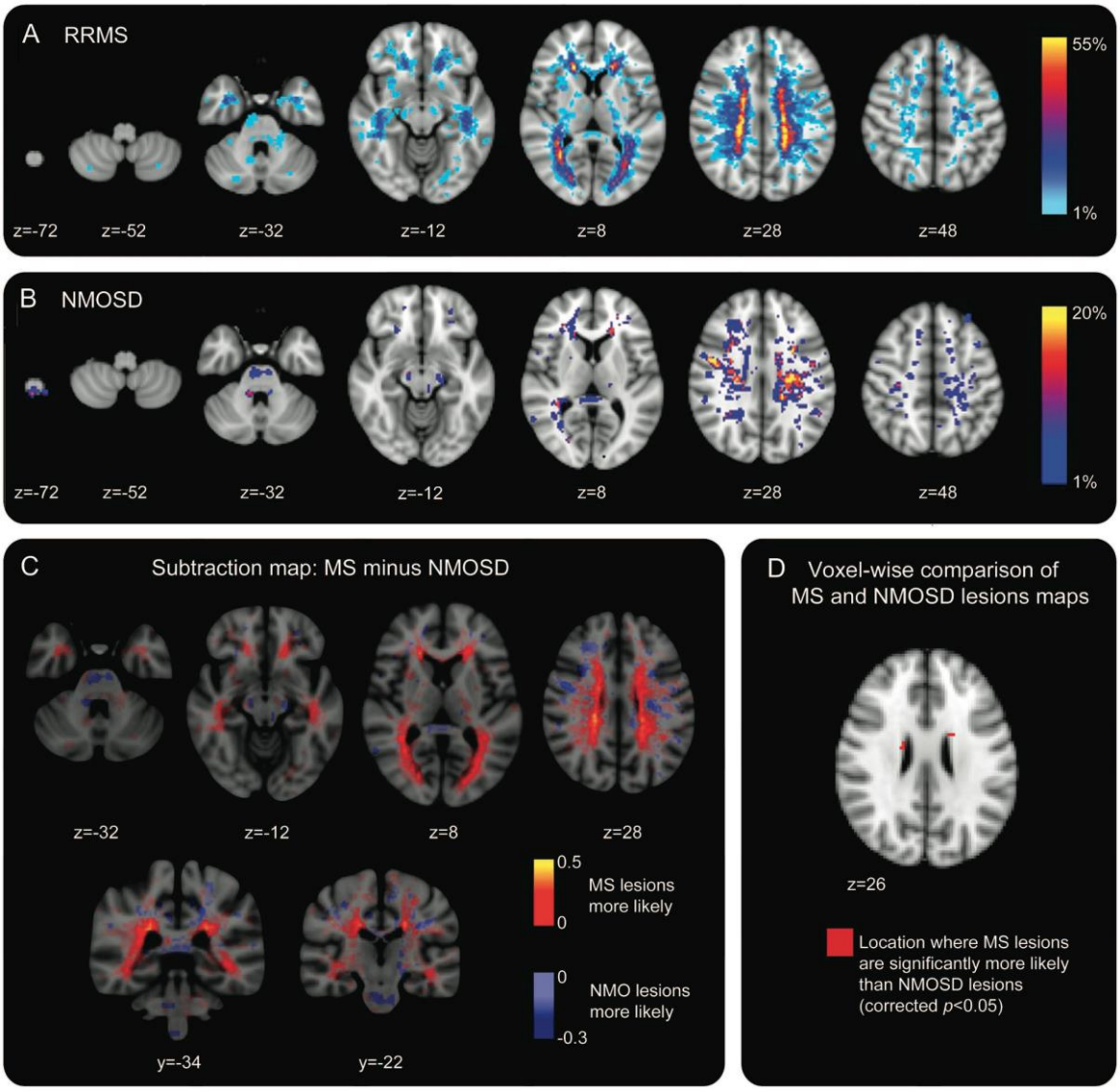
unlike the RRMS cohort. It is also of note that lesions adjacent to the lateral ventricles in NMOSD tend to be located at the anterior and posterior horns (Figure 6.1B), and that no patients had ovoid lesions in a perpendicular alignment (Dawson's fingers).

Within the individual patients of the NMOSD cohort a range of 0-83.3% T2 lesions showed T1 hypointensity (38% of all T2 lesions). This compares with 25-95% of MS lesions (53.4% of all T2 lesions).

Table 6.3: Lesion Location for 26 Aquaporin-4 antibody positive NMOSD patients

Lesion Location		Percentage
Supratentorial		92.8
	Adjacent to lateral ventricles	11.9
	Large hemispheric lesion	0.9
	Deep white matter	48.1
	Subcortical	30.7
	Deep grey matter	1.2
Infratentorial		7.2
	Brainstem	6.3
	Cerebellum	0.9

Figure 6.1: Figure 1 A: Lesion probability distribution for fifty subjects with relapsing MS. The colour scale (from 0 to 55 %) represents the minimum to maximum probability of a lesion occurring in a particular spatial location. MNI standard space template Z coordinate is shown in mm. B: Lesion probability distribution for twenty-six subjects with aquaporin-4 antibody positive NMOSD. The colour scale (from 0 to 20%) represents the minimum to maximum probability of a lesion occurring in a particular spatial location. MNI standard space Z coordinate is shown in mm. C. Subtraction map where the average NMOSD lesion map has been subtracted from the average RRMS map to allow direct statistical comparison of the lesion distributions. Red to yellow represents where RRMS lesions are more likely than NMOSD, and light blue to dark blue where NMOSD lesions are more likely than RRMS. D. Voxelwise comparison of lesion probability maps reveal that RRMS lesions are significantly more likely than NMOSD lesions adjacent to the body of the lateral ventricle, shown here in red (corrected $p<0.05$).



6.4.4 Formulation of Criteria for the Separation of RRMS and NMOSD:

Using the findings summarised above the hypothesis was made that RRMS could be distinguished from NMOSD on the basis of T2 brain lesion distribution. Table 6.4 shows the criteria tested. Having at least one lesion adjacent to the body of the lateral ventricle and at least one lesion in the inferior temporal lobe was able to identify RRMS with 78 % sensitivity, 96.2 % specificity, 97.5 % positive predicative value and 69.4 % negative predictive value. Of the RRMS who did not fulfill both criteria 7/11 had either an ovoid lesion perpendicular to a lateral ventricle or a subcortical lesion with morphology suggestive of location in the U-fibre. Adding this as a further criterion resulted in a 92 % sensitivity, 96.2 % specificity, 97.9 % positive predictive value and 86.2 % negative predictive value.

These criteria are formed on the basis of the cohort we had available i.e. an approximate 2:1 MS:NMOSD mix. This is likely to be representative of the final diagnosis of patients who are seen in a specialist clinic with a borderline syndrome and who present a diagnostic dilemma.

Table 6.4: Numbers of subjects fulfilling and the sensitivity and specificity of each criterion/ combination of criteria for the separation of RRMS from NMOSD.

	Number of subjects	Criterion 1: Lesion adjacent to the body of a lateral ventricle	Criterion 2: Inferior temporal lobe lesion	Criteria 1+2	Criterion 3: U-fibre or Dawson's finger type lesion	Criteria 1+2 or 3
NMOSD	26	6	5	1	0	1
RRMS	50	46	40	39	41	46
Sensitivity of distinguishing RRMS from NMOSD	-	92 %	80 %	78 %	82%	92 %
Specificity of distinguishing RRMS from NMOSD	-	76.9 %	80.8 %	96 .2 %	100%	96 .2 %
Positive Predictive Value	-	88.5 %	88.9 %	97.5 %	100%	97.9 %
Negative Predictive Value	-	83.3 %	67.7 %	69.4 %	74%	86.2 %

6.5 Discussion

This work provides practical diagnostic assistance with distinguishing RRMS and NMOSD when presented with an overlap syndrome, and could help to implement correct and early treatment, which is of particular gravity in NMO patients to prevent relapses. This work has used quantitative analysis techniques to identify important differences between the brain lesion distribution in NMOSD and RRMS but when applied at an individual level requires only a good quality clinical MRI brain examination that should be available to all neurologists.

To fully test the criteria for the separation of NMOSD and MS prospective application to patients of initially unknown diagnosis is required, with audit against the definitive clinical diagnosis once established.

The limitation of conventional imaging is that it does not provide disease specific biomarkers. At the level of a single voxel the increase in T2 signal intensity that is seen in both conditions is indistinguishable. We simply look for patterns in T2 lesion distribution and anatomical features that are more likely to occur in one condition than another. Although NMOSD and RRMS are both inflammatory demyelinating diseases the underlying pathophysiology differs, and therefore quantitative imaging methods that have the power to detect differences in microstructure and metabolism could provide more disease specific imaging biomarkers. The next chapter explores the use of a careful selection of such techniques in the differentiation of NMOSD and RRMS.

7.0 The Application of Quantitative Brain MRI to Differentiate Neuromyelitis Optica Spectrum Disorder and Multiple Sclerosis

This experimental chapter explores the potential of complimentary quantitative MRI techniques to aid the diagnosis of neuromyelitis optica spectrum disorder (NMOSD).

7.1 Introduction

Quantitative (or non-conventional) imaging can probe the biological and microstructural properties of central nervous system tissue. A variety of such MRI modalities have been used to study the MS brain with the consistent finding of abnormalities that indicate a diffuse neurodegenerative process. Examples from the literature are diffusion tensor imaging (DTI; Larsson *et al.* 1992; Griffin *et al.* 2001; Tortorella *et al.* 2006), magnetisation transfer imaging (Cercignani *et al.* 2001; Tortorella *et al.* 2006), proton spectroscopy (Davie *et al.* 1997; Anik *et al.* 2011) and myelin water imaging (Kolind *et al.* 2012). In keeping with these MR findings, MS is associated with substantial axonal loss in the normal appearing white matter on *post mortem* examination (Evangelou *et al.* 2000) and a clinically observed progressive neurodegenerative phase.

In contrast NMO pathology is lesion-centric (Lucchinetti *et al.* 2002) and is not known to be have the same degree of normal appearing white matter changes on *post mortem examination*. The differences between NMO and MS therefore should be detectable with MRI measures of non-lesional neurodegeneration and demyelination. Several quantitative MRI techniques that measure these two pathological mechanisms were considered for the research presented in this thesis. Factors influencing the final selection of the imaging protocol included:

- That the modalities had been shown in previous studies to reproducibly detect changes in normal appearing tissue in neurodegenerative neurological conditions including MS
- That they have the potential to be analysed in an automated way that could be translated into clinical practice
- That they can be acquired in a feasible acquisition time for a patient MRI examination
- That they provide complementary *in vivo* pathological information

Semi-automated volumetric analysis of structural MRI was chosen to detect whole brain and regional atrophy, diffusion tensor imaging to detect changes in axonal integrity and myelin water imaging as a relatively specific measure of myelin density. An overview of these measures and the previous literature relating to them was presented in Chapter 3. This study is unique in its methods by the definition of the study cohorts, ensuring all NMOSD are aquaporin-4 antibody positive and all RRMS patients are aquaporin-4 antibody negative. Myelin water imaging and structural analysis of subcortical volumes has not previously been applied to the study of NMOSD.

7.2 Objectives

- To determine whether volumetric structural analysis can distinguish NMOSD and MS
- To determine whether complimentary measures of normal appearing white matter integrity (DTI and MWI) can distinguish the two conditions

7.3 Methods

7.3.1 Study Participants

The recruitment for this experiment is as outlined for the core study cohort in section 5.3, and the baseline characteristics (age, sex, disease duration, type of relapses and disability assessment scores) of the subjects are detailed in Appendix I. There were three study groups: 18 aquaporin-4 antibody positive NMO spectrum disorder (NMOSD); 15 RRMS and 17 healthy controls.

7.3.2 Study Examinations

Each subject underwent a baseline brain and spinal cord MRI with collection of clinical disability data and serum (detailed in Chapter 5). This process was repeated after one year.

7.3.3 MRI Acquisition Protocol

The MRI brain scan was performed at 3T (Siemens Magnetom Verio, Erlangen, Germany) using a 32 channel receive head coil.

Sequence parameters: DTI: 60 diffusion directions with B-value 1000 and 8 volumes with no diffusion weighting, TR 9600ms, TE 87 ms, FOV 190 x 190mm, voxel-size 2.0x2.0x2.0mm, 65 slices, 1 average. Acquisition time = 12mins.
MWI: Acquired with mcDESPOT (Deoni *et al.* 2008). FOV=22x22x16cm, 1.7mm isotropic resolution; SPGR: TE/TR = 2.5ms/5.6ms, $\alpha=\{3,4,5,6,7,9,13,18\}°$, BW=±24kHz; SSFP: TE/TR=2.2ms/4.4ms, $\alpha=\{10,13.3,16.6,20,23.3,30,43.2,60\}°$, BW=±36kHz, phase-cycling patterns = 0º and 180º (for correction of off-resonance effects). A reduced

resolution IR-SPGR image was also acquired with TE/TR/TI/α = 2.5ms/5.6ms/450ms/5° to correct for flip angle inhomogeneity. Acquisition time = 14mins.

Structural Imaging: 3 dimensional MPRAG sequence with voxel size 1x1x1mm, TR 2040ms, TE 4.7ms, 1 average.

Sequences for Lesion Detection: T2: 2 dimensional turbo spin echo, 48 slices, slice thickness 3mm, voxel size 0.5x0.5mm, FOV 220x220mm, TR 5690ms, TE 71ms, 1 average. Flair: 2 dimensional turbo spin echo 48 slices, slice thickness 3mm, TE 73.0ms, TR 9000ms, voxel size 0.9x0.9. 1 average. PD: 2 dimensional turbo spin echo, 48 slices, slice thickness 3mm, voxel size 0.5x0.5mm, FOV 220x220mm, TR 3000ms, TE 18ms, 1 average.

7.3.4: MRI Data Analysis and Statistical Testing

7.3.4.1 Whole Brain Volume

Brain tissue volume, normalised for subject skull size, was estimated with SIENAX (Smith *et al.* 2001; Smith, *et al.* 2002), part of FSL (Smith *et al.* 2004). Brain extraction (removal of non-brain signal) was applied (Smith 2002) then the brain image affine-registered to MNI152 space (Jenkinson 2001, Jenkinson 2002) using the skull image to determine the registration scaling, which was used to normalise for head size. Next, tissue-type segmentation with partial volume estimation was carried out (Zhang 2001) in order to calculate the total volume of brain tissue.

Statistical analysis was conducted using the software SPSS Statistics (Version 20, IBM Corp.). A Kolmogorov-Smirnov test of the normality of the distribution and a Levene's test of the equality of error variance of the data was run and directed the further use of parametric statistical tests. A one-way analysis of co-variance (ANCOVA) was used to detect between group differences with age as a nuisance co-variable and a

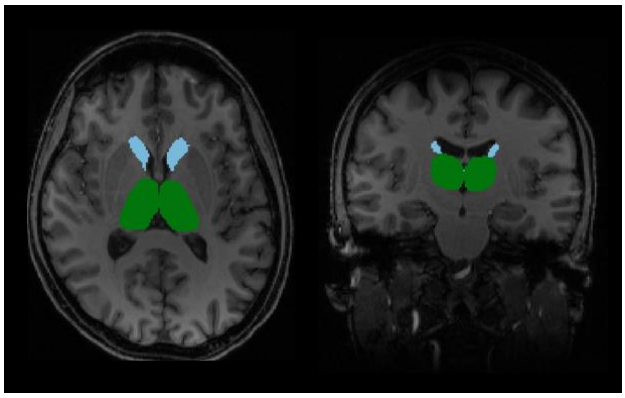
Bonferroni multiple comparisons correction applied. *Post hoc* pairwise comparisons were made between the groups using Tukey's test (which adjusts for multiple comparisons).

7.3.4.2 Thalamic and caudate volumes

The volumes of these subcortical structures were calculated using the automated segmentation tool FIRST (Patenaude *et al*., 2011), part of FSL, for each subject. This method is described and illustrated in Figure 7.1. The thalamus was chosen to study as it is the junction through which many of the brain's white matter tracts pass and therefore susceptible to the effects of white matter disease, as well as giving a measure of deep grey matter atrophy. Previous research has demonstrated that volumetric analysis of structural imaging can detect atrophy of the thalami in MS (Wylezinska *et al.* 2003). In addition to the thalamus, segmentation of the caudate by the FIRST automated tool was judged to be consistently accurate and therefore also included in the study. The caudate is a structure that is important for memory and other cognitive functions, which are often disordered in the neurodegenerative phase of MS.

Prior to segmentation the images were bias-field corrected and lesions filled as described by (Gelineau-Morel *et al.* 2011). They were then normalized for skull size. A one-way ANCOVA was run with age as a nuisance factor and a *post hoc* pairwise comparison made using Tukey's test to statistically compare the mean volume in each subject group.

Figure 7.1: Example of the segmentation of the thalamus (green) and caudate (blue) achieved with the automated tool FSL FIRST. This is a model-based segmentation tool. The shape models used in FIRST are constructed from manually segmented images provided by the Center for Morphometric Analysis, MGH, Boston. FIRST searches through linear combinations of shape modes of variation for the most probable shape given the observed intensities to the T1 image inputted.



7.3.4.3 Voxel Based Morphometry

Structural data was analysed with FSL-VBM, a voxel-based morphometry style analysis (Ashburner and Friston 2000; Good *et al.* 2001) part of FSL (Smith *et al.* 2004). First, structural images were brain-extracted using BET (Smith 2002). Next, tissue-type segmentation was carried out using FAST4 (Zhang *et al.* 2001). The resulting grey-matter partial volume images were then aligned to MNI152 standard space using the affine registration tool FLIRT (Jenkinson and Smith 2001; Jenkinson *et al.* 2002) followed by nonlinear registration using FNIRT (Andersson 2007a, 2007b). The resulting images were averaged to create a study-specific template, to which the native grey matter images were then non-linearly re-registered. The registered partial volume images were then modulated (to correct for local expansion or contraction) by dividing by the Jacobian of the warp field. The modulated segmented images were then smoothed with an isotropic Gaussian kernel with a sigma of 2 mm. Finally, a voxelwise general linear model was applied using permutation-based non-parametric testing with age and lesion masks included as nuisance regressors, correcting for multiple comparisons across space.

7.3.4.4 Diffusion tensor imaging of the normal appearing white matter

Voxelwise statistical analysis of the fractional anisotropy (FA) data was carried out using Tract-Based Spatial Statistics (Smith *et al.* 2006), part of FSL (Smith *et al.* 2004). First, FA images were created by fitting a tensor model to the raw diffusion data and then brain-extracted using BET (Smith 2002). All subjects' FA data were then aligned to a standard space template using the nonlinear registration tool FNIRT (Andersson *et al.* 2007a,b). Next, the mean FA image was created and thinned to form a mean FA skeleton that represents the centres of all tracts common to the group. Each subject's aligned FA data was then projected onto this skeleton and the resulting data compared voxel-wise according to group using permutation-based non-parametric testing, and corrected for multiple comparisons. Lesion maps were created from the FLAIR images and registered to 1mm MNI standard space, using a non-linear transformation, as described in Chapter 6, and entered as a nuisance regressor in the final model so that lesioned voxels would be disregarded in the statistical comparison of groups.

Subgroup ROI analysis: The mean derived TBSS skeleton for the NMOSD versus controls group analysis was used to manually define a region of interest (ROI) within the optic radiations. The mean FA and standard deviation for each subject's optic radiations were extracted for right and left separately excluding lesions. The NMOSD group was divided into a subgroup of patients with bilateral severe visual impairment (visual acuity $\leq$ 0.1) due to previous optic neuritis (n=5) and a subgroup of patients with good functional vision (visual acuity $\geq$6/9; n=6). A one-way ANOVA was used to statistically compare the difference in groups with a *post hoc* Student's t-test and an appropriate multiple comparisons correction.

7.3.4.5 *Myelin water imaging of the normal appearing white matter*

mcDESPOT processing was performed as described by Deoni *et al*. (2008) and Kolind *et al.* (2012). mcDESPOT volume data were linearly co-registered to correct for subtle motion during the acquisition of the data using FLIRT (Jenkinson *et al.* 2002) part of FSL (Smith *et al.* 2004). The images were brain extracted using an automated method (Smith 2002). This MWF data was aligned to standard space using FNIRT and then projected onto a white matter skeleton using the projections that were derived from the TBSS analysis of FA described above, and the voxel-wise group comparisons were made as described above.

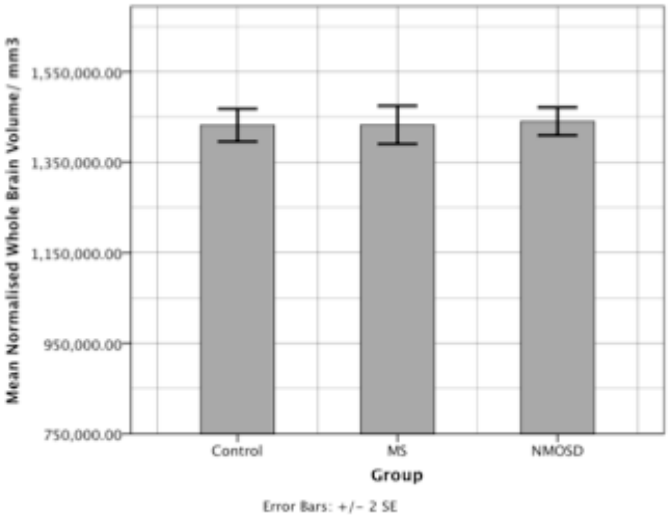
7.4 Results

7.4.1 Whole brain, thalamus and caudate volumes

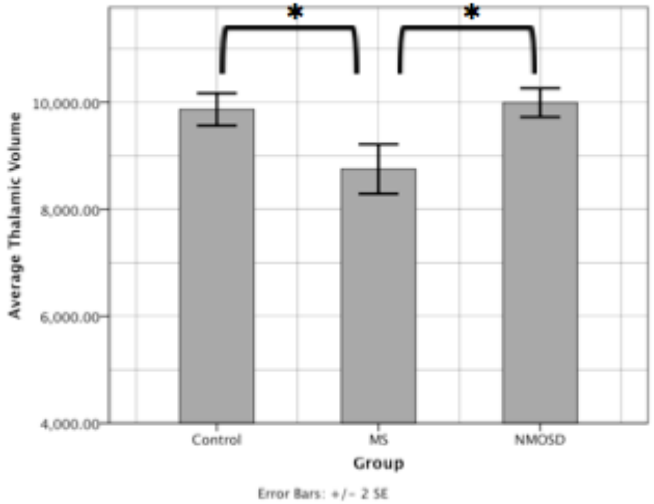
There was no significant difference in normalised brain volume between the three subject groups. Right/ left average thalamic and caudate volumes however were significantly lower in RRMS patients when compared to both NMOSD and controls (Figure 7.2). The results of the ANCOVA analysis and pairwise comparisons are shown in Tables 7.1 - 7.5.

*Figure 7.2: Bar charts showing the differences in volumetric measures between subject groups. Error bars are +/- 2 standard errors of the mean. * = significant difference (p<0.05) when corrected for age and multiple comparisons.*

a. Normalised brain volumes



b. Normalised thalamic volumes



c. Normalised caudate volumes

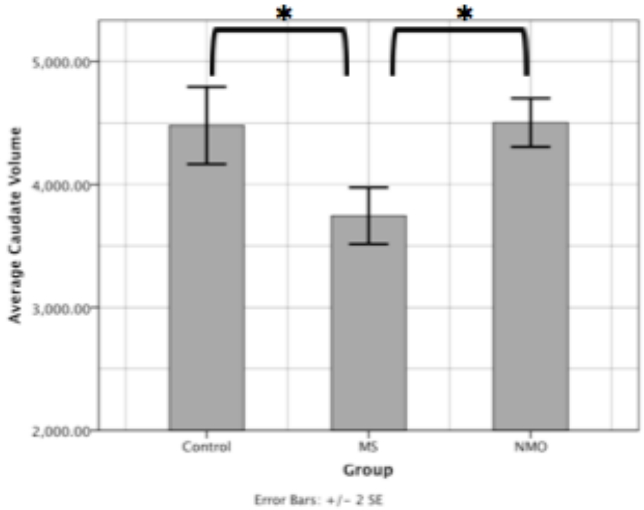


Table 7.1: Brain Volume ANCOVA

	Sum of Squares (Type III)	df	Mean Square	F	Sig.
Corrected Model (Age as covariate)	**1.804E+10**	**3**	**6.012E+9**	**1.144**	**0.341**
Age	1.727E+10	1	1.727E+10	3.286	0.076
Group	952763611	2	476381805	0.091	0.913

Tables 7.2 and 7.3 Thalamic Volume ANCOVA and Pairwise Comparison

	Sum of Squares (Type III)	df	Mean Square	F	Sig.
Corrected Model (Age as covariate)$^{+}$	**15182888**	**3**	**5060962.71**	**10.343**	**<0.001***
Age	413263.9	1	413263.9	0.845	0.363
Group	14960973.5	2	7480486.73	15.288	<0.001

$^{+}R^2 = 0.403$ (adjusted $R^2 = .364$)

Group	Group	Mean Difference	Std. Error	Sig.	95% Confidence Interval for Difference	
Control	MS NMO	1124.048* -126.772	247.980 236.574	<0.001*	507.895 -714.585	1740.201 461.040
MS	Control NMO	-1124.048* -1250.820*	247.980 244.746	<0.001* <0.001*	-1740.201 -1858.938	-507.895 -642.702
NMO	Control MS	126.772 1250.820*	236.574 244.746	< 0.001*	-461.040 642.702	714.585 1858.938

*=Significant mean difference with multiple comparisons correction ($\alpha = 0.05$)

Tables 7.4 and 7.5: Caudate Volume ANCOVA and Pairwise Comparison

	Sum of Squares (Type III)	df	Mean Square	F	Sig.
Corrected Model (Age as covariate)$^{+}$	**3977467.9**	**3**	**1325822.63**	**4.450**	**0.008***
Age	81345.804	1	81345.804	0.273	0.604
Group	3938118.69	2	1969059.34	6.609	0.003

$^{+}R^2 = 0.225$ (Adjusted R squared =0.174)

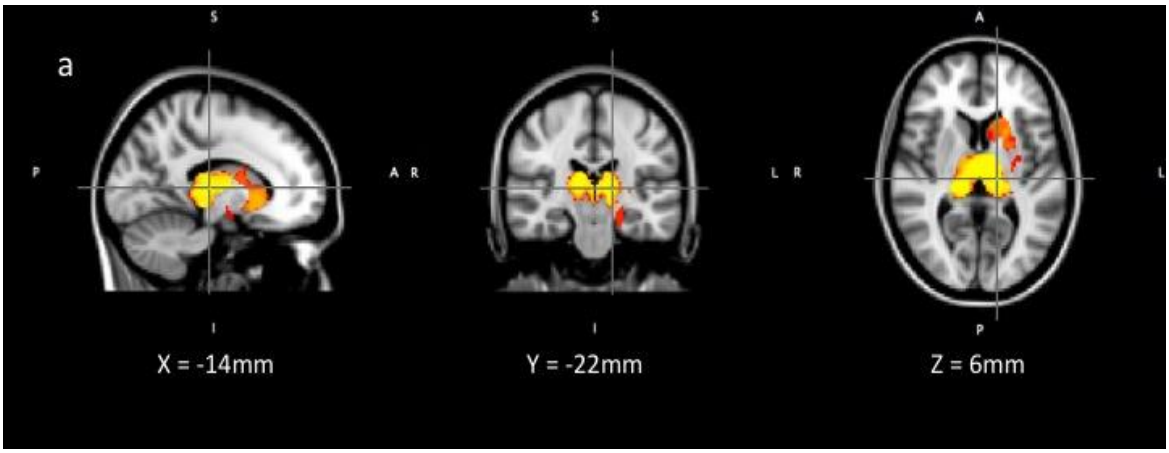
Group	Group	Mean Difference	Std. Error	Sig.	95% Confidence Interval for Difference	
Control	MS NMO	659.947* 106.275	193.497 184.597	0.004*	179.166 -352.392	1140.728 564.942
MS	Control NMO	-659.947* -553.672*	193.497 190.974	0.004* 0.017*	-1140.728 -1028.183	-179.166 -79.161
NMO	Control MS	-106.275 553.672*	184.597 190.974	0.017*	-564.942 79.161	352.392 1028.183

*=Significant mean difference with multiple comparisons correction ($\alpha = 0.05$)

7.4.2 Voxel-Based Morphometry

Voxel-based morphometry comparing RRMS with controls showed prominent grey matter volume loss in the thalami of RRMS patients (Figure 7.3) and also in the region of the left caudate nucleus and putamen consistent with the FIRST results. There was no significantly different area of grey matter volume between the controls and NMOSD patients.

Figure 7.3: Voxel-based morphology showing in a scale of red to yellow (from lower to higher significance) areas where there is significantly less grey matter contrast in the RRMS patients than controls ($p<0.05$ corrected for multiple comparisons).



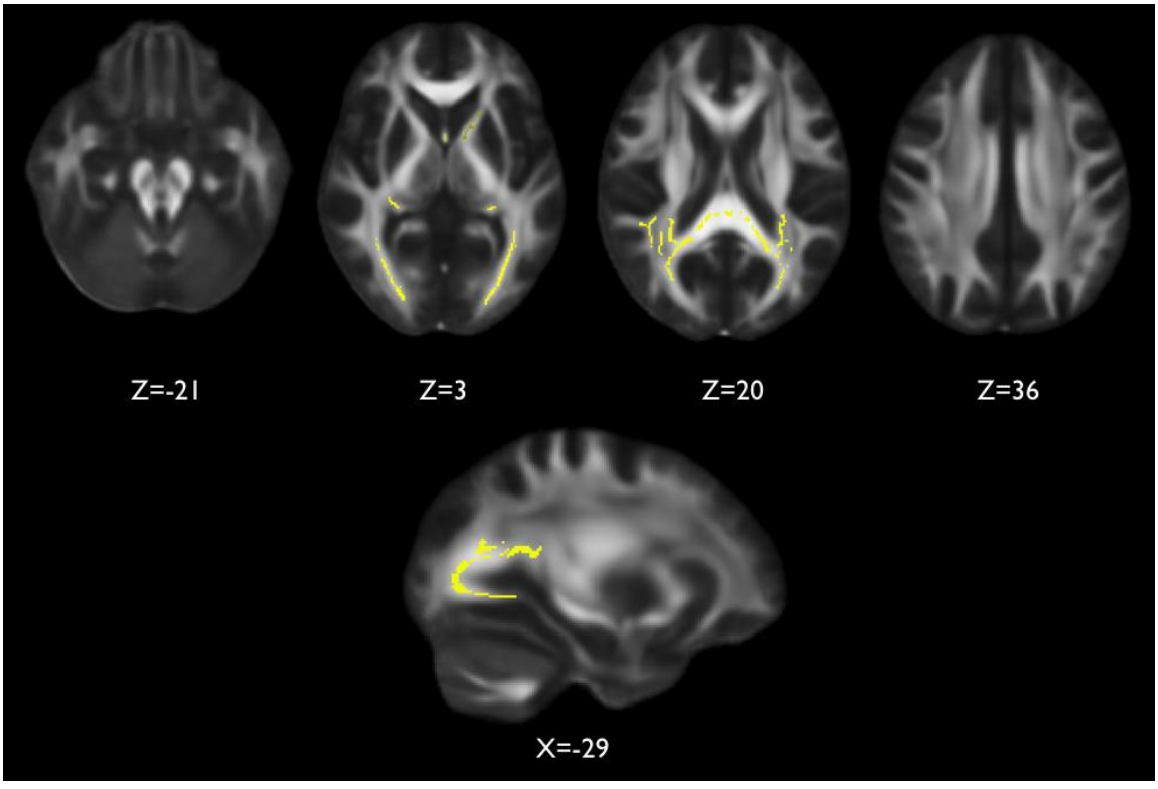
7.4.3 Diffusion tensor imaging of the normal appearing white matter

Voxel-wise comparison of normal appearing white matter fractional anisotropy (FA) between NMOSD patients and controls, and RRMS patients and controls, reveals important differences in the location of abnormalities in each condition. NMO is associated with a significantly reduced FA in the normal appearing white matter (NAWM) of the optic radiations (Figure 7.4a). There are also some significant FA reductions in parts of the splenium of the corpus callosum and the posterior corona radiata. RRMS is associated with widespread changes throughout the normal appearing

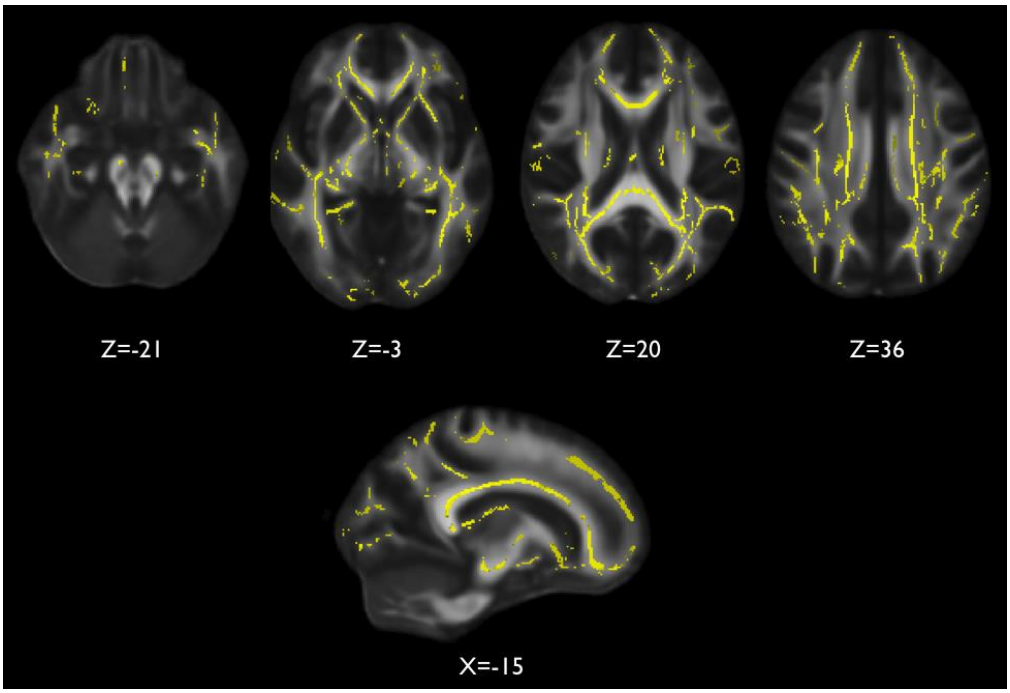
white matter (Figure 7.4b) when compared to controls. Figure 7.4c shows a comparison in FA between the NMOSD and RRMS cohorts, showing significant reductions in the FA of the RRMS cohort when compared to NMOSD. Significant voxels are scattered throughout the supra and infratentorial white matter in regions that include the superior longitudinal fasciculus, the corpus callosum, the corona radiata, the internal and external capsule, the inferior longitudinal fasciculus and the cerebellum. There were no areas of significant reduction in FA values in the NMOSD cohort when compared to RRMS.

Figure 7.4: Diffusion tensor imaging of the normal appearing white matter showing in yellow significant reductions ($p<0.05$) in fractional anisotropy in a. NMOSD patients compared to controls b. RRMS patients compared to controls and c. RRMS patients compared to NMOSD patients. Results are shown on the FMRIB_FA template, which is in 1mm MNI standard space. MNI coordinates are shown.

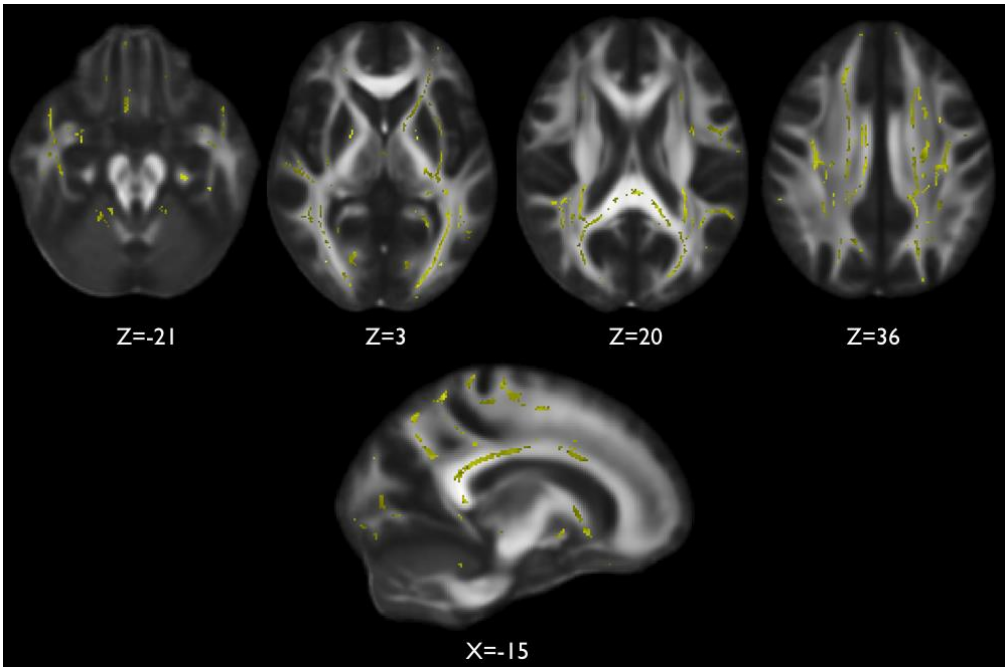
a. *Regions where FA is less in NMOSD patients compared to controls*



b. Regions where FA is less in RRMS patients compared to controls

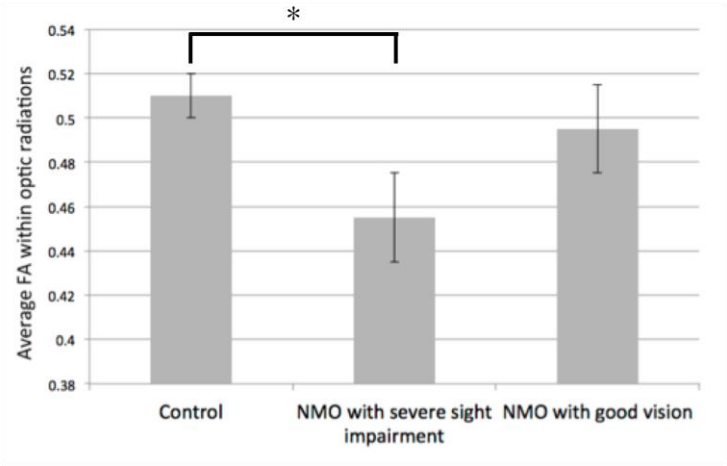


c. Regions where FA is less in RRMS patients compared to NMOSD



Region of interest analysis comparing the mean FA within the optic radiations of a subgroup of NMOSD patients with bilateral severe visual impairment (visual acuity ≤ 0.1) due to previous optic neuritis (n=4), a subgroup of NMOSD patients with good functional vision (visual acuity ≥6/9; n=6) and healthy controls (n=17) shows significantly lower FA in the patients with bilateral blindness only (Figure 7.5). This suggests that the low FA within the optic radiations in the NMOSD group could be due to secondary neurodegeneration in patients with no or little visual sensory input.

*Figure 7.5: Bar graph showing the average FA within the non-lesioned voxels of the optic radiations in controls (n=8), NMOSD patients with severe sight impairment (n=4) and NMOSD patients with good residual vision (n=6). *= significant difference (p<0.05). Error bars are +/- two standard errors.*

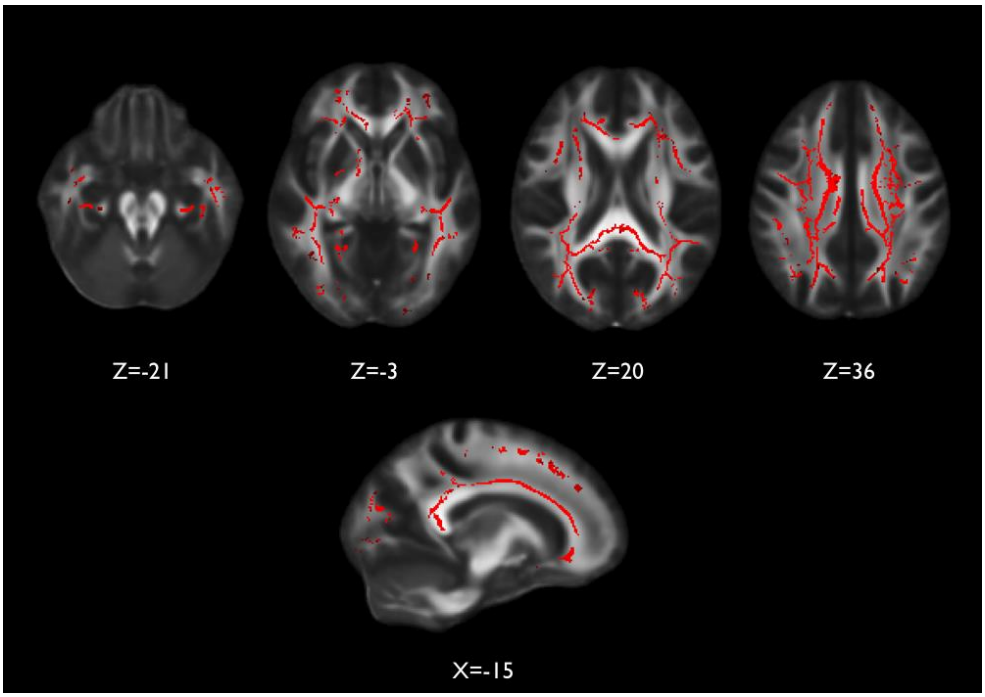


7.4.4 Myelin water imaging of the normal appearing white matter

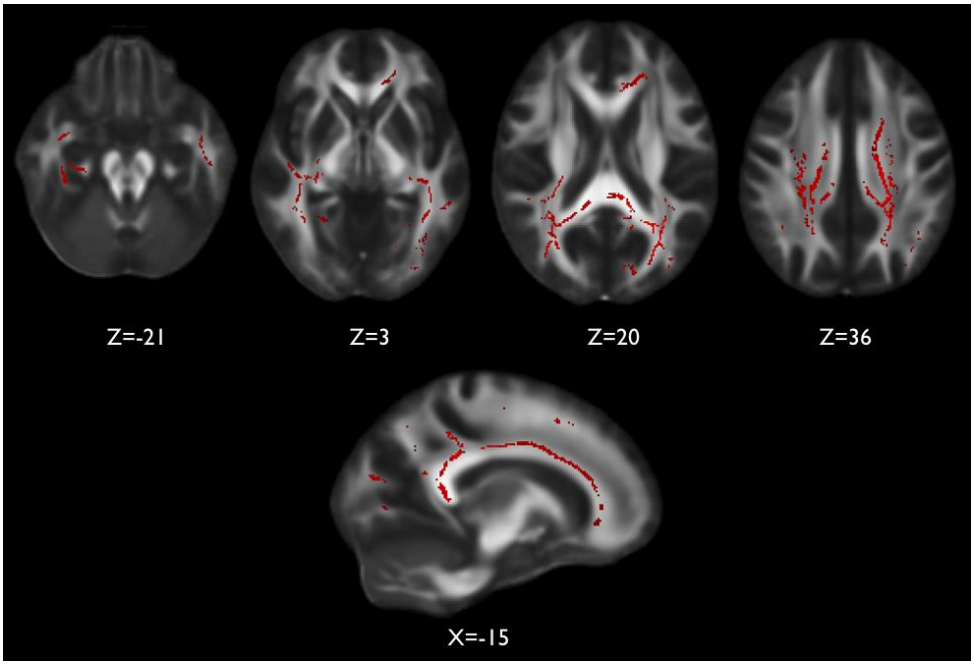
Voxel-wise analysis of NAWM myelin water fraction (MWF) in RRMS and controls is consistent with the DTI findings, with widespread significant reductions in the RRMS group (corrected p<0.05) relative to controls (Figure 7.6a) and to NMOSD (Figure7.6b). There was no significant difference between NMOSD MWF and control MWF.

Figure 7.6: Myelin Water Imaging of the normal appearing white matter showing in red significant reductions ($p<0.05$) in myelin water fraction in a. RRMS patients compared to controls and b. RRMS patients compared to NMOSD patients. Results are shown on the FMRIB_FA template, which is in 1mm MNI standard space. MNI coordinates are shown.

a. Regions where MWF is less in RRMS patients compared to controls



b. Regions where MWF is less in RRMS patients compared to NMOSD patients



7.4.5 Correlation of thalamic volume with fractional anisotropy and myelin water fraction

In this Chapter an automated method for calculating thalamic volume has been used. This tool offers relative simplicity in its application to clinical practice in comparison with calculating measures of NAWM integrity such as FA and MWF. Figure 7.7 shows that there is a significant level of correlation between thalamic volume and NAWM FA and MWF for the multiple sclerosis cohort, and therefore that thalamic volume is a useful representation of more widespread demyelination and neural damage.

Interestingly no correlation exists between these measures for the control (R=-0.4 for FA vs thalamic volume; R = 0.346 for MWF vs thalamic volume) and NMOSD cohorts (R=0.37 for FA vs thalamic volume; R=0.211 for MWF vs thalamic volume).

7.4.6 Individualised Measures

It has been shown in the results above that NMOSD and RRMS can be discriminated at a group level using thalamic volume, caudate volume or patterns in the normal appearing white matter FA and MWF reductions when compared with controls. The spread of the data is shown in Figure 7.8 to illustrate that a clear separation in groups cannot be made due to the overlap of the data.

In Chapter 10 a ‘discriminant analysis’ investigates whether a linear combination of the cross-sectional measures presented here, the spinal cord imaging outcomes and a serum measure of neurodegeneration (serum N-acetylaspartate) can accurately discriminate NMOSD and MS.

Figure 7.7: Partial correlation between thalamic volume and measures of normal appearing white matter integrity controlling for age for the multiple sclerosis cohort

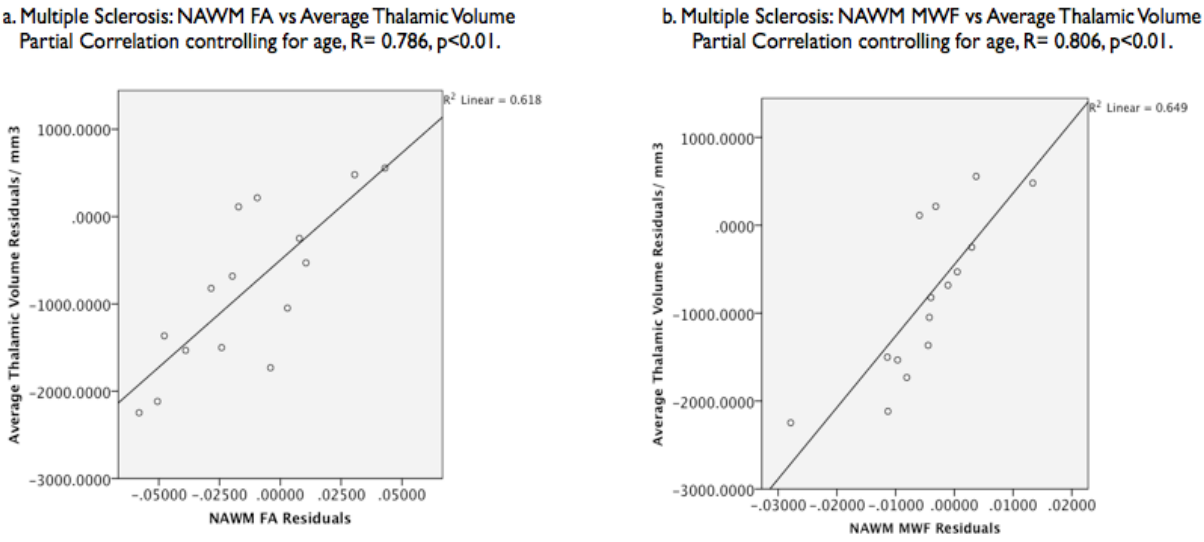
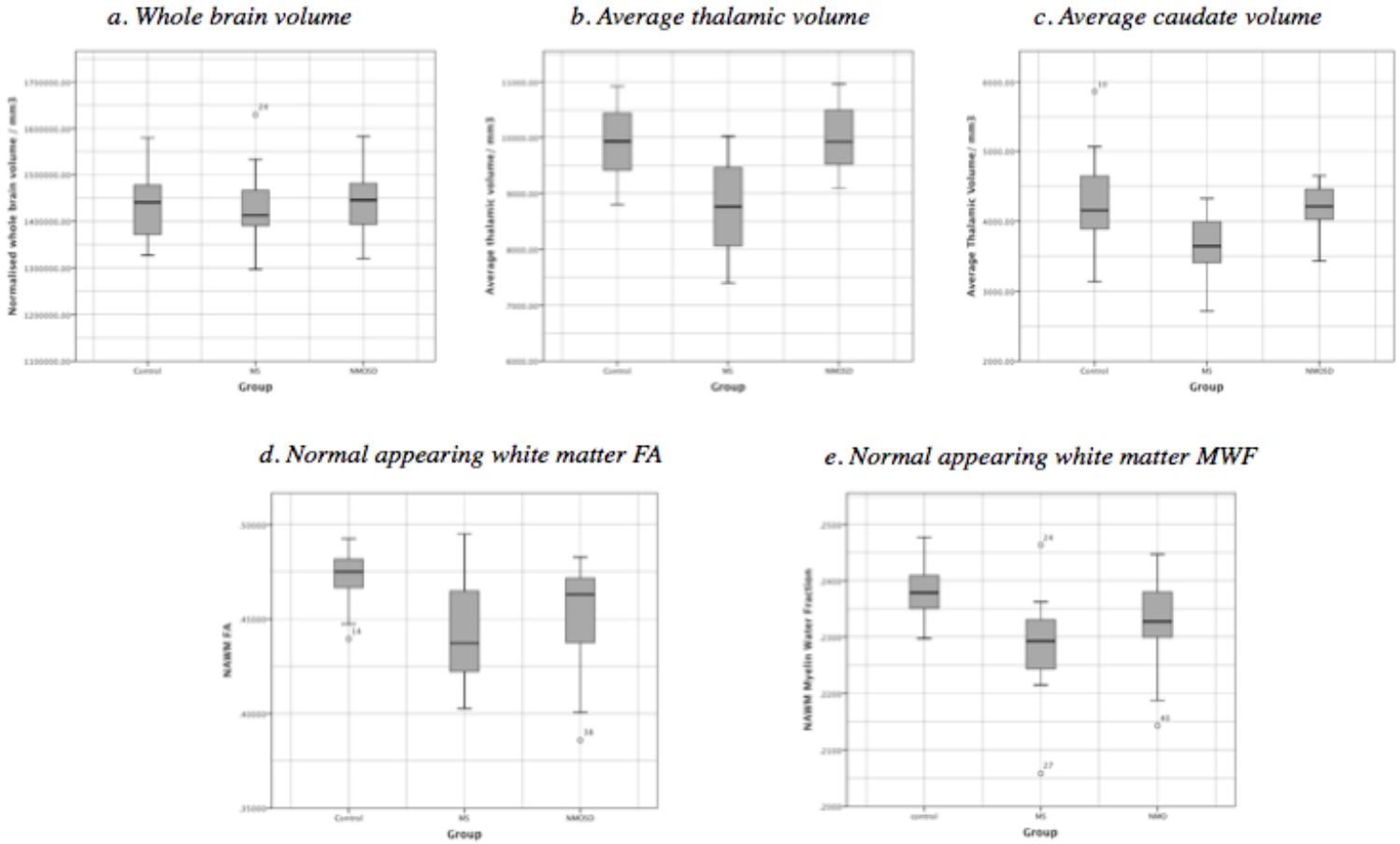


Figure 7.8: Box plots indicating the median, 25th and 75th centiles and the range of data for:



7.6 Discussion

The quantitative MRI results derived are reassuringly consistent; measures of diffuse neurodegeneration (normal appearing white matter FA and atrophy measures of subcortical structures) reveal significant abnormalities in MS compared to both controls and NMOSD patients, and no diffuse change in NMO (outside the optic pathways at the group level). In fact there is a high level of correlation between these indices as shown in Figure 7.7. In chapter 10 a 'discriminant analysis' is applied to all the cross-sectional outcome measures presented in this thesis to explore whether a linear combination can separate NMOSD and MS.

This is the first time that myelin imaging has been applied to NMOSD and it has been shown to provide useful complimentary information to discriminate between NMOSD and RRMS.

Comparing NMOSD and RRMS directly there are significant voxelwise reductions in FA in the RRMS group. This decrease in FA is seen scattered throughout the white matter, both supra and infratentorial. Similarly there is a significant reduction in MWF in the RRMS group when compared to NMOSD, but not *visa versa*.

The results presented in this chapter are in-keeping with previous studies, which utilized tractographic analysis of diffusion data and reported FA abnormalities in the optic radiations of patients with NMO (Yu *et al.* 2008; Pichiecchio *et al.* 2012). These patients were clinically defined and not all antibody positive (in the Chinese study the antibody status was unknown). Therefore the work presented here greatly strengthens this finding, and gives further insight into the cause of the low FA which appears to be driven by subjects with bilateral severe visual impairment and a lack of visual sensory input. Changes in the optic radiations have also been described in MS patients following optic neuritis (Ciccarelli *et al.* 2005).

In contrast other literature reports incongruent results, with more widespread abnormalities using diffusion imaging (Liu, Duan *et al.* 2012; Rueda Lopes *et al.* 2012). This in part could be due to the difficulty in controlling for brain lesions (which have been carefully excluded before statistical analysis in this chapter), or perhaps due to the inclusion of both antibody positive and negative patients increasing the risk that opticospinal forms of MS could be misclassified as NMOSD.

The positive correlation shown between the volume of subcortical structures and FA in Figure 7.7 indicate that automated measurement of the volume of these structures (normalized for skull size) to detect atrophy could be a relatively straightforward way of identifying wider neurodegenerative abnormalities in the brain tissue.

The key aim of this chapter was to detect differences in quantitative imaging between NMOSD and RRMS. Future work may include an investigation into imaging correlates with disability in the NMOSD cohort.

7.7 Conclusions

The ability of quantitative imaging to provide *in vivo* information that mirrors *post mortem* and clinical observations has been demonstrated. NMOSD is not associated with the widespread neurodegenerative abnormalities that are seen in RRMS. By identifying important group differences between NMOSD and RRMS, this work has highlighted candidate modalities and semi-automated analysis methods for future development.

8.0 Differentiating Between NMOSD And RRMS With Quantitative Imaging Of The Spinal Cord

In this chapter the accuracy and practicality of two quantitative spinal cord MRI techniques to differentiate between NMOSD and RRMS are explored.

8.1 Introduction

Pathology within the spinal cord is often the most important contributor to disability in both NMOSD and RRMS (Losseff *et al.* 1996; Bjartmar *et al.* 2000; Kitley *et al.* 2012). NMOSD in particular is characterized by longitudinally extensive lesions, which are one of the more specific conventional MRI indicators of the condition (Wingerchuk *et al.* 2006). Therefore this is clearly an important site to study when looking for biomarkers of NMOSD, and in particular differentiating it from MS, which is the more prevalent cause of myelitis.

However the spinal cord has been relatively neglected in MRI research and the reasons are clear; its diameter is a maximum of 15mm and therefore it is difficult to apply sequences that require relatively large voxels to gather signal. It moves unpredictably due to a combination of arterial pulsation, respiration and swallowing. Furthermore the spinal cord is not only surrounded by CSF but also has a central canal containing the dynamic fluid risking the degradation of images with flow artifacts. However progress continues to be made with new acquisition and analysis methods to overcome these problems.

As for chapter 7, factors taken into account in the selection of suitable modalities with which to study the spinal cord in the subject cohort included whether they had the potential to be translated into clinical practice – i.e. could be examined by a reporting radiographer with automated tools and did not require complex analysis methods, in particular co-registration of spinal images which is fraught with difficulty (and thus the

potential to introduce error) due to the aforementioned movement of the spinal cord between acquisition volumes. Two methods have here been tested: semi-automated calculation of spinal cord volume and magnetization transfer contrast normalized to CSF signal (or MTCSF).

Spinal cord atrophy is a well-described feature of MS and a number of clinical studies have shown that that atrophy measures correlate with disability (Losseff *et al.* 1996; Bjartmar *et al.* 2000). The pathological substrate of MS cord atrophy is thought to be tissue loss throughout the whole spinal tissue rather than lesion-focused volume loss (Evangelou *et al.* 2005). Spinal cord atrophy has also been reported in NMOSD but only at sites of previous spinal cord lesions (Krampla *et al.* 2009). Horsfield *et al.* (2010) pioneered an automated method for measuring spinal cord volume, which is based on an active-surface model of the cord surface. This method has been used successfully to show longitudinal progression in spinal cord atrophy (Horsfield *et al.* 2010) and to differentiate different subtypes of MS (Rocca *et al.* 2011).

The basis of magnetization transfer imaging, which was discovered by Wolff and Balabin in 1989, and the MTCSF method, described by Smith *et al*. in 2005 is outlined in detail in Chapter 3. This method is capable of detecting abnormalities in the macromolecular pool, which are generally considered a surrogate for the integrity of myelin and neurons. When there is efficient magnetization exchange between macromolecules and protons, MT signal is reduced. Hence there is lower MT signal (or contrast) in the white matter than the grey matter. When there is disruption to CNS microstructure (e.g. demyelination or axonal loss) the MT signal increases. The great advantage over other modalities that could also provide this micropathological information (such as DTI and myelin water imaging) is that co-registration of averages or to a structural image is not required. In fact MT contrast abnormalities (e.g. lack of

distinction between white and grey matter contrast as has been found in white matter diseases such as adrenoleukodystrophy (Smith *et al.* 2005)) can be viewed immediately from the images reconstructed by a clinical grade MR scanner. To allow comparison between subjects normalisation with the CSF signal intensity from the non-MT weighted acquisition volume is required (shown in the methods section below).

8.2 Objectives

1. To compare the spinal cord volumes in the NMO, MS and healthy control groups.

2. To compare the magnetization transfer contrast intensities of lesions in the NMO and MS groups.

3. To compare MTCSF intensity values in the normal appearing white matter and normal appearing grey matter in the NMO, MS and control groups.

8. 3 Methods

8.2.1 Subject Characteristics

The subjects including in this investigation are described in Chapter 5.3 as the core study cohort. There were three study groups: 18 aquaporin-4 antibody positive NMOSD; 15 RRMS and 17 healthy controls. 14 of the NMO patients and 10 of the RRMS patients had evidence of spinal cord lesions within the cervical spinal cord (the area of interest) at the time of the baseline scan, as visualized on the T2 weighted sagittal and axial images. These lesions are detailed in Appendix 1. Lesioned tissue was excluded for examination of the normal appearing spinal cord tissue.

8.3.2 Acquisition protocol

Spinal Cord Atrophy: Both a 3-dimensional T1 and an axial Siemen's MEDIC (a multi echo gradient echo sequence with T2 contrast) sequences were piloted with the spinal cord segmentation software. Segmentation was found to be more accurate with the MEDIC. This sequence was acquired with 30 consecutive axial slices with a distance factor of 10% of 3mm slice thickness. In plane voxel size 0.7x0.7mm. TE 17ms, TR 470ms. 2 averages. The most superior slice was positioned at the superior border of C2 (i.e. the odontoid peg).

MTCSF: 2-dimensional gradient-echo sequence with twenty consecutive axial slices with a distance factor of 10% positioned at the superior border of the C2 vertebra. FOV 180mm x180mm, slice thickness 4mm, voxel-size 0.8x0.7 mm, TR 600ms, TE 8.6ms, two averages. Acquired with magnetization transfer weighting both on and off. Total acquisition time 8 minutes.

Other clinical sequences: In order to localize lesions and position the axial slices a sagittal T2 turbo spin echo sequences were acquired. Sagittal: 15 slices of 3mm, voxel size 0.6x0.6, TE 67ms, TR 4590ms.

8.3.3 Analysis

Spinal Cord Volume: The superior cervical spinal cord was used for atrophy measurements as it is relatively straight and has less movement associated with it. During acquisition the first (or most superior) axial slice was positioned at the superior border of C2 (i.e. the odontoid process of the epistropheus or "axis") using a sagittal T2 image (Figure 8.1). The spinal cord was segmented using the Horsfield method that segments the spinal cord using a contrast based method and an active surface model, and is now incorporated into the software Jim 6.0 (Xinapse Systems). The volume of the spinal cord

was measured over 11 axial slices of 3.3mm starting with the most superior slice. This approximately covered the C1 – C3 spinal segments.

The 'Cord Finder' tool requires the user to mark the centre of each slice and then it automatically segments the cord with the option to the user to manually edit this segmentation. The options used were 32 shape coefficients to describe the complexity of the cord outline and an order of 12 polynomial variations of the shape coefficient along the cord. An example of the segmentation is shown in Figure 8.2.

MTCSF: The MTCSF slices were acquired from the top of the superior border of C2, i.e. the superior border of the odontoid peg, positioned using a T2 sagittal image. The most superior six slices of 4mm were examined which covered approximately the C1-C2 spinal cord segment. One of the advantages of MTCSF is that the relative intensity values in the MT weighted image can be viewed from the image reconstructed by the MR scanner without further analysis. However to allow inter-subject comparison the contrast values have to be normalized and this is achieved by dividing the intensity values in each slice by the mean intensity value of the CSF in a region of interest (ROI) taken from the non-MT weighted volume of the same slice.

After normalization of the MT weighted image ROIs were taken in lesions, grey matter and white matter as shown in Figure 8.3. On initial inspection of the MT weighted images it was noted that there was apparent loss of architecture, seen as a lack of contrast between the white and grey matter, in the MS group. These results are shown and discussed in section 8.4. To quantify this lack of contrast, and to take into account the differences in spinal architecture at each spinal level a ratio of white:grey matter normalized contrast was calculated for each patient, in each separate slice from C1-C6, averaged across each group and compared.

Statistics: Spinal cord volume and white:grey matter contrast ratios were compared across groups using an ANCOVA test (controlling for age and multiple comparisons) with a *post hoc* Tukey's test (which is adjusted for multiple comparisons). Lesion values were compared with a Mann–Whitney U test.

Figure 8.1 The spinal cord volume and MTCSF was taken from slices starting at the superior border of the odontoid process of the C2 vertebrae and moving inferiorly.



Figure 8.2: The automated outline of the spinal cord as derived by the 'cord finder' tool of Jim 6.0 (Xinapse Systems). This performed over 11 consecutive slices of 3.3mm and the volume derived by the tool. A healthy control spinal cord is shown in this image.

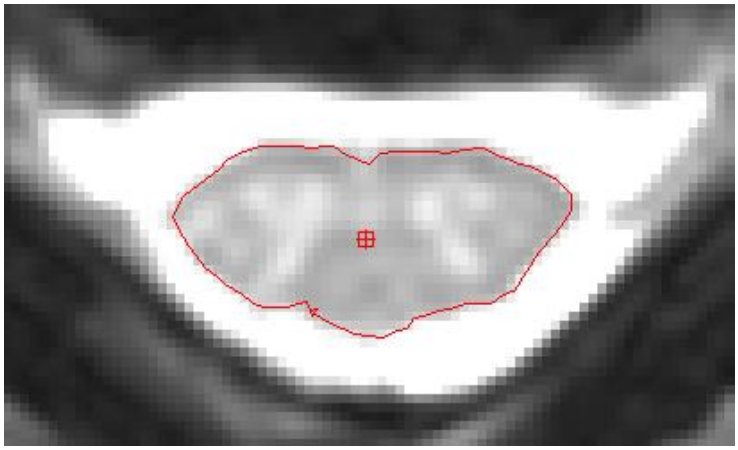
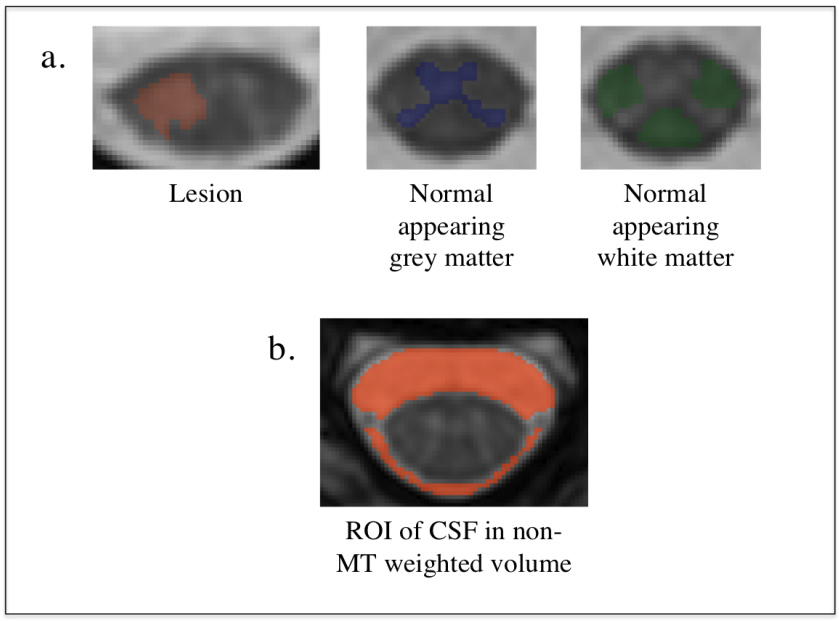


Figure 8.3: The ROIs sampled in the analysis of the MTCSF data b. The normalization of MTCSF involves dividing the image acquired with MT contrast by the average intensity value from an ROI of the CSF in the corresponding slice of the non-MT weighted volume.

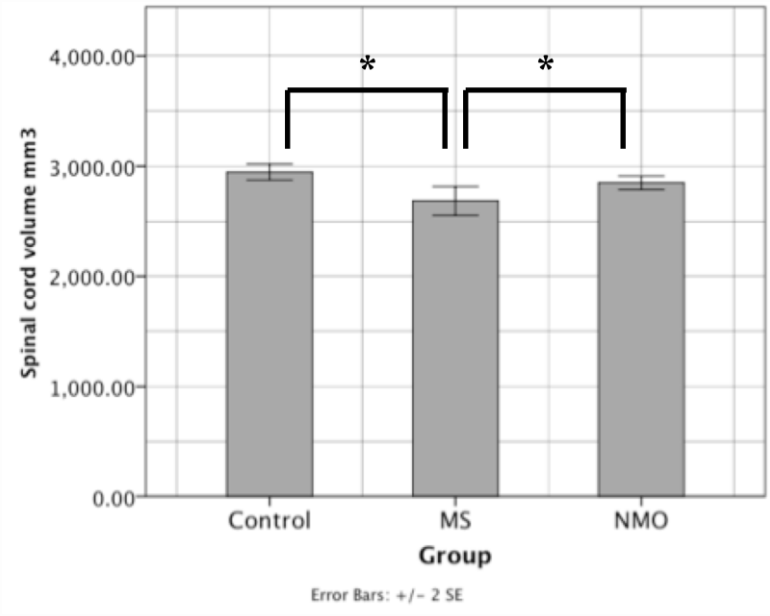


8.4 Results

8.4.1. Spinal Cord Atrophy

The bar graph in Figure 8.4 shows the mean spinal cord volumes for the C1 and C2 segments of the NMOSD, RRMS and control groups. An ANCOVA was run to compare the three groups, controlling for age and corrected for multiple comparisons with Bonferroni's method. This showed a significant between groups difference (Table 8.1). Table 8.2 details a *post hoc* pairwise comparison that showed significantly lower mean spinal cord volume in the RRMS patients when compared to both controls and NMOSD, but no difference between NMOSD and controls (significance threshold 0.05).

*Figure 8.4: Bar graph showing the mean spinal cord volumes for the c1-c3 segments in the control, RRMS and NMOSD groups. Error bars are +/- 2 standard errors of the mean. * = significant difference*



Tables 8.1 and 8.2: ANCOVA analysis comparing spinal cord volume in controls, RRMS and NMOSD patients (controlling for age) with a Bonferroni type multiple comparisons correction, and post hoc pairwise comparisons using Tukey's test (adjusted for multiple comparisons).

	Sum of Squares (Type III)	df	Mean Square	F	Sig.
Corrected Model (Age as covariate)	**552331.71**[+]	**3**	**184110.57**	**5.477**	**0.003***
Age	1.360	1	1.369	0.00	0.995
Group	551345.642	2	275672.821	8.200	0.001

[+]*R squared = 0.263 (adjusted R squared = 0.215)*

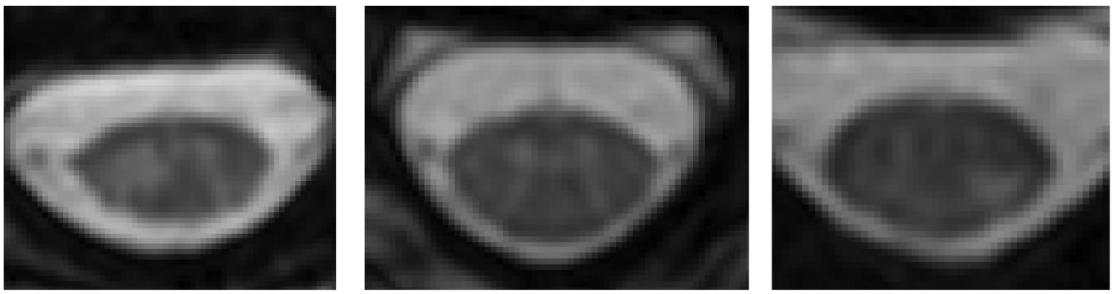
Group	Group	Mean Difference	Std. Error	Sig.	95% Confidence Interval for Difference	
Control	MS	261.458*	64.999	0.001*	99.955	422.961
	NMO	97.017	62.010	0.374	-57.057	251.902
MS	Control	-261.458*	64.999	0.001*	-422.961	-99.955
	NMO	-164.440*	64.152	0.041*	-323.837	-5.043
NMO	Control	-97.017	62.010	0.374	-251.092	57.057
	MS	164.440*	64.152	0.041*	5.043	323.837

* Significant mean difference, corrected for multiple comparisons

8.4.2 Comparison of lesion magnetization transfer contrast in NMOSD and RRMS

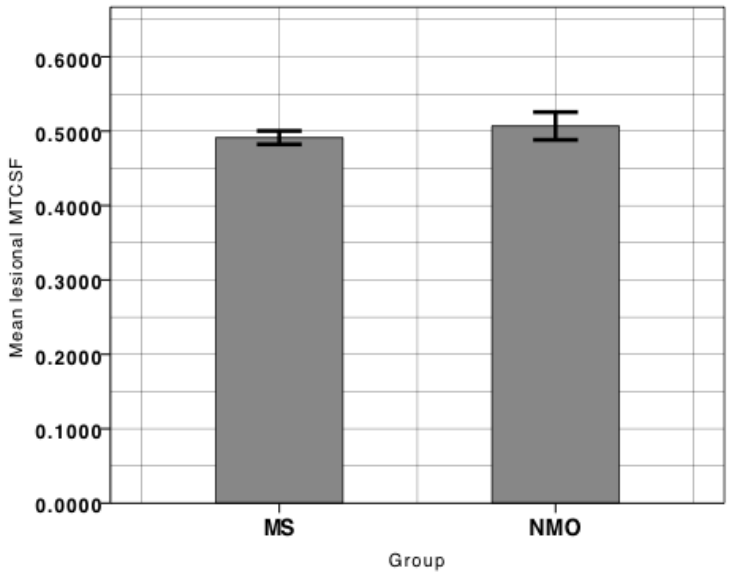
MT contrast normalized with the non-MT weighted CSF contrast (i.e. MTCSF) was compared across 10 clearly demarcated spinal cord lesions in the NMOSD group and 10 RRMS spinal lesions. Examples of these lesions are shown in Figure 8.5a. There was higher MTCSF in the NMOSD group however this was not significant using a Mann–Whitney U test (Figure 8.5b).

Figure 8.5: a. Examples of NMO and MS lesions seen on MT contrast



NMOSD lesion Control RRMS lesion

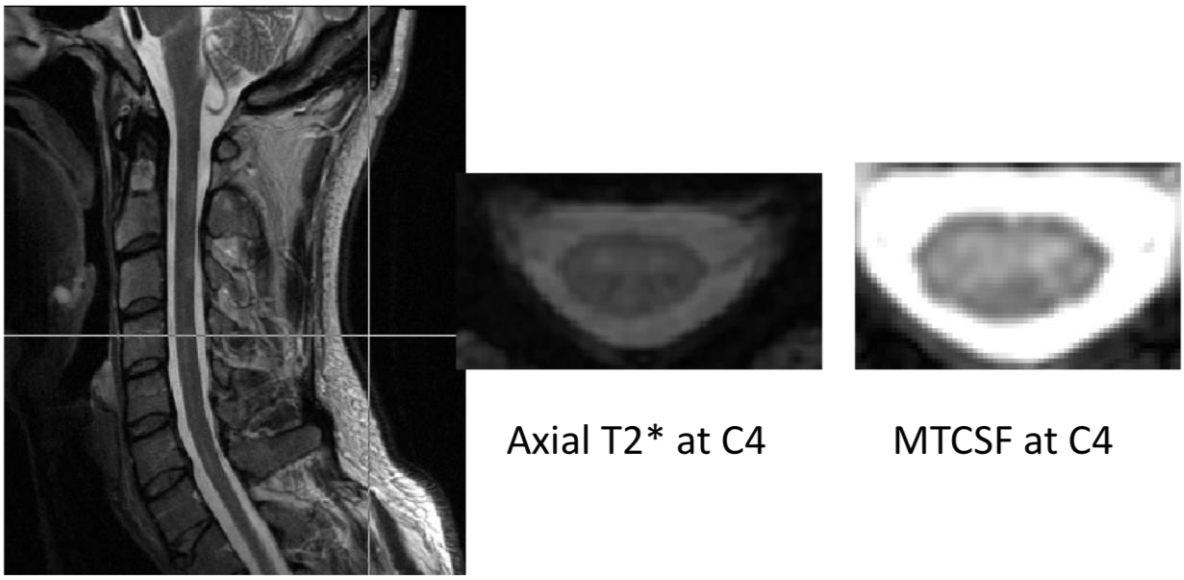
b. Bar graph showing mean lesion MTCSF in NMOSD versus RRMS. Error bars are +/- 2 standard errors.



8.4.3 Comparison of NAWM and NAGM magnetization transfer contrast in NMOSD, RRMS and healthy controls

Examples of white:grey matter contrast in RRMS patients is shown in Figure 8.6. In some RRMS patients there appears to be a clear loss of white:grey matter contrast and architecture within spinal cord tissue which does not appear lesioned on the T2 image. This is consistent with myelin and/or axonal loss within the normal appearing tissue in the RRMS patients. Figure 8.7a shows the average white:grey matter ratios in each group for each slice (starting at slice 1 positioned at the superior border of the odontoid peg of C2 and moving inferiorly). Figure 8.7b shows a comparison of the study groups averaged across slices and subjects. ANCOVA and pairwise comparison results are shown in table 8.3 and 8.4. There is a significantly lower white:grey matter ratio in the RRMS group than the control and NMOSD groups ($p<0.05$).

Figure 8.6: Examples of where MTCSF can reveal abnormalities not seen on the T2 in two RRMS patients (a and b), with an apparent loss of white:grey matter contrast.
a.



b.

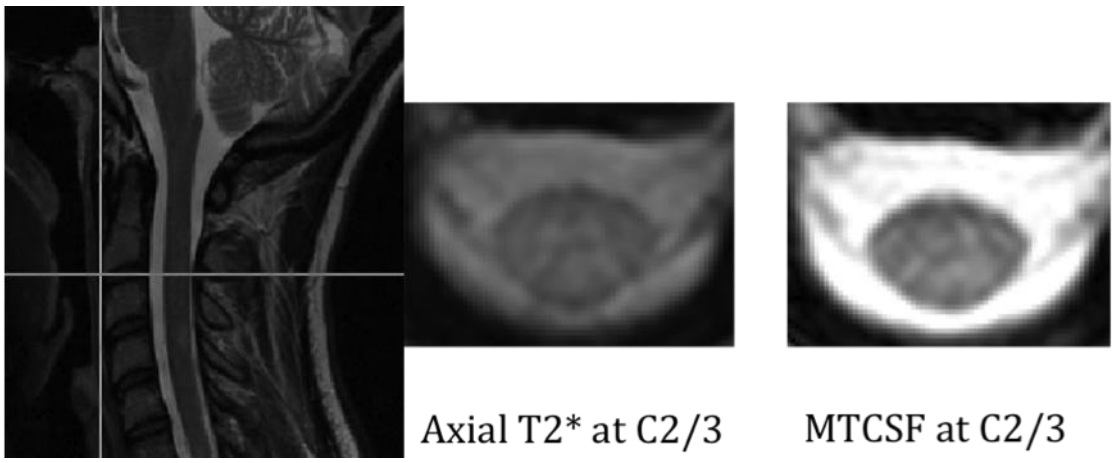
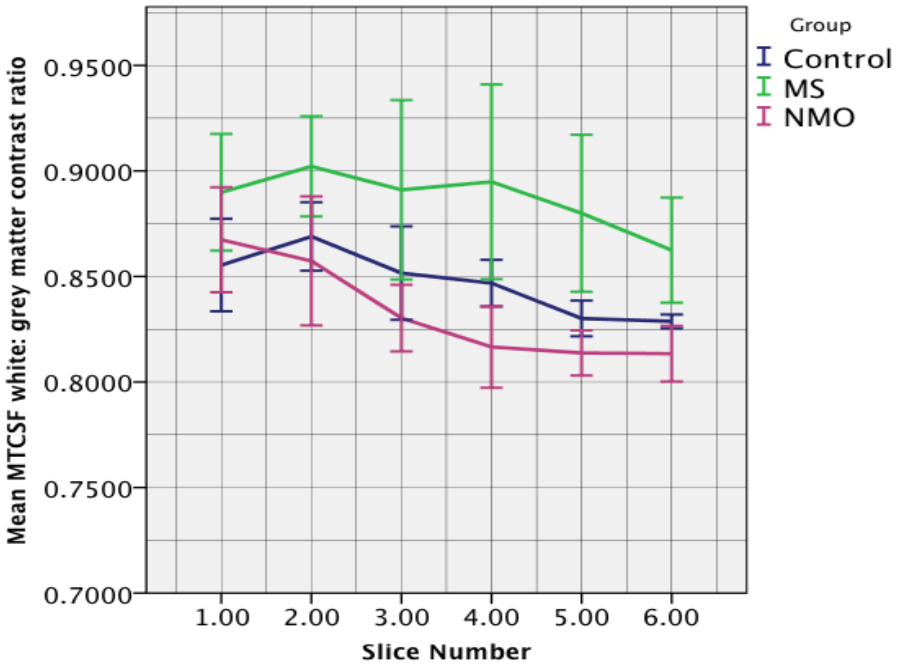
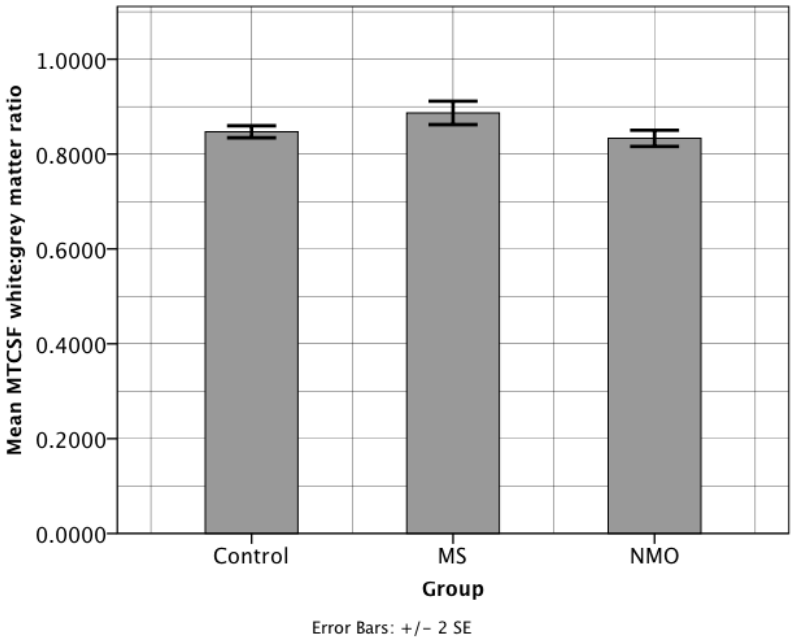


Figure 8.7: a. Average MTCSF white:grey matter contrast ratio in each group across slices from 1 moving inferiorly. Lesioned slices are excluded. Slice 1 is positioned at the superior border of the odontoid process of C2. 95% confidence intervals are shown. b. Average white:grey matter contrast ratio in each group, with lesioned slices excluded. Error bars are +/- 2 standard errors of the mean.

a.



b.



Tables 8.3 and 8.4: ANOVA analysis and post hoc pairwise comparisons, with Bonferonni correction, comparing the mean MTCSF white:grey matter ratio across the C1-C2 segments of the spinal cord excluding lesioned tissue.

	Sum of Squares (Type III)	df	Mean Square	F	Sig.
Between Group Effects	0.33	2	0.016	8.477	0.001*

R squared = 0.212 (adjusted R squared = 0.187)

Group	Group	Mean Difference	Std. Error	Sig.	95% Confidence Interval for Difference	
Control	MS	-0.39794*	0.0146690	0.026*	-0.075874	-.003715
	NMO	0.013800	0.013	0.891	-0.018471	0.046071
MS	Control	0.039794*	0.0146690	0.026*	0.003715	0.075874
	NMO	0.053594*	0.0131204	<0.001*	0.021324	0.085865
NMO	Control	-0.013800	0.0131204	0.891	-0.046071	0.018471
	MS	-0.053594*	0.0131204	<0.001*	-0.085865	-0.021324

* significant mean differences, corrected for multiple comparisons.

8.5 Discussion

The quantitative spinal cord imaging results corroborate with those of the brain presented in Chapter 7. There appears to be relative atrophy within the cervical spinal

cord in the RRMS group, and abnormalities within the normal appearing spinal cord tissue detected with magnetization transfer imaging. Again individuals are not clearly separated according to diagnosis. The measures assess different pathological phenomena and therefore the power of a combination of these indices is explored in Chapter 10.

The normal appearing tissue of the spinal cord in NMOSD has not been extensively studied *post mortem*, due to a relative shortage of available specimens. Here it is shown *in vivo* that seropositive NMOSD is not associated with the same level of the neurodegeneration as the RRMS cohort despite more extensive lesions.

This work has shown that quantitative spinal cord imaging is feasible in a patient cohort, and that automated analysis techniques (in this case the spinal cord volume calculator provide by Mark Horsfield and colleagues) can detect the neurodegenerative changes in the RRMS group that have been described in *post mortem* studies. This tool is straight-forward to use and if a range of 'normal for age' values or perhaps a normal control atlas could be produced, individuals could be compared against these.

It has also been shown here that MT contrast images, immediately viewable from the scanner, can reveal abnormalities of the normal appearing tissue when compared to a T2 image of the same level. A loss of the differentiation of the contrast between white and grey matter in the spinal cord is seen independently of spinal cord atrophy.

8.6 Conclusion

RRMS and NMOSD patients can be discriminated at the group level by quantitative spinal cord MRI measures of neurodegeneration.

9.0 Comparison of NMOSD and RRMS with Longitudinal MRI Measures of Neurodegeneration

This chapter examines the longitudinal changes in quantitative MRI measures, namely percentage change in whole brain volume, change in thalamic volume, change in fractional anisotropy and myelin water fraction, over a one year time period.

9.1 Introduction:

It has been shown in the chapters preceding this experiment that cross-sectional measures of lesion location, atrophy and the integrity of the normal appearing white matter can distinguish neuromyelitis optica spectrum disorder (NMOSD) and relapsing multiple sclerosis (RRMS) at the group level. Multiple quantitative MRI modalities have evidenced that tissue abnormalities in NMOSD are contained within the lesions visible on T2 scans in contrast to established RRMS, which is associated with widespread neurodegenerative type changes both within and between the lesions. As well as providing a potential tool for distinguishing the two conditions, the lack of widespread neurodegeneration in NMOSD despite the presence of severe demyelinating lesions raises questions about the pathophysiology of MS. It suggests that the neurodegeneration associated with MS might not be secondary to inflammatory and demyelinating lesions, and raises the question as to whether it could be a primary or separate process. Thus the study of NMO may aid the understanding of MS.

The mechanisms behind the degenerative component of MS have been in debate for a long time – pre-existing evidence suggests that neurodegeneration is an early phenomenon in MS includes demonstrations of atrophy and changes in the normal appearing white matter in patients who present with the very first inflammatory

symptoms of MS (known as clinically isolated syndrome) (Dalton *et al.* 2004; Bester *et al.* 2008; Bergsland *et al.* 2012). In contrast the group of Prof Hans Lassmann published a pathological study in 2009 showing high levels of inflammation present in the neurodegenerative phenotypes of MS (i.e. primary and secondary progressive MS) and a highly significant association of inflammation with axonal injury (Frischer *et al.* 2009).

To further affirm that NMOSD is not associated with progressive non-lesional neurodegeneration, a longitudinal component of the study was completed where the subjects were invited for a follow-up brain MRI at one year. The rate of whole brain atrophy across one year was selected as a measure of neurodegeneration using the semi-automated SIENA tool, which is part of the FMRIB software library of tools. This has previously been shown to be a sensitive and reproducible measure of neurodegeneration in MS clinical trials (Bakshi *et al.* 2008) with an expected annual atrophy rate in RRMS of -0.61 to -1.33% change in brain parenchyma volume (Bermel and Bakshi 2006).

Average thalamic volume was found to be a good discriminator of NMOSD and RRMS at the group level in Chapter 7, and therefore has been included in the longitudinal analysis. Voxelwise changes in DTI and MWI normal appearing white matter have also been investigated.

9.2 Objectives

- To investigate whether NMO is associated with neurodegenerative changes as measured by longitudinal volumetric imaging (whole brain volume and thalamic volume), and diffusion and myelin water fraction measures of the normal appearing white matter over one year.
- To investigate whether there are differences within the subject groups in the changes of these measures between the baseline and one year MRI brain scans.

9. Methods

9.3.1 Subject Details

16 NMOSD, 13 RRMS and 16 control subjects returned for a follow-up MRI scan at one year. The disability measures taken at baseline (as outline in chapter 7) were repeated and are given in full in Appendix 1. Table 9.1 summarizes the average age, time to follow-up and changes in EDSS and timed walk.

As expected in this cohort of patients with relapsing conditions, some patients improved over the course of the year in both the RRMS and the NMOSD groups, and there were no significant differences between the change in clinical scores between groups over the one year time period.

Table 9.1: Demographic features of the patients attending follow-up

Group	Number attending follow-up	Median age of those attending follow-up (range)	Median number of days to follow-up (range)	Median Change in EDSS (range)
NMOSD	16	20-76 (46)	350 - 456 (386)	0(-1⇒ +0.5)
RRMS	13	29 – 62 (40)	346 – 420 (378)	0 (-0.5 ⇒+1)
Control	16	21-77 (47)	340 – 430 (372)	-

9.3.2 MRI Acquisition

MRI brain scans at one year were acquired with the MRI brain protocol that was unchanged from that presented in Chapter 7 and comprised of a 3-dimensional structural T1 (MPRAG), T2, FLAIR and proton density scans, myelin water imaging using the mcDESPOT protocol and diffusion tensor imaging.

There were no changes made to the acquisition hardware i.e. the MR scanner (Siemens 3T Verio) and the 32-channel head coil.

9.3.3 Data Analysis

MRI analysis was carried out with FSL version 4.1.9 (www.fmrib.ox.ac.uk/fsl).

SIENA: Two-timepoint percentage change in brain parenchymal volume was estimated with SIENA (Smith *et al*. 2001, Smith *et al.* 2002), part of FSL (Smith *et al.* 2004). The 3-dimensional structural MPRAG T1 brain images entered into the SIENA analysis pipeline were first bias field corrected and lesions filled using the method described by (Gelineau-Morel *et al.* 2011). SIENA is a semi-automated method that begins by extracting brain and skull images from the two-timepoint whole-head MRI data (Smith *et al.* 2002). The two brain images are then aligned to each other (Jenkinson *et al.* 2001, Jenkinson *et al.* 2002) and are resampled into the space halfway between the two. Next, tissue-type segmentation is carried out (Zhang *et al.* 2001) in order to find brain/non-brain edge points, and then perpendicular edge displacement (between the two timepoints) is estimated at these edge points. Finally, the mean edge displacement is converted into an (global) estimate of percentage brain volume change between the two timepoints.

The SIENA output, i.e. percentage change in brain parenchymal volume, was further statistically analysed in two ways. The first method was to perform an analysis of co-variance (ANCOVA) with age and the time between scans as co-variates, to compare between groups effects, with a Bonferonni multiple comparisons correction. The second method was a voxelwise within-group analysis, to investigate whether there was any statistically significant atrophy or growth in each individual subject group, and the location of this change. The process involves taking the edge displacement image between both timepoints for each subject and registering them to a standard space image before running voxelwise statistics to calculate the average change with the group using the permutation testing tool *Randomise* (part of FSL) and correcting for multiple comparisons across space.

Thalamic Volume:

Thalamic volume at one year was calculated from the structural 3-dimensional T1 image using the FSL tool FIRST, as described for the baseline scans in Chapter 7. The images were bias field corrected before the thalamic volumes were calculated. Raw thalamic volumes from each timepoint were compared, rather than those normalized to brain size.

Statistics: Thalamic volume was compared in each group using a repeated-measures ANCOVA with age and time between scans as co-variates. A Bonferonni type multiple comparisons correction was made. *Post hoc* pairwise comparisons (with a paired Student's t-test) were made between the subject groups with a Bonferonni multiple comparisons correction.

DTI and MWI: Diffusion tensor imaging data and myelin water imaging data were processed in the way described in Chapter 7 to produce fractional anisotropy and myelin water fraction maps respectively. Baseline and one year normal appearing white matter was compared with Tract Based Spatial Statistics (TBSS). To avoid bias, a mid-space template, between the two timepoints, was created for each subject, and the data from each timepoint was registered to the midspace template using an affine transformation. TBSS was then run as outlined in Chapter 7, by using a non-linear transformation to register the maps to the FMRIB FA template in the case of the FA data, and an average of the subjects in the case of the MWF data. These registered images were then averaged for each subject group and thresholded at a value of 0.2 to generate a mean white matter skeleton. FA and MWF data was then projected onto this skeleton and the two time points compared voxelwise using a paired t-test design matrix and the permutation tool Randomise, and corrected for multiple comparisons. Lesion maps for the disease subjects

were included in the statistical analysis as regressors to allow the lesioned voxels to be disregarded i.e. only the normal appearing white matter was compared between timepoints.

9.4: Results

9.4.1: Whole Brain Atrophy (SIENA analysis)

The average percentage change in brain volume over one year in each subject group is shown in Figure 9.1. It is greatest in the RRMS group, and least in the control group but ANCOVA statistical testing with age as a co-variate found there was no significant difference between groups (between groups effect is p=0.375) as shown in Table 9.2.

However a voxelwise examination of whether there were any significant areas of atrophy within the group showed a small area in the left temporal lobe in the RRMS group (corrected P <0.05; Figure 9.2) but no significant areas within the control and NMOSD groups.

Figure 9.1: Bar graph showing the average percentage change in brain volume over 1 year in each subject group. Error Bars are +/- 1 standard error of the mean.

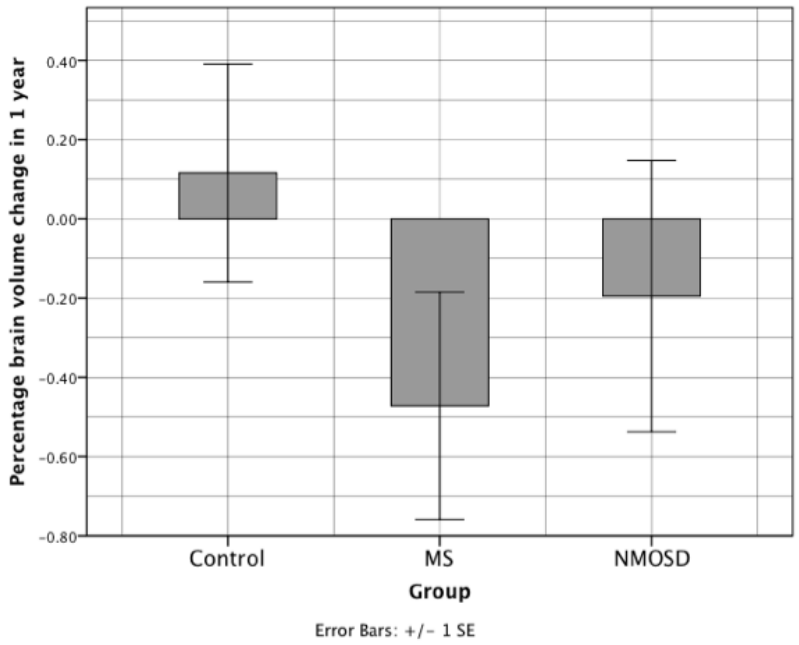


Table 9.2: ANCOVA results for a comparison between percentage brain volume change in one year between the subject groups (NMOSD, RRMS and controls).

	Sum of Squares (Type III)	df	Mean Square	F	Sig.
Corrected Model (Age as covariate)	6.829[+]	**4**	**1.707**	**1.089**	**0.375**
Age	2.348	1	2.348	1.498	0.228
Time	2.242	1	2.242	1.429	0.239
Group	2.535	1	1.268	0.808	0.453

[+]*R squared = 0.098 (adjusted R squared = 0.008)*

Figure 9.2: Results of a voxelwise SIENA analysis showing a significant cluster of brain atrophy (shown in red/yellow) over the one-year period in the RRMS group projecting onto the MNI standard space template.

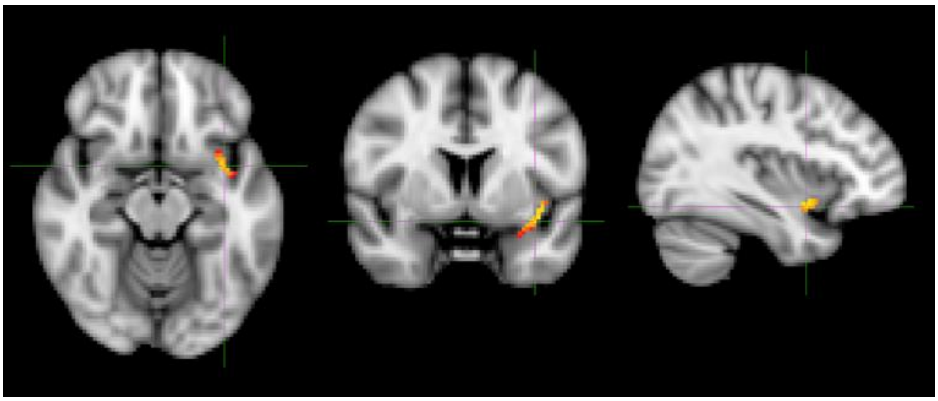
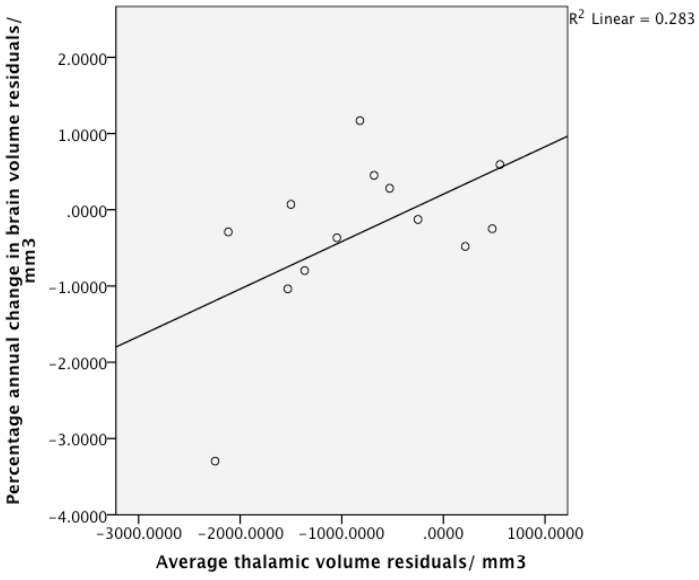


Figure 9.3 shows that thalamic volume predicts percentage brain volume change over one year in the MS cohort (correlation coefficient R= 0.532, p=0.031), but not the NMOSD or control cohorts. There is no significant correlation between baseline brain volume and percentage brain volume change in one year in any of the study groups.

Figure 9.3: Scatter graph with line of best fit showing the partial correlation, corrected for age, between baseline left/right average thalamic volume and percentage brain volume change in one year for the multiple sclerosis group.



9.4.2 Thalamic Volume

Baseline and one year thalamic volumes are highly correlated in all cohorts as expected (Figure 9.4). The change in the estimated means of the thalamic volumes is shown in Figure 9.5. There is a significant within-subjects effect of visit*group ($p<0.001$), and a between-subjects effect of group i.e. RRMS, Control and NMOSD ($p=0.043$) when using age and time between scans as co-variates and correcting for multiple comparisons with the Bonferonni method. *Post hoc* paired t-test analysis shows that there is a significant difference between timepoints one and two in the RRMS group ($p=0.01$) with a reduction in thalamic volume, but not within the control ($p=0.21$) or NMOSD groups ($p=0.054$).

Figure 9.4: Correlation between individual subject's baseline (x axis) and follow-up thalamic volumes for each group

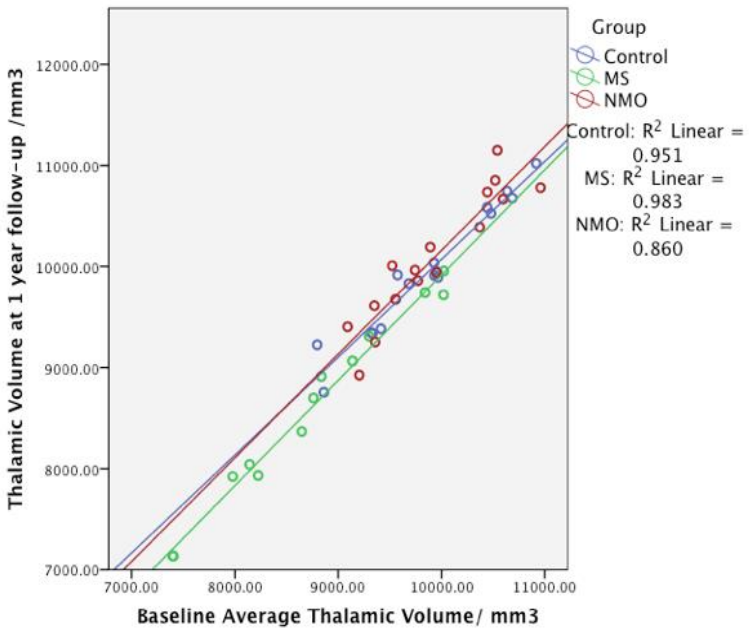
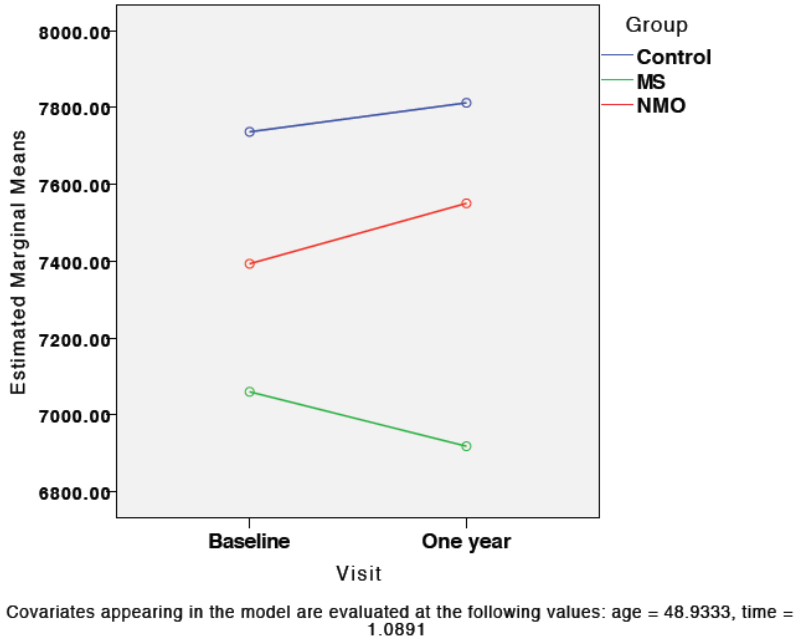


Figure 9.5: The estimated means, corrected for age and time between scans, for each subject group for each timepoint. Note these thalamic volumes have not been normalized with respect to brain size.



9.4.3 Diffusion Tensor Imaging

There were no significant changes in the normal appearing white matter FA between timepoints 1 and 2 in the control and NMOSD groups. In the RRMS group there were scattered areas of significant reduction in FA throughout the normal appearing white matter as shown in Figure 9.6. These regions include the right uncinate fasciculus, right corticospinal tract, right internal capsule, right inferior longitudinal fasciculus, left anterior thalamic radiation, right corona radiata, right juxtacortical white matter.

9.4.4 Myelin Water Imaging

Similar findings were revealed with the myelin water imaging with no significant changes between timepoints 1 and 2 in the control and NMOSD groups. As displayed in Figure 9.7 there are some areas of the significant reduction in MWF in the normal appearing

white matter of the RRMS group. These are in the regions of the left and right juxtacortical white matter, the left and right corticospinal tracts, left and right internal capsule, the body and genu of the corpus callosum, the right anterior and posterior thalamic radiations, the right optic radiation, the left and right cerebral peduncles and inferior longitudinal fasciculi.

Figure 9.6: Significant areas of reduction in fractional anisotropy over the one year follow-up period in the RRMS cohort shown in red-yellow, overlaid on the FMRIB FA standard space template. MNI coordinates of each slice are shown.

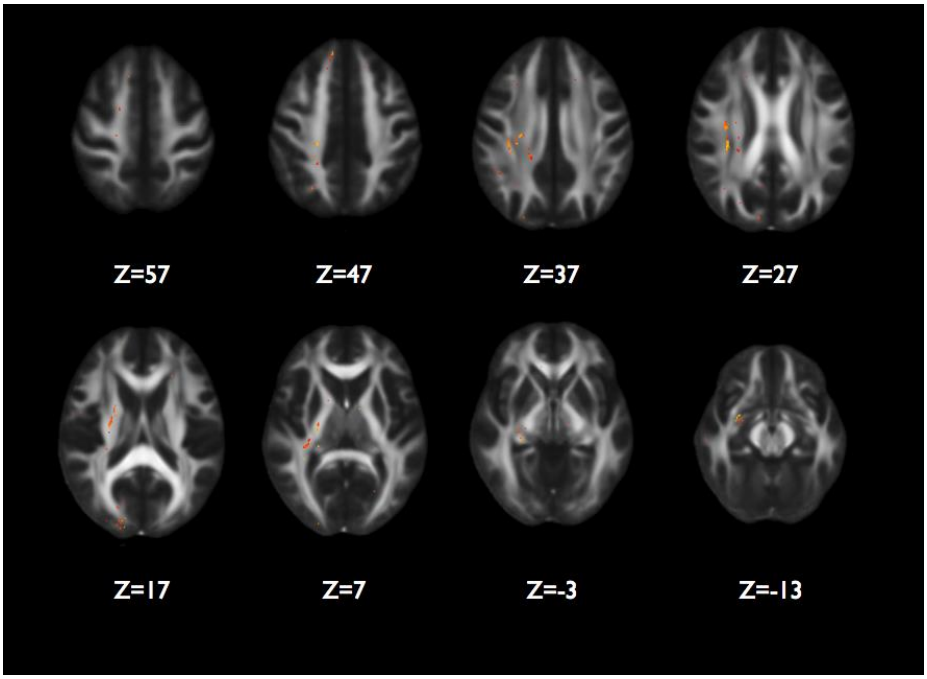
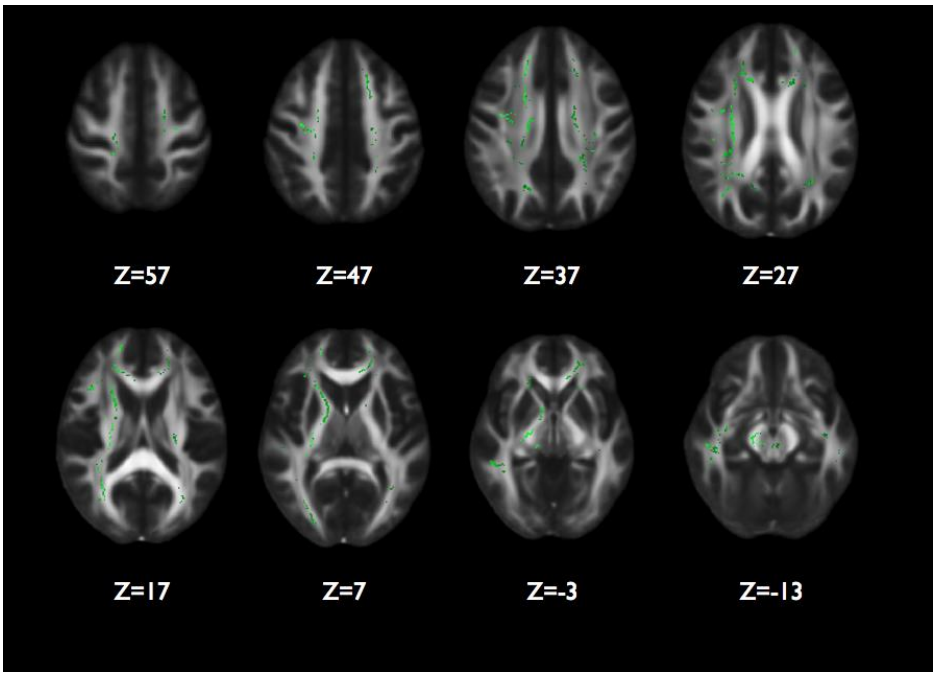


Figure 9.7: Significant areas of reduction in MWF in the RRMS cohort over a one year period shown in green, overlaid on the FMRIB FA standard space template. MNI coordinates for each slice are shown.



9.5 Discussion

This is the first known study that has examined longitudinal changes in quantitative MRI measures in a cohort of NMOSD patients. The main finding is that NMOSD is not associated with any measurable changes over a one year follow-up period in MRI markers of neurodegeneration.

One limitation of the longitudinal component of this study is that it is a relatively short period of follow-up, particularly if it is considered in terms of the usual length of development of disability in the progressive form of MS. However in favor of the finding that neurodegeneration does not occur in NMOSD is the fact that reduction in thalamic volume and fractional anisotropy have been measurable in a smaller RRMS cohort over the same time period. A further limitation is that spinal cord atrophy measures at one year are not presented in this thesis.

The reported finding of longitudinal grey matter atrophy in this chapter is in-keeping with a previous study of brain atrophy in RRMS by Fisher *et al.* (2008) that found that grey matter atrophy, measured over four years, is approximately four times that of a healthy control. Atrophy was found in this research at the earliest stage of MS (i.e. a clinically isolated syndrome converting to RRMS), a finding corroborated in cross-sectional studies (Chard *et al.* 2002; Chard, Miller 2009; Pirko *et al.* 2008). Grey matter atrophy is thought to be a useful surrogate marker of long-term disability in MS (Fisniku *et al.* 2008; Ramasamy *et al.* 2009), indicating that it may be representative of the neurodegenerative component of the disease.

Some longitudinal changes in FA have been found in this group of RRMS patients. A previous longitudinal study by Rashid *et al.* (2008) of 28 subjects with early relapsing MS over a two-year period did not find any differences in the rates of change of DTI metrics with controls. However in MS of longer disease duration, measurable reduction in FA has been found within a year particularly within the corpus callosum (Harrison *et al.* 2011). Diffusion tensor imaging has therefore been included as an outcome measure in clinical trials of new disease modifying therapies for MS, particularly those targeted at neuroprotection (e.g. Arun *et al.* 2013). Measuring MWF in MS patients with the mcDESPOT technique is a relatively new area, however previous work using this protocol has found reductions in MWF over a one-year period in primary progressive MS patients (Kolind *et al.* 2012). The work presented in this chapter shows that myelin water imaging has the power to detect longitudinal changes in a relatively small group of people with RRMS, which appear more widespread than those seen with diffusion tensor imaging.

The primary objective of this thesis was to detect differences in NMOSD and RRMS, which may be useful for diagnosis, rather than look for correlations of

quantitative MRI with clinical measures as has previously been investigated in existing literature in MS (overviewed in reviews by Ceccarelli *et al.* 2012 and Bakshi *et al.* 2008). However, as this is the first longitudinal study of NMOSD with DTI and volumetric imaging, this area may be an interesting focus for future analysis of the dataset.

The results presented in this chapter highlight that MRI markers of neurodegeneration can be useful in detecting progressive changes that clinical disability scores are insensitive to over a relatively short time period.

An interesting outcome of this thesis is that semi-automated measurement of thalamic volume appears to be a more sensitive marker of degeneration than whole brain volume in the RRMS cohort. Therefore, as well as its utility in distinguishing NMOSD and MS, this measure has potential as an adjunct outcome measure in clinical treatment trials of neuroprotective agents in this group of patients, and the usefulness in this context should be further explored with a longer period of follow-up and a larger number of subjects.

9.6 Conclusion

The longitudinal results support the cross-sectional findings that the absence of widespread neurodegeneration and atrophy in NMOSD could provide a means of discrimination from RRMS. The next chapter investigates which combination of outcome measures derived in this thesis are the most useful for distinguishing the study groups.

Experimental Chapter 10: Serum N-Acetyl Aspartate Measurement and Formulation Of A Function To Discriminate Between NMOSD And RRMS

10.1 Introduction

Serum immunoassay for aquaporin-4 antibodies is currently the most sensitive and specific method of diagnosing NMOSD, however, as discussed diagnostic problems can arise when a patient is negative. The most prevalent mimic of NMOSD is RRMS, hence this thesis has concentrated on methods of distinguishing the two conditions. We have already shown that qualitative analysis using lesion location and lesion characteristics may distinguish NMOSD and RRMS at an individual level in those patients with abnormal brain scans. However our findings from quantitative MRI analysis suggest that RRMS and NMOSD can be distinguished by volumetric measures and examination of the normal appearing tissue only at a group level – RRMS is characterised by widespread diffuse neurodegenerative changes whereas neurodegenerative changes in NMOSD are limited to lesions.

It therefore follows that a serum measure of neurodegeneration could provide accessory information to aid the distinction of the two conditions. N-acetylaspartate (NAA) is specifically located in neurons, and is one of the most abundant molecules in the central nervous system (Moffett *et al.* 2007). Widespread reduction of NAA has been detected in the MS brain using MR proton-spectroscopy (Arnold *et al.* 1990; Wolinsky *et al.* 1990; De Stefano *et al.* 2005), and previous research has distinguished NMO and MS at the group level using this method by comparing to control values (Aboul-Enein *et al.* 2010; de Seze *et al.* 2010).

Intuitively one may think that if NAA is being lost from brain tissue due to neurodegeneration then higher levels (than healthy controls) will be found in serum or cerebrospinal fluid. In clinically isolated demyelinating syndromes CSF NAA levels have been found to be significantly raised when compared to controls (Khalil *et al.* 2012). However other work has shown that with disease progression, possibly due to cumulatively reduced number of axons within the CNS, serum and CSF NAA levels reduce (Jasperse *et al.* 2007; Teunissen *et al.* 2009). In agreement with this lowered levels of NAA are found in healthy aging (Ruggieri *et al.* 2011). However in the neurodegenerative disease amyotrophic lateral sclerosis, serum NAA was found to be significantly increased when compared to healthy controls (Simone *et al.* 2011).

In this thesis NAA levels in serum samples taken at the same time as the baseline brain MRI are determined, and correlations with the MRI measures of neurodegeneration presented in earlier chapters are investigated. In addition, to attempt to find a method of distinguishing NMO, MS and healthy controls a discriminant analysis is conducted using the cross-sectional quantitative measures derived in this thesis.

Discriminant analysis is a method akin to regression that is used for classification when the dependent variables are categorical, and the predictor variables are at interval level. In this chapter, linear equations for discriminating NMO, MS and Controls were derived using the cross-sectional outcomes of this thesis, namely normalised whole brain volume, normalised thalamic volume, normalised caudate volume, normal appearing white matter FA and MWF, normal appearing grey matter FA and MWF, cervical spinal cord volume and serum NAA. Discriminant equations take the form:

$$D = v_1X_1 + v_2X_2 + v_3X_3 + ...v_iX_1 + a$$

where D = *discriminant function*
v = *the discriminant coefficient or weight for that variable*
X = *the subjects score for that variable*
a = *a constant*
i = *the number of predictor variables*

10.2 Objectives

- To investigate whether a serum measure of neurodegeneration, namely NAA, can distinguish NMO and RRMS
- To test if the NAA in serum correlates with imaging markers of neurodegeneration
- To investigate whether a linear equation can be formed from the cross-sectional quantitative measures derived in this thesis that would allow the distinction of NMO from both controls and RRMS.

10.3 Methods

10.3.1 Subject Cohort

Accurate measurement of serum NAA was achievable in 15 RRMS patients, 17 NMOSD patients and 16 controls from serum that was taken at the baseline assessment on the same day as the MRI brain examination. The subject characteristics are shown in Table 10.1.

Table 10.1: Subject Characteristics:

Subject Group	Number	Age, range (median)	Sex	Aquaporin-4 antibody positive	EDSS, range (median)	Disease Duration, range (median)
NMOSD	17	20-70 (42)	14F 3M	17 (100%)	2-6 (3.5)	12-186 (57.5)
RRMS	15	22-62 (38)	11F 4M	0 (0%)	0-5 (2)	24-240 (72)
Control	17	21-77 (47)	13F 4M	0 (0%)	-	-

10.3.2 Serum Collection

Serum was collected into tubes containing clot activator and gel for serum separation. Blood was left for 30minutes to clot and then centrifuged. The separated serum was pipetted off and frozen at -80˚C until analysis.

10.3.3 NAA Analysis

NAA was measured with the gas-chromatography-mass-spectroscopy method by the Department of Molecular Cell Biology and Immunology, VU University Amsterdam, Netherlands in collaboration with Dr Charlotte Teunissen (Teunissen *et al.* 2009).

10.3.4 Statistical Testing

NAA levels in each subject group were compared using an analysis of covariance (ANCOVA) using the SPSS statistics package version 19, with age included as a co-variate.

In order to test whether NAA has any relationship with the measures of neurodegeneration, partial correlation (controlling for age) was sought with brain volume, percentage brain volume change in one year, thalamic volume, change in thalamic

volume in one year, baseline caudate volume, cervical spinal cord area, baseline normal appearing white matter (NAWM) myelin water fraction (MWF) and fractional anisotropy (FA), and disease duration. To achieve this all the variables were entered into a linear regression model to correct for the multiple comparisons.

Changes consistent with neurodegeneration were seen over the one-year period in the MS group, and not NMO (because there was no difference found with control subjects in these outcome measures). Separate models were therefore created for each subject group to test for partial correlation (corrected for age) of NAA with the above listed variables.

10.3.5 Discriminant Analysis

A discriminant analysis was run using SPSS version 19. The outcome variable was group (i.e. MS, control or NMOSD), the predictor variables were normalised whole brain volume, normalised thalamic volume, normalised caudate volume, normal appearing white matter FA and MWF, cervical spinal cord volume and serum NAA. The first discriminant analysis also included the longitudinal measures of annual percentage change in brain parenchymal volume and thalamic volumes.

Two approaches for this analysis were taken: first including all the predictor variables, and second a stepwise approach were the derivation is simplified by removing variables that highly correlate.

10.4 Results

10.4.1 Serum NAA:

A box plot (Figure 10.1) shows the range of serum NAA values in each subject group.

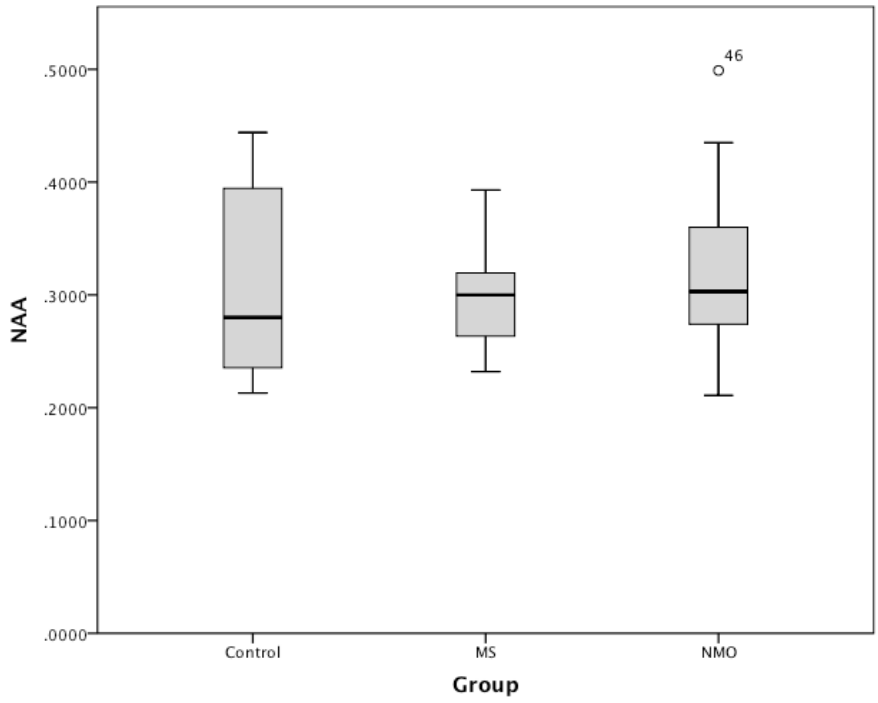
ANCOVA analysis accepted the null hypothesis that there was no significant difference between groups as shown in Table 10.2, with age as a co-variable.

Table 10.2 *ANCOVA results for a comparison of NAA between the subject groups (NMOSD, RRMS and controls).*

	Sum of Squares (Type III)	df	Mean Square	F	Sig.
Corrected Model (Age as covariate)	**0.17**[+]	**3**	**0.006**	**1.137**	**0.344**
Age	0.013	1	0.013	2.750	0.106
Group	0.003	2	0.001	0.269	0.765

[+]*R squared = 0.72*

Figure 10.1: Box plot showing range of serum NAA values in each subject group.



10.4.2 Correlation of NAA with MRI measures of neurodegeneration

Partial correlations of the whole cohort, with age as a nuisance regressor, are shown in Table 10.3a. A significant negative correlation was found between NAA and NAWM FA. Subgroup analysis showed significant negative correlations within the MS group alone of NAA with baseline average thalamic volume, annual thalamic volume change, baseline NAWM MWF and baseline NAWM FA (Table 10.3 b and Figure 10.2). A trend exists with annual percentage brain volume change.

Table 10.3. Partial Correlations from Regression Model of NAA with Quantitative MRI measures, corrected for age and multiple comparisons. For

a. Whole cohort

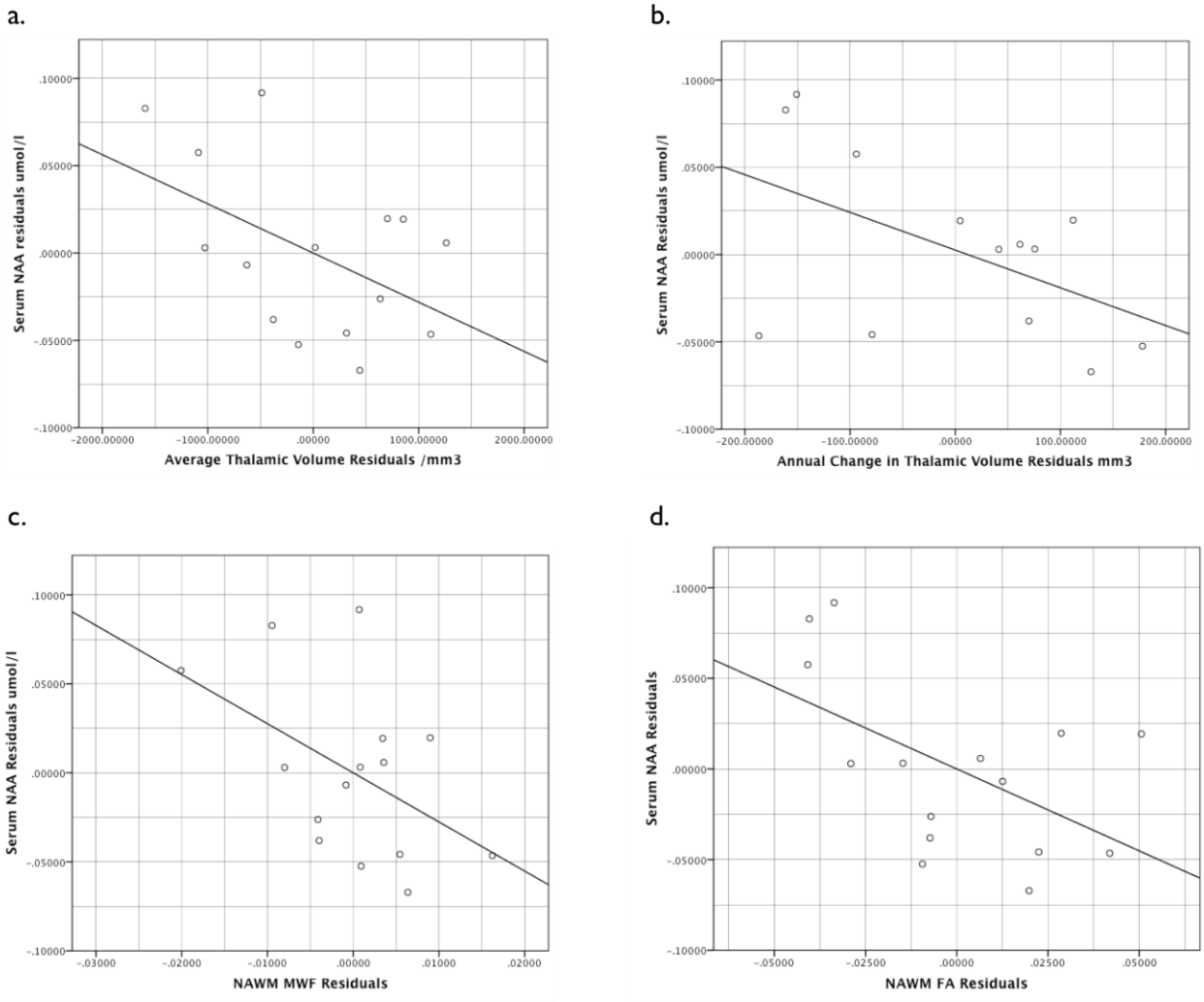
Variables	**Correlation Coefficient with NAA**	**Significance level (p)**
Baseline whole brain volume	-0.144	0.237
Baseline average thalamic volume	-0.019	0.463
Baseline average caudate volume	-0.229	0.126
Cord Area	0.120	0.211
Annual brain volume percentage change	-0.144	0.285
Annual thalamic volume change	0.200	0.158
Baseline NAWM myelin water fraction	-0.224	0.130
Baseline NAWM FA	-0.431	0.012*
Age	0.246	0.092

b. MS Group Alone

Variables	**Pearson's Correlation Coefficient with NAA**	**Significance level**
Baseline whole brain volume	-0.126	0.349
Baseline average thalamic volume	-0.502	0.048*
Baseline average caudate volume	-0.361	0.124
Cord Area	0.090	0.380
Annual brain volume percentage change	-0.401	0.098
Annual thalamic volume change	-0.504	0.047*
Baseline NAWM myelin water fraction	-0.561	0.048*
Baseline NAWM FA	-0.542	0.037*
Age	-0.046	0.435
Disease Duration (controlling for age)	-0.156	0.315

Figure 10.2: Statistically significant partial correlations of NAA with quantitative MRI outcomes for the MS cohort, corrected for age

a. Average thalamic volume
b. Annual change in thalamic volume
c. NAWM MWF
d. NAWM FA



10.4.3 Discriminant Analysis

Cross-sectional predictor variables were normalised whole brain volume, normalised thalamic volume, normalised caudate volume, NAWM FA, NAWM MWF, cervical spinal cord volume and serum NAA. The first discriminant analysis also included the longitudinal measures of annual percentage change in brain parenchymal volume and thalamic volumes.

Analysis 1: All outcome measures:

Two discriminant functions are required to separate the three groups.

- **Discriminant Function 1:** To separate Controls and NMOSD from RRMS: The discriminate function (Function 1) showed a significant association between groups and all predictors, accounting for 79.8% of between group variability, although closer analysis of the structure matrix revealed that the most significant predictors where average thalamic volume (correlation with Function 1 = 0.627), change in thalamic volume (correlation with Function 1 = 0.551) and cord area (correlation with Function 1 = 0.461).

- **Discriminant Function 2**: To separate NMOSD and Controls: This function (Function 2) accounted for 20.2% of the between group variability. The most significant predictors were NAWM FA (correlation coefficient with Function 2 = 0.544), NAWM MWF (correlation coefficient with Function 2 = 0.541) and cord area (correlation coefficient with Function 2 = 0.428).

The cross-validated classification showed that overall 74% were correctly classified. Separation of the groups using the Canonical discriminant functions is shown in Figure 10.3.

Analysis 2: Cross-sectional outcome measures only

Removing the longitudinal measures (to allow the discriminant function to be useful for cross-sectional MRI examinations) did not significantly affect the Canonical function's ability to discriminate between the groups. Discriminate Function 1 (which separates RRMS from NMO and Controls) explains 83.0% of the between group variability. Function 2 (for the separation of NMO and Controls) explains 17% of the between group variability. The most useful predictors for Function 1 are normalised thalamic volume (correlation coefficient with Function 1 = 0.706), cord area (correlation coefficient with Function 1 = 0.516) and caudate volume (correlation coefficient with Function 1 = 0.473). For Function 2 the most useful predictors are NAWM FA (correlation coefficient with Function 2 = 0.566) and NAWM MWF (correlation coefficient = 0.522). The cross-validated classification showed that overall 74% were correctly classified.

Analysis 3: Simplified Function for Discriminating RRMS and NMOSD:

To derive an equation for separating NMOSD and RRMS, the analysis was repeated with only these options as the output classifying groups. Thalamic volume (correlation coefficient 0.665), caudate volume (correlation coefficient 0.485) and cord area (correlation coefficient 0.320) were the most useful variables for separation. This is able to separate 93.9% of the cases accurately.

To simplify the equation to create a more practical tool, a stepwise approach was taken where factors that highly correlate are removed from the final function.

The discriminant function derived was:

$$D = (-0.01NWBV) + (2ATV) - 0.891$$

Where *NWBV* = normalised whole brain volume in **cm^3**

and *ATV* = average (of left and right) thalamic volume in **cm^3**

NMOSD cases would be expected to centre around 0.983 and RRMS around -1.114 (Table 10.4). It is able to correctly classify 90.9% of subjects when cross-validated shown in Table 10.5. This equates to 89.5% sensitivity, 92.9% specificity, 94.4% positive predictive value and 86.7% negative predictive value for the diagnosis of NMOSD. The outcome of the application of this function to the NMOSD, RRMS and control groups is shown in Figure 10.4 a and b, with good separation of the NMOSD and RRMS cohorts.

Table 10.4: Group centroids and standard deviations for function to discriminate NMOSD and RRMS with cross-sectional quantitative measures:

Group	*Centroid value*	*Centroid -/+ 1 SD*	*Centroid + 2 SDs*
NMOSD	*0.983*	*0.123 to 1.843*	*-0.737 to 2.703*
RRMS	*-1.114*	*- 2124 to – 0.104*	*-3.134 to 0.906*

SD = standard deviation

Figure 10.3: Plot showing the separation of the NMOSD, RRMS and control groups using the derived canonical discriminant functions.

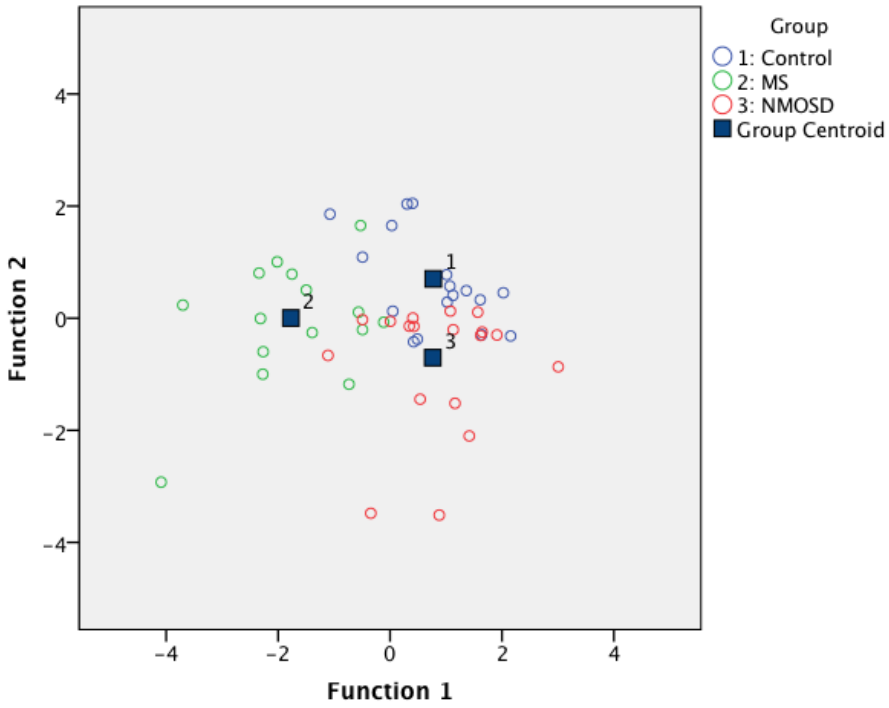
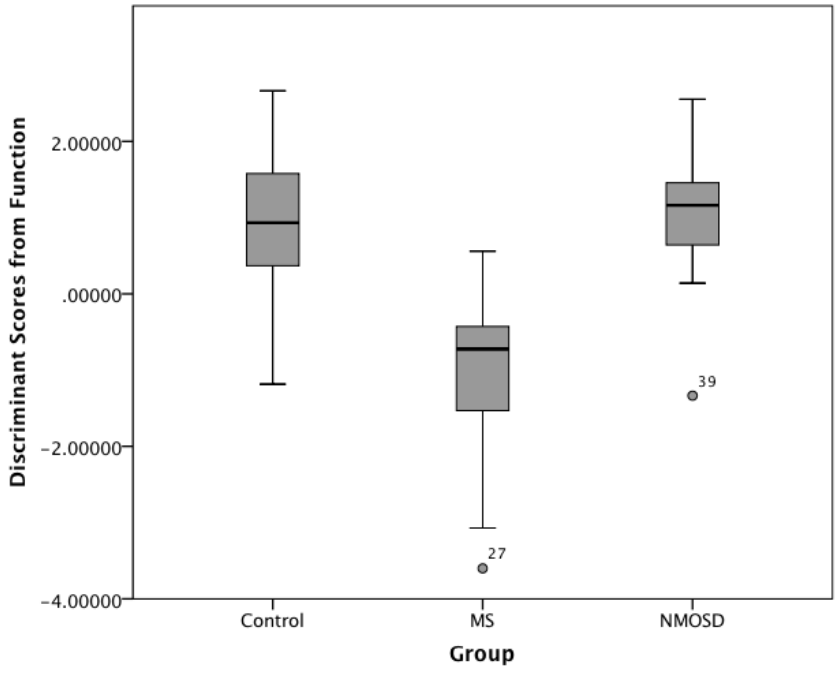


Figure 10.4: a. Box plot showing the grouping of the data when the simplified function for the separation of RRMS and NMO is applied to the NMO and MS. The function has also been applied to the control group in this plot.



b. Histogram demonstrating the discriminant function's separation of NMOSD and RRMS

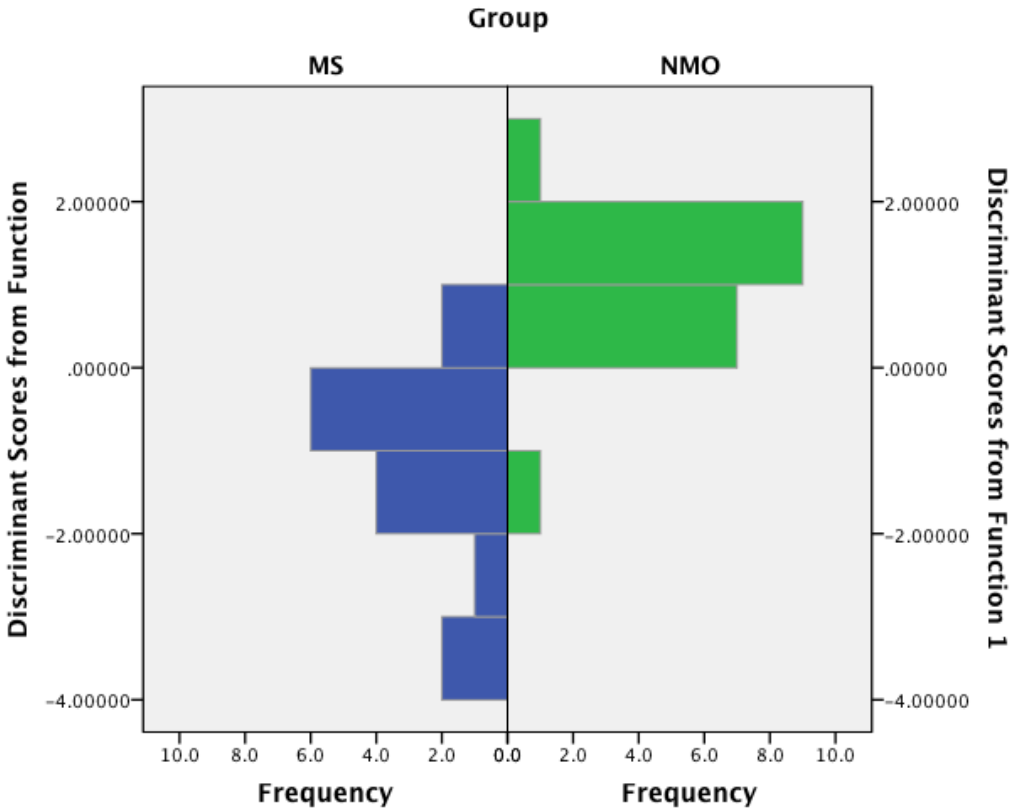


Table 10.5: Cross-validation of function for the separation of NMOSD and RRMS

		Predicted Group Membership		
		RRMS	NMOSD	Total
Original Group Membership	RRMS	13	2	15
	NMOSD	1	17	18

10.5 Discussion:

In this experiment serum NAA has not proven to be a useful adjunct to the imaging measures for the separation of an antibody positive NMOSD cohort from RRMS. Yet the negative correlations with imaging measures of CNS tissue integrity, particularly within the RRMS group, show an association of higher NAA levels with greater degrees of neurodegeneneration. RRMS is generally thought of as an earlier form of MS, with the secondary progressive phase heralding clinically eloquent neurodegeneration. One

explanation for the contradictory results with some of the previous literature (Jasperse *et al.* 2007; Teunissen *et al.* 2009) may be that the low NAA levels found in progressive forms of MS and aging represent a point where there becomes a significantly lower density of neuronal axons producing NAA within the CNS.

Limitations of the methods presented in this chapter include the fact that NAA was measured in only a single serum sample for each participant at one time point. It is therefore difficult to assess the biological variability of the measure, for instance whether it changes according to the time of day at which the sample was taken or due to other metabolic factors.

The discriminant analysis ties together the work from previous chapters, and has allowed the formulation of a function for distinguishing NMSOSD and RRMS. This formula requires the calculation of normalised whole brain and thalamic volume, a task that automated MRI analysis tools exist for (Smith *et al.* 2002; Smith *et al.* 2004; Patenaude *et al.* 2011). Therefore it is feasible that this could be translated into clinical practice however further validation is required in independent cohorts.

10.6 Conclusion

A discriminant function, $D = (-0.01NWBV) + (2ATV) - 0.891$, can aid the separation NMOSD and RRMS, with a 89.5% sensitivity and 92.9% specificity for the diagnosis of NMOSD when cross-validated. This requires further testing and validation on an independent cohort.

11.0 Discussion

The research reported in this thesis enhances our knowledge of neuromyelitis optica spectrum disorder (NMOSD) in terms of both conventional and quantitative imaging features. It has shown that lesion characteristics can be a useful identifier for NMOSD, and supports the potential for the use of quantitative imaging in clinical practice.

11.1 Summary of Key Findings:

The key findings are summarized below as a response to the research questions posed:

Research Questions (as stated in Chapter 4):

- Can MRI, either conventional or quantitative, provide an additional biomarker for NMO to allow prompt and accurate diagnosis?
- Is neurodegeneration a feature of NMOSD?
- Can serum N-acetylaspartate (NAA) levels be used as adjunctive information to allow the distinction of NMOSD and relapsing remitting multiple sclerosis (RRMS)?

Key Findings:

- In an approximately 2:1 cohort of RRMS:NMOSD patients, brain lesion distribution can identify RRMS with a 92 % sensitivity and 96 % specificity.

- At the group level cross-sectional thalamic volume, caudate volume, normal appearing white matter FA and normal appearing white matter MWF can separate NMOSD from RRMS. RRMS is associated with significant changes consistent with neurodegeneration (subcortical grey matter atrophy and the loss of structural

integrity of the white matter) when compared to controls. In NMOSD the changes are focal, with low FA within the optic pathways that appear to be driven by a lack of visual sensory input in patients with severe visual impairment.

- The RRMS group also have a reduction in cervical spinal cord volume and white:grey matter MT contrast within the normal appearing spinal cord tissue, again consistent with neurodegeneration.

- Cross-sectional normalised brain (NWBV) and thalamic volume (ATV) can be used in an equation (D = (-0.01NWBV) + (2ATV) – 0.891) to aid the separation of NMOSD and RRMS.

- Over a one-year period, longitudinal changes consistent with neurodegeneration can be found within the RRMS group but not the NMOSD and control cohorts. There was a significant reduction in thalamic volume, a significant area of brain atrophy in the left temporal lobe region, and reductions in normal appearing white matter FA and MWF.

- Serum NAA measurement cannot differentiate between NMOSD and RRMS, however does show association with MRI measures of neurodegeneration whereby NAA is increased in patients with greater atrophy or white matter damage.

11.2 Interpretation of Key Findings:

NMOSD and RRMS are both inflammatory demyelinating diseases, which in the clinical setting can be diagnostically confused. The pathophysiology of the diseases is otherwise clearly distinct: NMOSD is caused by a disease specific antibody (Lennon *et al.* 2004; Lennon *et al.* 2005), neurodegenerative changes have been documented in normal appearing tissue on pathological examination in RRMS (Evangelou *et al.* 2000) but not NMOSD, the pathological characteristics of lesions differ (Lucchinetti *et al.* 2002) and immunomodulatory treatments can have very different effects (Palace *et al.* 2010; Kleiter *et al.* 2012).

It follows, therefore, that these differences in underlying pathophysiology should be detectable with MRI, which is the best tool we have available for studying inflammatory diseases *in vivo*. Results of existing MRI studies of NMOSD in the literature have been inconclusive, and therefore this thesis takes the approach of using a relatively large cohort of NMOSD patients who have been defined by their antibody positive status to avoid any diagnostic uncertainty.

Conventional Imaging

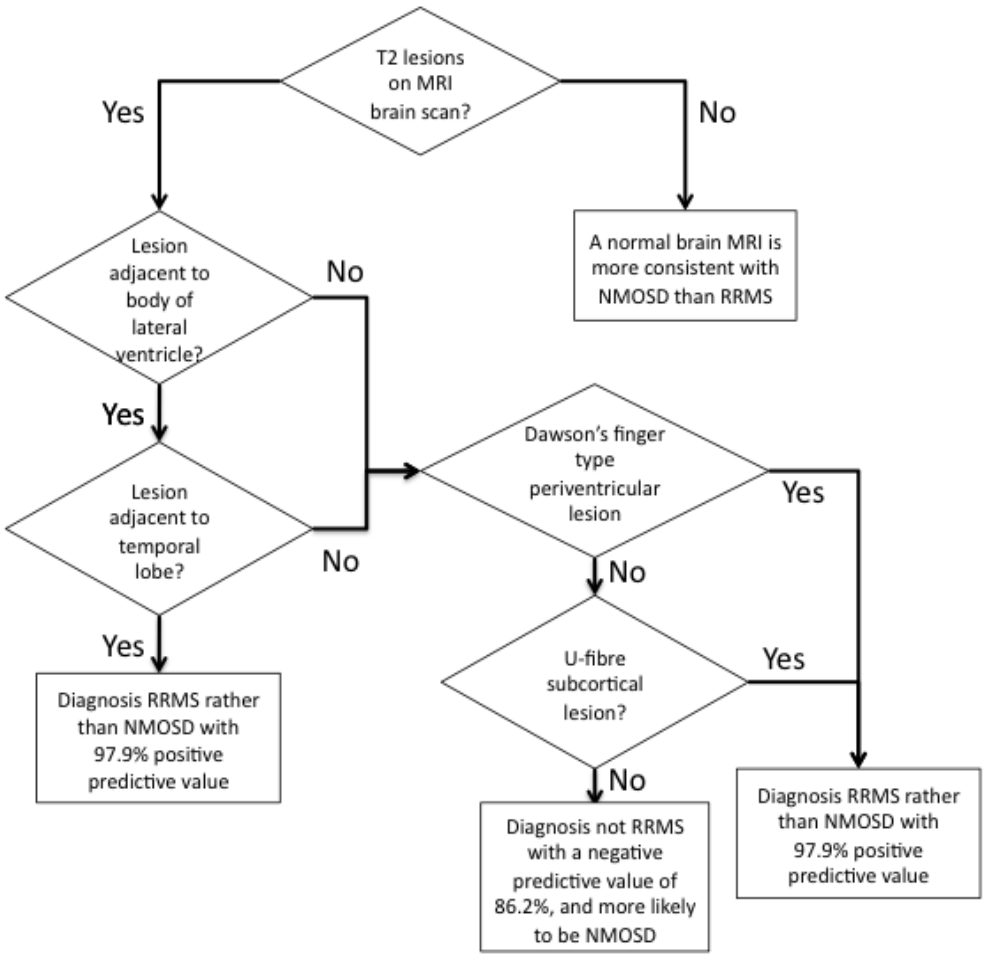
The first experimental chapter of this thesis (Chapter 6) explored whether conventional MRI - more specifically imaging with T2 weighted images could distinguish NMOSD and RRMS. Brain lesions represented by T2 hyperintensity is a known feature of both RRMS and NMOSD. In the cohort studied in this work, 15 of the 44 NMOSD patients did not have brain lesions - a feature far more indicative of NMOSD than RRMS (Wingerchuk *et al.* 2006), as for reasons that are still not entirely clear NMOSD has a predilection for the optic nerves and spinal cord. This left a 29:50 NMOSD:RRMS cohort with which to try to identify consistent differences in the patterns of lesion

distribution. To do this quantitative analysis techniques, lesion probability mapping and voxelwise analysis, were for the first time applied to the problem. The outcome was the identification of certain features that were more common in each group directing the formulation of criteria for the identification of RRMS over NMOSD (summarised in the flow diagram below (Figure 11.1)). The reason that RRMS was 'more identifiable' was because of the higher lesion load, presence of more consistent features (i.e. lesions adjacent to the body of the lateral ventricle) as shown with the high probabilities on the lesion maps, and the presence of features that have previously been identified in the literature as being very suggestive of RRMS (i.e. Dawson's fingers and U-fibre subcortical lesions). The criteria need further validation in an independent cohort. They also need prospective application to the problem of classifying antibody negative patients with an opticospinal syndrome by applying them to patients whose diagnosis is in doubt and auditing against eventual diagnosis (once more of the clinical features have unfolded) – it would be in this clinical setting that the criteria prove especially useful particularly as they only require MRI information which is collected during routine work-up in this population.

The aim of this thesis was to identify disease specific features of antibody positive NMOSD and the work presented in Chapter 6 has affirmed previous work that conventional brain imaging features in most are non-specific (Pittock *et al.* 2006). This is an interesting observation in itself because the reason often given for the predilection of this disease process for the optic nerves and spinal cord is the high concentration of AQP-4 antibody (Pittock *et al.* 2006), however the majority of brain lesions are within the deep white matter, that is not known to be an AQP-4 rich region. Therefore there must be other factors at play in the development of NMO lesions, such as blood brain barrier permeability, and future work should be to look into these factors, as a better

understanding could help to prevent relapses. T2 imaging also has the disadvantage that high signal purely represents an increase in the amount of water in that region and does not give any specific information as to the underlying pathogenic cause. The search for a specific imaging biomarker of NMOSD therefore moved onto quantitative imaging which is the topic of experimental chapters 7-10.

Figure 11.1: Flow chart outlining the application of conventional MRI criteria for distinguishing NMOSD and RRMS



Quantitative Imaging

Because of existing knowledge of the pathological examination findings in NMOSD and RRMS (i.e. that axonal loss and grey matter atrophy are features of RRMS but have not been documented in NMOSD), an assumption was made that RRMS would be associated with neurodegenerative changes that have previously shown to be detectable on quantitative imaging (Bakshi *et al.* 2008) and NMOSD would not. In addition, because of differences in the target of the disease process in each condition (astrocytes in NMOSD versus primary oligodendrocyte damage in RRMS) it was a possibility that there may be detectable differences in myelination and therefore myelin water imaging was also included in the investigation.

The findings, as summarised above, were indeed in favor of this assumption, and at a group level RRMS and NMOSD could be separated on the basis of the absence of widespread neurodegenerative changes in the NMOSD group both from a cross-sectional and longitudinal point of view. There were however some localised reductions in FA in the optic radiations of the NMOSD group, which appear to be driven by the subjects who had bilateral severe visual impairment.

Both RRMS and NMOSD involve brain lesions, but the diffuse neurodegenerative changes have only been found in RRMS suggesting that the neurodegenerative process in RRMS may be 'primary' or separate from the inflammatory component. In favour of this finding is the clinical observation that progression is very rare/ absent in NMOSD (Wingerchuk *et al.* 2007; Kitley *et al.* 2012), whereas it can be the first presenting feature of MS in the primary progressive phenotype.

An alternative explanation that must be considered is that the greater lesions load in RRMS leads to greater reciprocal neurodegeneration, and that at a group level the

neurodegeneration due to lesions in NMOSD cannot be detected due to far lower average lesion load (some patients have no brain lesions at all).

Although reductions in FA and basal ganglia volumes have been found in RRMS over a one-year interval (Simon *et al.* 1999; Harrison *et al.* 2011), a further potential limitation of this work is that the follow-up period may not have been long enough to detect neurodegenerative changes in NMOSD. It is difficult to say when one would expect neurodegenerative changes to occur in NMOSD if they are not present at one year, however further work could involve a longer term study – perhaps over 5 years or more, whereby one may expect to also detect differences in the changes in disability scores between the RRMS and NMOSD group.

Previous literature in the field of quantitative MRI has been reviewed in the introduction to this thesis and it is clear that the findings are inconsistent. Some research supports the notion that widespread neurodegeneration is absent in NMOSD (Filippi *et. al* 2004; Yu *et al.* 2006; Yu *et al.* 2008). However other reports suggest more diffuse changes (Rocca *et al.* 2004; Liu *et al.* 2012; Rueda Lopes *et al.* 2012). Possible explanations include population differences such as race. The work presented in this thesis is the first quantitative imaging research where all the patients were AQP-4 antibody positive. In previous studies the inclusion of seronegative patients introduces the risk that subjects may have an opticospinal form of MS and be misclassified. In fact in more than one of the studies the antibody status of the population is unknown, which would seem to be vital information in a disease that is defined by its associated antibody.

A further potential reason for the incongruous outcomes in the historical literature could be due to data analysis issues. Extremely careful and complex methodology is required to exclude lesions from the quantitative analysis of normal appearing white matter to avoid contamination.

N-acetylaspartate measurement

Two main factors directed the selection of serum NAA measurement as an additional outcome of the study. Firstly biomarkers of disease that are detectable within the serum, such as the aquaporin-4 antibody, are advantageous due to the ease of sample collection particularly in the outpatient clinic setting. Second, NAA is known to be a neuronal marker with reduced levels found in several neurodegenerative diseases using *in vivo* MR spectroscopy (Aboul-Enein *et al.* 2010; de Seze *et al*. 2010). The findings in our study suggest that a cross-sectional measure of serum NAA cannot accurately discriminate the subject groups, however negative correlations found between NAA levels and MRI measures of neurodegenerative change in the RRMS cohort suggest that serum NAA may reflect the degree of neuronal damage. Further work is required to investigate whether this measure is a useful method for monitoring the efficacy of neuroprotective agents in clinical trials. Previous literature suggests that in the more progressed stages of neurodegenerative diseases NAA levels drop (Jasperse *et al.* 2007; Teunissen *et al.* 2009).

Discriminant Analysis

The final part of this investigation was to bring together the quantitative outcome measures derived in the previous experiments by applying a discriminant analysis. The objective was to select a combination of indices that could be useful in clinical practice for helping to discriminate NMOSD and RRMS. Using a stepwise approach a simplified function was derived which has the power to discriminate our NMOSD cohort with 90.9% accuracy using cross-sectional MRI data.

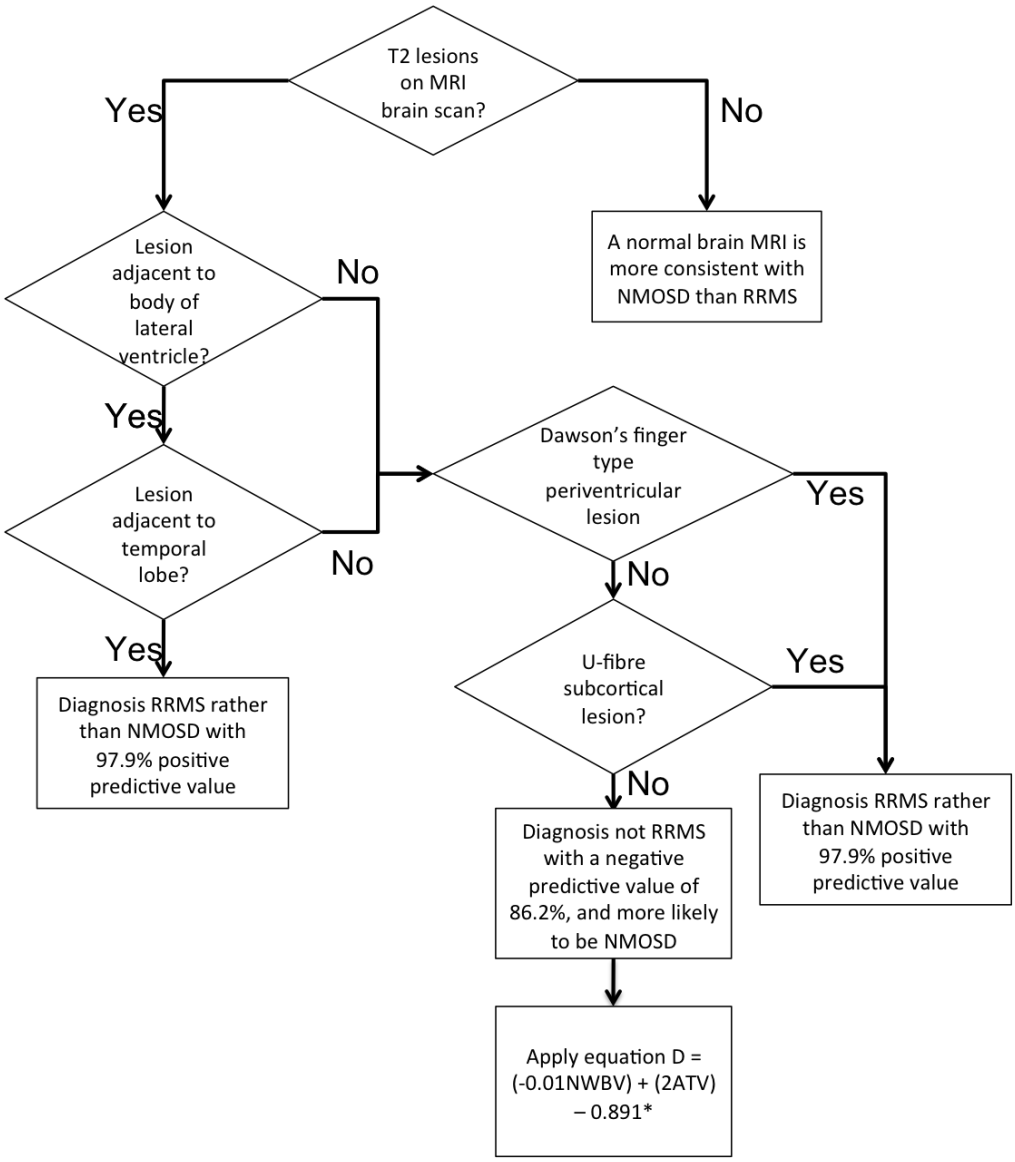
From a translational point of view it is fortuitous that the two indices that combine to discriminate the greatest number of cases (i.e. brain and thalamic volume) can be

measured from 3-dimensional T1 images, which are commonly used in conventional MRI. An additional advantage is that the analysis tools used to derive these measures are already semi-automated (Smith *et al.* 2002; Patenaude *et al.* 2011).

As with the lesion location criteria presented in Chapter 6, this function requires validation with an independent cohort of patients, and application to aquaporin-4 antibody negative patients with a phenotype that overlaps the features of NMOSD and RRMS.

The function could be fitted to the algorithm shown in Figure 11.1, whereby it would be most useful in the context of a conventional MRI scan that is not typical of RRMS (Figure 11.2). It could also be applied in addition to the conventional MRI algorithm to provide further evidence/ reassurance of a diagnosis of RRMS as opposed to NMOSD.

Figure 11.2: Flow chart outlining the application of conventional MRI criteria and the function using whole brain volume and normalized thalamic volume derived from the discriminant analysis.



** NWBV = Normalised Whole Brain Volume, ATV = Average Thalamic Volume. RRMS patients have a value 'D' within the range -2124 to - 0.104 and patients with NMOSD have a value within the range 0.123 to 1.843. On cross-validation this function separates NMOSD and RRMS with a 90.9% accuracy.*

11.3 Implication to clinical practice:

- Criteria have been developed that can be applied to the conventional brain image of a patient with an NMOSD/RRMS borderline syndrome to aid in diagnosis. Correct diagnosis has important treatment implications.
- Quantitative imaging analysis may further assist diagnosis. Cross-sectional thalamic volume has been shown to be most predictive of group. In combination with normalised brain volume NMOSD patients are diagnosed with 89.5% sensitivity and 92.9% specificity in this study cohort.
- The data suggest that NMO is lesion focused, and therefore disease prevention should be targeted at lesion prevention with immunosuppression.
- Work exploring measurable predictors of relapse could also improve disease control. Interestingly the location of NMOSD lesions predominantly within the deep white matter shows that the factors that lead to relapse may not be as straight forward as a rise in antibody levels.
- One exception to the rule is the reduced FA levels found within the optic radiations in the NMOSD group associated with severe visual loss due to previous optic neuritis. It is not known whether this degeneration could worsen eyesight in patients with optic neuritis and already compromised vision, and this question could be addressed in future work.
- In contrary to this RRMS seems to be associated with primary neurodegenerative pathology that in many previous studies has been shown to be the main substrate of the development of disability (Trapp and Nave 2008), therefore the target of treatment for this condition needs to be both anti-inflammatory and, possibly more importantly, neuroprotective.

11.4 Implication to MRI research

- The usefulness of quantitative, 'non-conventional', imaging methods such as DTI in a neuroscience research context have been clear for many years. This study shows that translational application of techniques that can probe CNS microstructure and measure anatomical volumes can help solve a clinical problem.
- The ability of quantitative imaging to reflect neuropathological findings has been demonstrated. With future development of methods this could help to avoid invasive brain biopsy procedures.
- Quantitative spinal cord imaging is a relatively poorly explored area. The potential utility of MTCSF imaging and spinal cord volume measurement in the study of patients with demyelinating disease has been reported in this research.
- This is the first time that myelin water imaging has been applied to the study of NMO.

11.5 Recommendations for Future Work

- The proposed criteria for differentiating NMOSD and RRMS using lesion characteristics, and the function derived from thalamic and whole brain volume, require validation in independent cohorts and antibody negative patients.
- A useful focus for future imaging, clinical and immunological NMO research would be to investigate ways of trying to predict when patients are about to relapse so that they can be treated expectantly with high dose immunosuppressive agents or plasma exchange.
- The pathological process by which the autoimmune attack of aquaporin-4 antibodies causes demyelination and neurological damage remains unclear, but hypotheses include disruption in glutamate homeostasis. MR spectroscopy now has the potential

to measure glutamate particularly at ultra high field (7 Tesla). A patient with a new relapse could be sequentially scanned to look for changes in glutamate levels associated with the development of brain or spinal cord lesions.

Furthermore the study of demyelinating lesions in the NMOSD and RRMS cohort with high field spectroscopy may allow diagnostic distinction.

- One approach to taking quantitative imaging further into clinical practice and allowing the individualisation of measures could be to create normative atlases for DTI, volumetric and myelin water indices from healthy control data. Data from a single patient could then be compared to these atlases.

11.6 Overall Conclusion

Conventional and quantitative MRI modalities can identify important distinguishing features of RRMS and NMOSD.

The marker of NMOSD is a relapsing inflammatory demyelinating disease with T2 brain lesions that are not typical for RRMS, and that is not associated with diffuse neurodegenerative features on quantitative imaging.

-REFERENCES-

- Aboul-Enein, F., M. Krssak, et al. (2010). "Diffuse white matter damage is absent in neuromyelitis optica." AJNR Am J Neuroradiol 31(1): 76-79.

- Agre P, Preston GM, Smith BL, Jung JS, Raina S, Moon C, Guggino WB, Nielsen S (1993) "Aquaporin CHIP: the archetypal molecular water channel." American Journal of Physiology 265:F463–476.

- Amiry-Moghaddam and Otterson (2003) "The molecular basis of water transport in the brain." Nat Rev Neurosci. 2003 Dec;4(12):991-1001.

- Anik, Y., A. Demirci, et al. (2011). "Evaluation of Normal Appearing White Matter in Multiple Sclerosis : Comparison of Diffusion Magnetic Resonance, Magnetization Transfer Imaging and Multivoxel Magnetic Resonance Spectroscopy Findings with Expanded Disability Status Scale." Clin Neuroradiol.

- Apiwattanakul, M., B. F. Popescu, et al. (2010). "Intractable vomiting as the initial presentation of neuromyelitis optica." Ann Neurol 68(5): 757-761.

- Arnold, D. L., P. M. Matthews, et al. (1990). "Proton magnetic resonance spectroscopy of human brain in vivo in the evaluation of multiple sclerosis: assessment of the load of disease." Magn Reson Med 14(1): 154-159.

- Arun T, Tomassini V, Sbardella E, de Ruiter MB, Matthews L, Leite MI, et al. Targeting ASIC1 in primary progressive multiple sclerosis: evidence of neuroprotection with amiloride. Brain. 2013 Jan;136(Pt 1):106-15.

- Ashburner, J. and K. J. Friston (2000). "Voxel-based morphometry--the methods." Neuroimage 11(6 Pt 1): 805-821.

- Bakshi, R., A. J. Thompson, et al. (2008). "MRI in multiple sclerosis: current status and future prospects." Lancet Neurol 7(7): 615-625.

- Balcer, L. J. and E. M. Frohman (2010). "Evaluating loss of visual function in multiple sclerosis as measured by low-contrast letter acuity." Neurology 74 Suppl 3: S16-23.

- Barkhof, F., M. Filippi, et al. (1997). "Comparison of MRI criteria at first presentation to predict conversion to clinically definite multiple sclerosis." Brain 120 (Pt 11): 2059-2069.

- Basser, P. J., J. Mattiello, et al. (1994). "Estimation of the effective self-diffusion tensor from the NMR spin echo." J Magn Reson B 103(3): 247-254.

- Basser, P. J., J. Mattiello, et al. (1994). "MR diffusion tensor spectroscopy and imaging." Biophys J 66(1): 259-267.

- Bergsland, N., D. Horakova, et al. (2012). "Subcortical and Cortical Gray Matter Atrophy in a Large Sample of Patients with Clinically Isolated Syndrome and Early Relapsing-Remitting Multiple Sclerosis." AJNR Am J Neuroradiol.

- Bermel, R. A. and R. Bakshi (2006). "The measurement and clinical relevance of brain atrophy in multiple sclerosis." Lancet Neurol 5(2): 158-170.
- Bester, M., C. Heesen, et al. (2008). "Early anisotropy changes in the corpus callosum of patients with optic neuritis." Neuroradiology 50(7): 549-557.

- Bitsch, A., T. Kuhlmann, et al. (2001). "A longitudinal MRI study of histopathologically defined hypointense multiple sclerosis lesions." Ann Neurol 49(6): 793-796.

- Bjartmar, C., G. Kidd, et al. (2000). "Neurological disability correlates with spinal cord axonal loss and reduced N-acetyl aspartate in chronic multiple sclerosis patients." Ann Neurol 48(6): 893-901.

- Bonavita, S., A. Gallo, et al. (2011). "Distributed changes in default-mode resting-state connectivity in multiple sclerosis." Mult Scler 17(4): 411-422.

- Bot, J. C., F. Barkhof, et al. (2004). "Spinal cord abnormalities in recently diagnosed MS patients: added value of spinal MRI examination." Neurology 62(2): 226-233.

- Bozzali, M., M. Franceschi, et al. (2001). "Quantification of tissue damage in AD using diffusion tensor and magnetization transfer MRI." Neurology 57(6): 1135-1137.

- Bradl, M., T. Misu, et al. (2009). "Neuromyelitis optica: pathogenicity of patient immunoglobulin in vivo." Ann Neurol 66(5): 630-643.

- Bruck, W., A. Bitsch, et al. (1997). "Inflammatory central nervous system demyelination: correlation of magnetic resonance imaging findings with lesion pathology." Ann Neurol 42(5): 783-793.

- Cabrera-Gomez, J. A. and I. Kister (2012). "Conventional brain MRI in neuromyelitis optica." Eur J Neurol 19(6): 812-819.

- Cabrera-Gomez, J., A. Saiz-Hinarejos, et al. (2008). "Brain magnetic resonance imaging findings in acute relapses of neuromyelitis optica spectrum disorders." Mult Scler 14(2): 248-251.

- Calabrese, M., M. S. Oh, et al. (2012). "No MRI evidence of cortical lesions in neuromyelitis optica." Neurology 79(16): 1671-1676.

- Ceccarelli A, Bakshi R, Neema M. MRI in multiple sclerosis: a review of the current literature. Curr Opin Neurol. 2012 Aug;25(4):402-9.

- Cercignani, M., M. Bozzali, et al. (2001). "Magnetisation transfer ratio and mean diffusivity of normal appearing white and grey matter from patients with multiple sclerosis." J Neurol Neurosurg Psychiatry 70(3): 311-317.

- Chard, D. T., C. M. Griffin, et al. (2002). "Brain metabolite changes in cortical grey and normal-appearing white matter in clinically early relapsing-remitting multiple sclerosis." Brain 125(Pt 10): 2342-2352.

- Chard DT, Griffin CM, Parker GJ, Kapoor R, Thompson AJ, Miller DH. Brain atrophy in clinically early relapsing-remitting multiple sclerosis. Brain. 2002 Feb;125(Pt 2):327-37

- Chard D, Miller D. Grey matter pathology in clinically early multiple sclerosis: evidence from magnetic resonance imaging. J Neurol Sci. 2009 Jul 15;282(1-2):5-11.

- Ciccarelli, O., A. T. Toosy, et al. (2005). "Optic radiation changes after optic neuritis detected by tractography-based group mapping." Hum Brain Mapp 25(3): 308-316.

- Ciccarelli, O., M. Catani, et al. (2008). "Diffusion-based tractography in neurological disorders: concepts, applications, and future developments." Lancet Neurol 7(8): 715-727.

- Coombs, B. D., A. Best, et al. (2004). "Multiple sclerosis pathology in the normal and abnormal appearing white matter of the corpus callosum by diffusion tensor imaging." Mult Scler 10(4): 392-397.

- Cossburn, M., G. Tackley, et al. (2012). "The prevalence of neuromyelitis optica in South East Wales." Eur J Neurol 19(4): 655-659.

- Dalton, C. M., D. T. Chard, et al. (2004). "Early development of multiple sclerosis is associated with progressive grey matter atrophy in patients presenting with clinically isolated syndromes." Brain 127(Pt 5): 1101-1107.

- Davie, C. A., G. J. Barker, et al. (1997). "1H magnetic resonance spectroscopy of chronic cerebral white matter lesions and normal appearing white matter in multiple sclerosis." J Neurol Neurosurg Psychiatry 63(6): 736-742.

- de Seze, J., F. Blanc, et al. (2010). "Magnetic resonance spectroscopy evaluation in patients with neuromyelitis optica." J Neurol Neurosurg Psychiatry 81(4): 409-411.

- de Seze, J., T. Stojkovic, et al. (2002). "Devic's neuromyelitis optica: clinical, laboratory, MRI and outcome profile." J Neurol Sci 197(1-2): 57-61.

- De Stefano, N., M. L. Bartolozzi, et al. (2005). "Magnetic resonance spectroscopy as a measure of brain damage in multiple sclerosis." J Neurol Sci 233(1-2): 203-208.

- Dehmeshki, J., D. T. Chard, et al. (2003). "The normal appearing grey matter in primary progressive multiple sclerosis: a magnetisation transfer imaging study." J Neurol 250(1): 67-74.

- Deoni, S. C., B. K. Rutt, et al. (2008). "Gleaning multicomponent T1 and T2 information from steady-state imaging data." Magn Reson Med 60(6): 1372-1387.

- Devic E Myélite subaiguë compliquée de névrite optique. Bull Med.1894;8:1033-1034.

- Douaud, G., N. Filippini, et al. (2011). "Integration of structural and functional magnetic resonance imaging in amyotrophic lateral sclerosis." Brain 134(Pt 12): 3470-3479.

- Douaud, G., S. Smith, et al. (2007). "Anatomically related grey and white matter abnormalities in adolescent-onset schizophrenia." Brain 130(Pt 9): 2375-2386.

- Downer, J. J., M. I. Leite, et al. (2011). "Diagnosis of neuromyelitis optica (NMO) spectrum disorders: is MRI obsolete?" Neuroradiology.

- Duan, Y., Y. Liu, et al. (2011). "Comparison of grey matter atrophy between patients with neuromyelitis optica and multiple sclerosis: A voxel-based morphometry study." Eur J Radiol.

- Evangelou, N., G. C. DeLuca, et al. (2005). "Pathological study of spinal cord atrophy in multiple sclerosis suggests limited role of local lesions." Brain 128(Pt 1): 29-34.

- Evangelou, N., M. M. Esiri, et al. (2000). "Quantitative pathological evidence for axonal loss in normal appearing white matter in multiple sclerosis." Ann Neurol 47(3): 391-395.

- Filippi, M., G. Mastronardo, et al. (1998). "Quantitative volumetric analysis of brain magnetic resonance imaging from patients with multiple sclerosis." J Neurol Sci 158(2): 148-153.

- Filippi, M. and M. A. Rocca (2004). "MR imaging of Devic's neuromyelitis optica." Neurol Sci 25 Suppl 4: S371-373.

- Filippi, M., G. Iannucci, et al. (2000). "A quantitative study of water diffusion in multiple sclerosis lesions and normal-appearing white matter using echo-planar imaging." Arch Neurol 57(7): 1017-1021.

- Filippi, M., M. A. Rocca, et al. (1999). "MRI and magnetization transfer imaging changes in the brain and cervical cord of patients with Devic's neuromyelitis optica." Neurology 53(8): 1705-1710.

- Filippi, M., M. A. Rocca, et al. (2002). "Correlations between structural CNS damage and functional MRI changes in primary progressive MS." Neuroimage 15(3): 537-546.

- Filippi, M., M. A. Rocca, et al. (2012). "Association between pathological and MRI findings in multiple sclerosis." Lancet Neurol 11(4): 349-360.

- Filippini, N., B. J. MacIntosh, et al. (2009). "Distinct patterns of brain activity in young carriers of the APOE-epsilon4 allele." Proc Natl Acad Sci U S A 106(17): 7209-7214.

- Fischl, B. and A. M. Dale (2000). "Measuring the thickness of the human cerebral cortex from magnetic resonance images." Proc Natl Acad Sci U S A 97(20): 11050-11055.

- Frischer, J. M., S. Bramow, et al. (2009). "The relation between inflammation and neurodegeneration in multiple sclerosis brains." Brain 132(Pt 5): 1175-1189.

- Fisher E, Lee JC, Nakamura K, Rudick RA. Gray matter atrophy in multiple sclerosis: a longitudinal study. Ann Neurol. 2008 Sep;64(3):255-65.
- Fisniku LK, Chard DT, Jackson JS, Anderson VM, Altmann DR, Miszkiel KA, et al. Gray matter atrophy is related to long-term disability in multiple sclerosis. Ann Neurol. 2008 Sep;64(3):247-54.

- Gelineau-Morel, R., V. Tomassini, et al. (2011). "The effect of hypointense white matter lesions on automated gray matter segmentation in multiple sclerosis." Hum Brain Mapp.

- Good, C. D., I. S. Johnsrude, et al. (2001). "A voxel-based morphometric study of ageing in 465 normal adult human brains." Neuroimage 14(1 Pt 1): 21-36.

- Griffin, C. M., D. T. Chard, et al. (2001). "Diffusion tensor imaging in early relapsing-remitting multiple sclerosis." Mult Scler 7(5): 290-297.

- Harrison, D. M., B. S. Caffo, et al. (2011). "Longitudinal changes in diffusion tensor-based quantitative MRI in multiple sclerosis." Neurology 76(2): 179-186.

- Hickman, S. J., A. T. Toosy, et al. (2004). "Visual recovery following acute optic neuritis--a clinical, electrophysiological and magnetic resonance imaging study." J Neurol 251(8): 996-1005.

- Hinson, S. R., S. J. Pittock, et al. (2007). "Pathogenic potential of IgG binding to water channel extracellular domain in neuromyelitis optica." Neurology 69(24): 2221-2231.

- Horsfield, M. A., S. Sala, et al. (2010). "Rapid semi-automatic segmentation of the spinal cord from magnetic resonance images: application in multiple sclerosis." Neuroimage 50(2): 446-455.

- Hu, W. and C. F. Lucchinetti (2009). "The pathological spectrum of CNS inflammatory demyelinating diseases." Semin Immunopathol 31(4): 439-453.

- Hutchinson, D., T. Solomon, et al. (2000). "Devic's neuromyelitis optica: a primary autoimmune disease?" Rheumatology (Oxford) 39(2): 215-217.

- Isose, S., M. Mori, et al. (2011). "Neurological pictures. Clumsy hand syndrome due to a localised cortical lesion in the primary sensory cortex in neuromyelitis optica." J Neurol Neurosurg Psychiatry 82(5): 559-560.

- Ito, S., M. Mori, et al. (2009). ""Cloud-like enhancement" is a magnetic resonance imaging abnormality specific to neuromyelitis optica." Ann Neurol 66(3): 425-428.

- J.L.R. Andersson, M. Jenkinson and S. Smith. Non-linear optimisation. FMRIB technical report TR07JA1 from www.fmrib.ox.ac.uk/analysis/techrep

- J.L.R. Andersson, M. Jenkinson and S. Smith. Non-linear registration, aka Spatial normalisation FMRIB technical report TR07JA2 from www.fmrib.ox.ac.uk/analysis/techrep

- Jacob, A., A. McKeon, et al. (2012). "Current concept of neuromyelitis optica (NMO) and NMO spectrum disorders." J Neurol Neurosurg Psychiatry.

- Jasperse, B., C. Jakobs, et al. (2007). "N-acetylaspartic acid in cerebrospinal fluid of multiple sclerosis patients determined by gas-chromatography-mass spectrometry." J Neurol 254(5): 631-637.

- Jenkinson, M. and S. Smith (2001). "A global optimisation method for robust affine registration of brain images." Med Image Anal 5(2): 143-156.

- Jenkinson, M., P. Bannister, et al. (2002). "Improved optimization for the robust and accurate linear registration and motion correction of brain images." Neuroimage 17(2): 825-841.

- Jung, J. S., R. V. Bhat, et al. (1994). "Molecular characterization of an aquaporin cDNA from brain: candidate osmoreceptor and regulator of water balance." Proc Natl Acad Sci U S A 91(26): 13052-13056.

- Kanbayashi, T., T. Shimohata, et al. (2009). "Symptomatic narcolepsy in patients with neuromyelitis optica and multiple sclerosis: new neurochemical and immunological implications." Arch Neurol 66(12): 1563-1566.

- Khalil, M., C. Enzinger, et al. (2012). "CSF neurofilament and N-acetylaspartate related brain changes in clinically isolated syndrome." Mult Scler.

- Kidd, D., B. Burton, et al. (2003). "Chronic relapsing inflammatory optic neuropathy (CRION)." Brain 126(Pt 2): 276-284.

- Kim, J. E., S. M. Kim, et al. (2011). "Brain abnormalities in neuromyelitis optica." J Neurol Sci 302(1-2): 43-48.

- Kinoshita, M., Y. Nakatsuji, et al. (2009). "Neuromyelitis optica: Passive transfer to rats by human immunoglobulin." Biochem Biophys Res Commun 386(4): 623-627.

- Kitley, J., M. I. Leite, et al. (2012). "Prognostic factors and disease course in aquaporin-4 antibody-positive patients with neuromyelitis optica spectrum disorder from the United Kingdom and Japan." Brain 135(Pt 6): 1834-1849.

- Kitley, J., M. Leite, et al. (2011). "The differential diagnosis of longitudinally extensive transverse myelitis." Mult Scler. 2012 Mar;18(3):271-85

- Kleiter, I., K. Hellwig, et al. (2012). "Failure of natalizumab to prevent relapses in neuromyelitis optica." Arch Neurol 69(2): 239-245.

- Kolind, S., L. Matthews, et al. (2012). "Myelin water imaging reflects clinical variability in multiple sclerosis." Neuroimage 60(1): 263-270.

- Krampla, W., F. Aboul-Enein, et al. (2009). "Spinal cord lesions in patients with neuromyelitis optica: a retrospective long-term MRI follow-up study." Eur Radiol 19(10): 2535-2543.

- Kurtzke, J. F. (1983). "Rating neurologic impairment in multiple sclerosis: an expanded disability status scale (EDSS)." Neurology 33(11): 1444-1452.

- Larsson, H. B., C. Thomsen, et al. (1992). "In vivo magnetic resonance diffusion measurement in the brain of patients with multiple sclerosis." Magn Reson Imaging 10(1): 7-12.

- Lassmann, H., W. Bruck, et al. (2007). "The immunopathology of multiple sclerosis: an overview." Brain Pathol 17(2): 210-218.

- Laule, C., E. Leung, et al. (2006). "Myelin water imaging in multiple sclerosis: quantitative correlations with histopathology." Mult Scler 12(6): 747-753.

- Laule, C., P. Kozlowski, et al. (2008). "Myelin water imaging of multiple sclerosis at 7 T: correlations with histopathology." Neuroimage 40(4): 1575-1580.

- Le Bihan, D; Breton E. et al. (1985). "MR Imaging of intravoxel incoherent motions : application to diffusion and perfusion in neurologic disorders". Annual Meeting of the RSNA, Chicago.

- Le Bihan, D; E. Breton (1985). "Imagerie de diffusion in-vivo par résonance". C R Acad Sci (Paris) 301 (15): 1109–1112.

- Le Bihan, D. and H. Johansen-Berg (2012). "Diffusion MRI at 25: exploring brain tissue structure and function." Neuroimage 61(2): 324-341.
- Lennon, V. A., D. M. Wingerchuk, et al. (2004). "A serum autoantibody marker of neuromyelitis optica: distinction from multiple sclerosis." Lancet 364(9451): 2106-2112.

- Lennon, V. A., T. J. Kryzer, et al. (2005). "IgG marker of optic-spinal multiple sclerosis binds to the aquaporin-4 water channel." J Exp Med 202(4): 473-477.

- Li, L., H. Zhang, et al. (2009). "Greatly attenuated experimental autoimmune encephalomyelitis in aquaporin-4 knockout mice." BMC Neurosci 10: 94.

- Li, Y., P. Xie, et al. (2008). "Brain magnetic resonance imaging abnormalities in neuromyelitis optica." Acta Neurol Scand 118(4): 218-225.

- Liang, P., Y. Liu, et al. (2011). "Regional homogeneity changes in patients with neuromyelitis optica revealed by resting-state functional MRI." Clin Neurophysiol 122(1): 121-127.

- Liu, Y., P. Liang, et al. (2011). "Abnormal baseline brain activity in patients with neuromyelitis optica: a resting-state fMRI study." Eur J Radiol 80(2): 407-411.

- Liu, Y., Y. Duan, et al. (2012). "A tract-based diffusion study of cerebral white matter in neuromyelitis optica reveals widespread pathological alterations." Mult Scler 18(7): 1013-1021.

- Losseff, N. A., S. L. Webb, et al. (1996). "Spinal cord atrophy and disability in multiple sclerosis. A new reproducible and sensitive MRI method with potential to monitor disease progression." Brain 119 (Pt 3): 701-708.

- Lu, Z., W. Qiu, et al. (2010). "Characteristic linear lesions and longitudinally extensive spinal cord lesions in Chinese patients with neuromyelitis optica." J Neurol Sci 293(1-2): 92-96.

- Lucchinetti, C. F., R. N. Mandler, et al. (2002). "A role for humoral mechanisms in the pathogenesis of Devic's neuromyelitis optica." Brain 125(Pt 7): 1450-1461.

- Lucchinetti, C., W. Bruck, et al. (2000). "Heterogeneity of multiple sclerosis lesions: implications for the pathogenesis of demyelination." Ann Neurol 47(6): 707-717.

- MacKay, A., K. Whittall, et al. (1994). "In vivo visualization of myelin water in brain by magnetic resonance." Magn Reson Med 31(6): 673-677.

- Magana, S. M., M. Matiello, et al. (2009). "Posterior reversible encephalopathy syndrome in neuromyelitis optica spectrum disorders." Neurology 72(8): 712-717.

- Manev, H., M. Favaron, et al. (1989). "Delayed increase of Ca2+ influx elicited by glutamate: role in neuronal death." Mol Pharmacol 36(1): 106-112.

- Matiello, M., A. Jacob, et al. (2007). "Neuromyelitis optica." Curr Opin Neurol 20(3): 255-260.

- Matiello, M., H. J. Kim, et al. (2010). "Familial neuromyelitis optica." Neurology 75(4): 310-315.

- Matsuoka, T., S. O. Suzuki, et al. (2011). "Reappraisal of aquaporin-4 astrocytopathy in Asian neuromyelitis optica and multiple sclerosis patients." Brain Pathol 21(5): 516-532.

- Matsuoka, T., T. Matsushita, et al. (2007). "Heterogeneity of aquaporin-4 autoimmunity and spinal cord lesions in multiple sclerosis in Japanese." Brain 130(Pt 5): 1206-1223.

- Matsushita, T., N. Isobe, et al. (2010). "Reappraisal of brain MRI features in patients with multiple sclerosis and neuromyelitis optica according to anti-aquaporin-4 antibody status." J Neurol Sci 291(1-2): 37-43.

- Matthews, L. A., F. Baig, et al. (2009). "The borderland of neuromyelitis optica." Pract Neurol 9(6): 335-340.

- McKeon, A., V. A. Lennon, et al. (2008). "CNS aquaporin-4 autoimmunity in children." Neurology 71(2): 93-100.

- Merle, H., S. Olindo, et al. (2007). "Natural history of the visual impairment of relapsing neuromyelitis optica." Ophthalmology 114(4): 810-815.

- Miller, D. H., B. G. Weinshenker, et al. (2008). "Differential diagnosis of suspected multiple sclerosis: a consensus approach." Mult Scler 14(9): 1157-1174.

- Misu, T., K. Fujihara, et al. (2005). "Intractable hiccup and nausea with periaqueductal lesions in neuromyelitis optica." Neurology 65(9): 1479-1482.

- Moffett, J. R., B. Ross, et al. (2007). "N-Acetylaspartate in the CNS: from neurodiagnostics to neurobiology." Prog Neurobiol 81(2): 89-131.

- Nagaishi, A., M. Takagi, et al. (2011). "Clinical features of neuromyelitis optica in a large Japanese cohort: comparison between phenotypes." J Neurol Neurosurg Psychiatry 82(12): 1360-1364.

- Nagelhus, E. A., T. M. Mathiisen, et al. (2004). "Aquaporin-4 in the central nervous system: cellular and subcellular distribution and coexpression with KIR4.1." Neuroscience 129(4): 905-913.

- Nakamura, M., I. Miyazawa, et al. (2008). "Preferential spinal central gray matter involvement in neuromyelitis optica. An MRI study." J Neurol 255(2): 163-170.

- Nakamura, M., T. Misu, et al. (2009). "Occurrence of acute large and edematous callosal lesions in neuromyelitis optica." Mult Scler 15(6): 695-700.

- Narayanan, S., L. Fu, et al. (1997). "Imaging of axonal damage in multiple sclerosis: spatial distribution of magnetic resonance imaging lesions." Ann Neurol 41(3): 385-391.

- Nishiyama, S., T. Ito, et al. (2009). "A case of NMO seropositive for aquaporin-4 antibody more than 10 years before onset." Neurology 72(22): 1960-1961.

- O'Riordan, J. I., H. L. Gallagher, et al. (1996). "Clinical, CSF, and MRI findings in Devic's neuromyelitis optica." J Neurol Neurosurg Psychiatry 60(4): 382-387.

- Palace, J., M. I. Leite, et al. (2010). "Interferon Beta treatment in neuromyelitis optica: increase in relapses and aquaporin 4 antibody titers." Arch Neurol 67(8): 1016-1017.

- Patenaude, B., S. M. Smith, et al. (2011). "A Bayesian model of shape and appearance for subcortical brain segmentation." Neuroimage 56(3): 907-922.

- Pichiecchio, A., E. Tavazzi, et al. (2012). "Advanced magnetic resonance imaging of neuromyelitis optica: a multiparametric approach." Mult Scler 18(6): 817-824.

- Pirko I, Lucchinetti CF, Sriram S, Bakshi R. Gray matter involvement in multiple sclerosis. Neurology. 2007 Feb 27;68(9):634-42.

- Pittock, S. J., B. G. Weinshenker, et al. (2006). "Neuromyelitis optica brain lesions localized at sites of high aquaporin 4 expression." Arch Neurol 63(7): 964-968.

- Pittock, S. J., V. A. Lennon, et al. (2006). "Brain abnormalities in neuromyelitis optica." Arch Neurol 63(3): 390-396.

- Pittock, S. J., V. A. Lennon, et al. (2008). "Neuromyelitis optica and non organ-specific autoimmunity." Arch Neurol 65(1): 78-83.

- Polman, C. H., S. C. Reingold, et al. (2005). "Diagnostic criteria for multiple sclerosis: 2005 revisions to the "McDonald Criteria"." Ann Neurol 58(6): 840-846.

- Polman, C. H., S. C. Reingold, et al. (2011). "Diagnostic criteria for multiple sclerosis: 2010 revisions to the McDonald criteria." Ann Neurol 69(2): 292-302.

- Popescu, B. F., V. A. Lennon, et al. (2011). "Neuromyelitis optica unique area postrema lesions: nausea, vomiting, and pathogenic implications." Neurology 76(14): 1229-1237.

- Poppe, A. Y., Y. Lapierre, et al. (2005). "Neuromyelitis optica with hypothalamic involvement." Mult Scler 11(5): 617-621.

- Qian, W., Q. Chan, et al. (2011). "Quantitative assessment of the cervical spinal cord damage in neuromyelitis optica using diffusion tensor imaging at 3 Tesla." J Magn Reson Imaging 33(6): 1312-1320.

- Qiu, W., J. S. Wu, et al. (2010). "Longitudinally extensive myelopathy in Caucasians: a West Australian study of 26 cases from the Perth Demyelinating Diseases Database." J Neurol Neurosurg Psychiatry 81(2): 209-212.

- Ramasamy DP, Benedict RH, Cox JL, Fritz D, Abdelrahman N, Hussein S, et al. Extent of cerebellum, subcortical and cortical atrophy in patients with MS: a case-control study. J Neurol Sci. 2009 Jul 15;282(1-2):47-54.

- R Rashid W, Hadjiprocopis A, Davies G, Griffin C, Chard D, Tiberio M, et al. Longitudinal evaluation of clinically early relapsing-remitting multiple sclerosis with diffusion tensor imaging. J Neurol. 2008 Mar;255(3):390-7.

- Rizzo, J. F., 3rd, C. M. Andreoli, et al. (2002). "Use of magnetic resonance imaging to differentiate optic neuritis and nonarteritic anterior ischemic optic neuropathy." Ophthalmology 109(9): 1679-1684.

- Rocca, M. A., F. Agosta, et al. (2004). "A functional MRI study of movement-associated cortical changes in patients with Devic's neuromyelitis optica." Neuroimage 21(3): 1061-1068.

- Rocca, M. A., F. Agosta, et al. (2004). "Magnetization transfer and diffusion tensor MRI show gray matter damage in neuromyelitis optica." Neurology 62(3): 476-478.

- Rocca, M. A., M. A. Horsfield, et al. (2011). "A multicenter assessment of cervical cord atrophy among MS clinical phenotypes." Neurology 76(24): 2096-2102.

- Roemer, S. F., J. E. Parisi, et al. (2007). "Pattern-specific loss of aquaporin-4 immunoreactivity distinguishes neuromyelitis optica from multiple sclerosis." Brain 130(Pt 5): 1194-1205.

- Rueda Lopes, F. C., T. Doring, et al. (2012). "The role of demyelination in neuromyelitis optica damage: diffusion-tensor MR imaging study." Radiology 263(1): 235-242.

- Ruggieri, M., C. Tortorella, et al. (2011). "Age-related changes of serum N-acetyl-aspartate in healthy controls." Age Ageing 40(3): 391-395.

- Saadoun, S., P. Waters, et al. (2010). "Intra-cerebral injection of neuromyelitis optica immunoglobulin G and human complement produces neuromyelitis optica lesions in mice." Brain 133(Pt 2): 349-361.

- Simon, J. H., L. D. Jacobs, et al. (1999). "A longitudinal study of brain atrophy in relapsing multiple sclerosis. The Multiple Sclerosis Collaborative Research Group (MSCRG)." Neurology 53(1): 139-148.

- Simone, I. L., M. Ruggieri, et al. (2011). "Serum N-acetylaspartate level in amyotrophic lateral sclerosis." Arch Neurol 68(10): 1308-1312.

- Sinclair, C., J. Kirk, et al. (2007). "Absence of aquaporin-4 expression in lesions of neuromyelitis optica but increased expression in multiple sclerosis lesions and normal-appearing white matter." Acta Neuropathol 113(2): 187-194.

- Smith, S. A., X. Golay, et al. (2005). "Magnetization transfer weighted imaging in the upper cervical spinal cord using cerebrospinal fluid as intersubject normalization reference (MTCSF imaging)." Magn Reson Med 54(1): 201-206.

- Smith, S. M. (2002). "Fast robust automated brain extraction." Hum Brain Mapp 17(3): 143-155.

- Smith, S. M., M. Jenkinson, et al. (2004). "Advances in functional and structural MR image analysis and implementation as FSL." Neuroimage 23 Suppl 1: S208-219.

- Smith, S. M., M. Jenkinson, et al. (2006). "Tract-based spatial statistics: voxelwise analysis of multi-subject diffusion data." Neuroimage 31(4): 1487-1505.

- Smith, S. M., N. De Stefano, et al. (2001). "Normalized accurate measurement of longitudinal brain change." J Comput Assist Tomogr 25(3): 466-475.

- Smith, S. M., Y. Zhang, et al. (2002). "Accurate, robust, and automated longitudinal and cross-sectional brain change analysis." Neuroimage 17(1): 479-489.

- Soares, D. P. and M. Law (2009). "Magnetic resonance spectroscopy of the brain: review of metabolites and clinical applications." Clin Radiol 64(1): 12-21.

- Tait, M. J., S. Saadoun, et al. (2008). "Water movements in the brain: role of aquaporins." Trends Neurosci 31(1): 37-43.

- Teunissen, C. E., E. Iacobaeus, et al. (2009). "Combination of CSF N-acetylaspartate and neurofilaments in multiple sclerosis." Neurology 72(15): 1322-1329.

- Tortorella, P., M. A. Rocca, et al. (2006). "MRI quantification of gray and white matter damage in patients with early-onset multiple sclerosis." J Neurol 253(7): 903-907.

- Trapp, B. D. and K. A. Nave (2008). "Multiple sclerosis: an immune or neurodegenerative disorder?" Annu Rev Neurosci 31: 247-269.

- Tso, M. O., C. Y. Shih, et al. (1975). "Is there a blood-brain barrier at the optic nerve head?" Arch Ophthalmol 93(9): 815-825.

- Vargas, M. I., J. Delavelle, et al. (2008). "Clinical applications of diffusion tensor tractography of the spinal cord." Neuroradiology 50(1): 25-29.

- Verkman, A. S., D. K. Binder, et al. (2006). "Three distinct roles of aquaporin-4 in brain function revealed by knockout mice." Biochim Biophys Acta 1758(8): 1085-1093.

- Viegas, S., A. Weir, et al. (2009). "Symptomatic, radiological and pathological involvement of the hypothalamus in neuromyelitis optica." J Neurol Neurosurg Psychiatry 80(6): 679-682.

- Vollmar C, O'Muircheartaigh J, Barker GJ, Symms MR, Thompson P, Kumari V, et al. Identical, but not the same: intra-site and inter-site reproducibility of fractional anisotropy measures on two 3.0T scanners. Neuroimage. 2010 Jul 15;51(4):1384-94.

- Wang, F., Y. Liu, et al. (2011). "Brain MRI abnormalities in neuromyelitis optica." Eur J Radiol 80(2): 445-449.

- Waters, P. J., A. McKeon, et al. (2012). "Serologic diagnosis of NMO: a multicenter comparison of aquaporin-4-IgG assays." Neurology 78(9): 665-671; discussion 669.

- Waters, P., S. Jarius, et al. (2008). "Aquaporin-4 antibodies in neuromyelitis optica and longitudinally extensive transverse myelitis." Arch Neurol 65(7): 913-919.

- Weinshenker, B. G., D. M. Wingerchuk, et al. (2006). "OSMS is NMO, but not MS: proven clinically and pathologically." Lancet Neurol 5(2): 110-111.

- Wingerchuk, D. M. (2007). "Diagnosis and treatment of neuromyelitis optica." Neurologist 13(1): 2-11.

- Wingerchuk, D. M. and B. G. Weinshenker (2003). "Neuromyelitis optica: clinical predictors of a relapsing course and survival." Neurology 60(5): 848-853.

- Wingerchuk, D. M., S. J. Pittock, et al. (2007). "A secondary progressive clinical course is uncommon in neuromyelitis optica." Neurology 68(8): 603-605.

- Wingerchuk, D. M., V. A. Lennon, et al. (2006). "Revised diagnostic criteria for neuromyelitis optica." Neurology 66(10): 1485-1489.

- Wingerchuk, D. M., V. A. Lennon, et al. (2007). "The spectrum of neuromyelitis optica." Lancet Neurol 6(9): 805-815.

- Wingerchuk, D. M., W. F. Hogancamp, et al. (1999). "The clinical course of neuromyelitis optica (Devic's syndrome)." Neurology 53(5): 1107-1114.

- Wolff, S. D. and R. S. Balaban (1989). "Magnetization transfer contrast (MTC) and tissue water proton relaxation in vivo." Magn Reson Med 10(1): 135-144.

- Wolff, S. D. and R. S. Balaban (1994). "Magnetization transfer imaging: practical aspects and clinical applications." Radiology 192(3): 593-599.

- Wolinsky, J. S., P. A. Narayana, et al. (1990). "Proton magnetic resonance spectroscopy in multiple sclerosis." Neurology 40(11): 1764-1769.

- Woolrich, M. W., S. Jbabdi, et al. (2009). "Bayesian analysis of neuroimaging data in FSL." Neuroimage 45(1 Suppl): S173-186.

- Wylezinska, M., A. Cifelli, et al. (2003). "Thalamic neurodegeneration in relapsing-remitting multiple sclerosis." Neurology 60(12): 1949-1954.

- Yu, C. S., C. Z. Zhu, et al. (2007). "Relapsing neuromyelitis optica and relapsing-remitting multiple sclerosis: differentiation at diffusion-tensor MR imaging of corpus callosum." Radiology 244(1): 249-256.

- Yu, C. S., F. C. Lin, et al. (2006). "Diffusion tensor imaging in the assessment of normal-appearing brain tissue damage in relapsing neuromyelitis optica." AJNR Am J Neuroradiol 27(5): 1009-1015.

- Yu, C., F. Lin, et al. (2008). "Pathogenesis of normal-appearing white matter damage in neuromyelitis optica: diffusion-tensor MR imaging." Radiology 246(1): 222-228.

- Zhang, Y., M. Brady, et al. (2001). "Segmentation of brain MR images through a hidden Markov random field model and the expectation-maximization algorithm." IEEE Trans Med Imaging 20(1): 45-57.

--APPENDICES--

APPENDIX I: PATIENT DETAILS
Neuromyelitis Optica Spectrum Disorder:

	Age*	Sex	Aquaporin-4 antibody status	Disease Duration/ months*	Previous Relapses**	Hand Dominance	Baseline EDSS	1 year EDSS	Baseline 25 ft timed walk/ seconds	1 year 25ft timed walk/ seconds	Baseline corrected visual acuity***	1 year corrected visual acuity***	Baseline 9 hole peg test/seconds	1 year 9 hole peg test/seconds	Cervical spina cord lesion leve at time o baseline scan
1	50	F	Positive	50	R+L ON	R	3.5	3.5	6.7	6.8	R= 6/36 L=6/9	R=6/36 L=6/9	R=17.5 L=21.5	R=18.1 L=20.3	No lesion
2	42	F	Positive	24	R ON, LETM	R	3.5	3.5	12.1	10.3	R=6/60 L=6/6	R<6/60 L=6/9	R=19.0 L=20.1	R=18.5 L=23/1	C5-C6
3	28	F	Positive	186	R+L ON	R	4.0	4.0	Blind	Blind	R=NPL L=LPA	R=NPL L=LPA	Blind	Blind	No lesion
4	33	F	Positive	69	R+L ON, LETM, B	R	5.5	6.0	8.2	18.3	R=NPL L=6/9	R=NPL L=6/9	R=unable L=26.85	R=unable L=29.1	C2-4
5	56	F	Positive	60	R+L ON, LETM	R	6.0	6.0	9.8	8.9	R=6/9 L=LPA	R=6/9 L=LPA	R=20.8 L=21.3	R=24.3 L=22.1	C4-7
6	20	F	Positive	84	R+L ON, LETM	R	3.5	3.5	6.8	7.3	R=6/24 L=6/60	R=6/18 L=6/60	R=22.5 L=24.5	R=24.2 L=22.6	C2-C3
7	33	M	Positive	48	R+L ON, LETM	R	4.0	4.0	Blind	Blind	R=NPL L=LPA	R=NPL L=NPL	Blind	Blind	C3
8	76	F	Positive	180	LETM	R	7.5	6.5	Unable	Unable	R=6/6 L=6/6	R=6/6 L=6/6	R=25.1 L=27	R=20.1 L=22.3	C3-C6
9	46	M	Positive	183	R+L ON, LETM	R	4.0	4.0	Blind	Blind	R=NPL L=NPL	R=NPL L=NPL	Blind	Blind	C2-C4
10	40	F	Positive	74	R+L ON, LETM	R	3.5	3.5	19.3	18.7	R=6/60 L=6/9	R=6/60 L=6/12	R=19.3 L=23.1	R=18.8 L=21.3	C5
11	63	F	Positive	24	R+L ON	R	2.0	2.0	6.1	6.6	R=6/9 L=6/12	R=6/9 L=6/12	R=18.1 L=18.3	R=17.2 L=20.1	No lesion
12	70	F	Positive	55	LETM	R	6.0	Did not attend	15	Did not attend	R=6/6 L=6/9	Did not attend	R=25.2 L=30	Did not attend	C4
13	66	F	Positive	72	LETM	R	6.0	6.0	20.2	22.1	R=6/6 L=6/6	R=6/6 L=6/6	R=28 L=29.3	R=22.1 L=28.6	C4-C7
14	60	F	Positive	60	LETM	R	3.0	2.0	15.6	11.2	R=6/6 L=6/6	R=6/6 L=6/6	R=22 L=21.2	R=19.9 L=23.2	C3, C6

15	40	M	Positive	36	LETM	R	5.0	4.5	14.8	9.8	R=6/6 L=6/6	R=6/6 L=6/6	R=20 L=23.7	R=22.4 L=21.9	C6-7
16	38	F	Positive	12	LETM, ON, B	R	6.0	Did not attend	13	Did not attend	R=6/6 L=6/9	Did not attend	R=18.3 L=21.9	Did not attend	C3
17	50	F	Positive	48	LETM, B	R	6.0	6.0	8.6	9.2	R=6/6 L=6/6	L=6/6 R=6/6	R=19.6 L=16.4	R=21.2 L=17.2	No residua cervical lesion
18	46	F	Positive	16	ON, B, LETM	R	4.0	4.5	9.1	12.4	R=LPA L=6/60	R=NPL L=6/60	Visual impairment	Visual impairment	C3, C5

* Age and disease duration at time of baseline scan
** R=Right, L=Left, ON=Optic Neuritis, LETM=Longitudinally Extensive Transverse Myelitis, B=symptoms of Brain origin
*** NPL=No Perception of Light, LPA=Light Perception Alone

Relapsing Remitting Multiple Sclerosis:

	Age*	Sex	Disease Duration/ months*	Previous Relapses**	Hand Dominance	Baseline EDSS	1 year EDSS	Baseline 25 ft timed walk/ seconds	1 year 25ft timed walk/ seconds	Baseline corrected Visual acuity	1 year corrected visual acuity	Baseline 9 hole peg test/ seconds	1 year 9 hole peg test / seconds	Cervical sp cord lesion l at time baseline scan
1	61	M	228	R+L ON, TM, B	L	5	5.5	11.1	14.2	L=6/36 R=6/6	L=6/36 R=6/6	L=115.9 R=55.7	L=123.2 R=42.1	Patchy char C2-C5
2	49	F	54	ON, TM, B	R	1.5	1.5	8.1	7.2	L=6/6 R=6/9	L=6/6 R=6/9	L=17.8 R=19.5	L=20.1 R=18.7	C3, C7
3	30	F	120	L ON, TM, B	R	1.0	Did not attend	6.9	Did not attend	L=6/4.8 R=6/4.8	Did not attend	L=20.7 R=19.1	Did not attend	C4
4	56	F	72	R ON, TM, B	R	5	4.5	10.8	10.2	L=6/6 R=6/6	L=6/6 R=6/6	L=25.1 R=32	L=21.1 R=25.1	No cerv lesion
5	29	F	36	TM, B	R	2	1.5	6.8	6.3	L=6/4.8 R=6/4.8	L=6/4.8 R=6/4.8	L=18 R=16.9	L=16.8 R=17.2	C4, C6
6	34	M	48	TM, ON, B	R	2	2.5	7.2	9.3	L=6/6 R=6/6	L=6/6 R=6/6	L=19 R=18.2	L=21.2 R=17.9	C3
7	38	F	156	TM, B	R	1	1	7.1	6.8	L=6/6 R=6/6	L=6/6 R=6/6	L=19.8 R=17.1	L=19.2 R=17.2	C4-5
8	40	M	72	TM, B	L	3.5	4.0	6	6.5	L=6/6 R=6/6	L=6/6 R=6/6	L=18 R=19.2	L=17 R=18.9	No cerv lesion
9	36	M	80	ON, TM, B	R	5	5	10.5	11.2	L=6/6 R=6/12	L=6/9 R=6/12	L=25.5 R=24.3	L=21.2 R=23.2	C2, C7
10	33	F	50	ON, TM, B	L	5	5	21.9	20.1	L=6/12 R=6/6	L=6/12 R=6/6	L=18.8 R=20	L=19.1 R=18.3	C3-5
11	22	F	24	ON, B	R	0	Did not attend	6.9	Did not attend	L=6/6 R=6/6	Did not attend	L=16.1 R=17.2	Did not attend	No lesion
12	34	F	26	ON, TM. B	R	2	1.5	7	8.6	L=6/6 R=6/9	L=6/6 R=6/6	L=19.7 R=19.3	L=18.6 R=20.6	C4
13	60	F	240	TM, B	R	5	5	8.5	9.1	L=6/6 R=6/6	L=6/6 R=6/6	L=23.2 R=24.9	L=21.4 R=23.2	C3-4, C6
14	62	F	156	R ON, B	R	2	2	6.8	7.2	L=6/4.8 R=6/15	L=6/4.8 R=6/15	L=22 R=21	L=23.1 R=18.1	No cerv lesion
15	47	F	36	B, TM	R	4	4	9	7.4	L=6/6 R=6/6	L=6/6 R=6/6	L=20.6 R=16.9	L=18.1 R=16.4	No cerv lesion

* Age and disease duration at time of baseline scan

** R=Right, L=Left, ON=optic neuritis, TM=transverse myelitis, B=symptoms of Brain origin

Appendix II. Full MRI Protocol used in the core study

Imaging Measure Required	MRI Sequence	Sequence Parameters
White matter integrity	Brain Diffusion Tensor Imaging (DTI)	60 diffusion directions with B-value 1000 and 8 volumes with no diffusion weighting, TR 9600ms, TE 87 ms, FOV 190 x 190mm, voxel-size 2.0x2.0x2.0mm, 65 slices, 1 average. Acquisition time = 12mins.
	Brain Myelin Water Imaging (MWI)	Acquired with mcDESPOT (Deoni, Rutt et al. 2008). FOV=22x22x16cm, 1.7mm isotropic resolution; SPGR: TE/TR = 2.5ms/5.6ms, α={3,4,5,6,7,9,13,18}°, BW=±24kHz; SSFP: TE/TR=2.2ms/4.4ms, α={10,13.3,16.6,20,23.3,30,43.2,60}°, BW=±36kHz, phase-cycling patterns = 0º and 180º (for correction of off-resonance effects). A reduced resolution IR-SPGR image was also acquired with TE/TR/TI/α = 2.5ms/5.6ms/450ms/5° to correct for flip angle inhomogeneity. Acquisition time = 14mins.
	Spinal Magnetisation transfer ratio (MTR)	Acquired with MTCSF protocol as described by Smith et al (Smith, Golay et al. 2005). 2D-gradient echo sequence with 20 consecutive axial slices with a distance factor of 10% positioned at the superior border of the C1 vertebra. FOV 180x180mm, slice thickness 4mm, voxel size 0.8 x0.7 mm, TR 600ms, TE 8.6ms, 2 averages. Acquired with magnetisation transfer weighting both on and off. Acquisition time = 8 mins.
	Spinal Myelin Water Imaging (MWI)	Acquired with mcDESPOT (Deoni, Rutt et al. 2008). SPGR:TE/TR=2.7/6.1ms, α= {2.25,4.5,6.75,9,11,25,13.5,15.75,18}°, BW=+/- 22kHz SSFP:TE/TR=2.3/4.6ms, α= {5.625, 11.25, 16.875, 22.5, 28.125, 33.75, 39.375, 45}°, BW=+/-34KHz, phase-cycling increments of 0° & 180° (for correction of off-resonance effects}. IRSPGR: TE/TR 2.7/6.3ms, TI = 450ms, α = 5°, BW = +/-22KHz (for correction of flip angle variation, acquired with half the spatial resolution in both phase-encode directions to reduce acquisition time. Sagittal FOV = 15(AP)x12(LR)x20(SI)cm, voxel size = 0.9(AP)x0.9(LR)x1.8(SI)mm. Acquisition time = 20mins.
Brain, spinal cord and regional atrophy	3-dimensional T1 weighting	Brain: 3 dimensional MPRAG sequence with voxel size 1x1x1mm, TR 2040ms, TE 4.7ms, 1 average.
		Spine: 3 dimensional MPRAG sequence with voxel size 1x1x1mm, TR 2300ms, TE 3.59 ms, 1 average.
Lesion volume and location	Brain axial T2	2 dimensional turbo spin echo, 48 slices, slice thickness 3mm, voxel size 0.5x0.5mm, FOV 220x220mm, TR 5690ms, TE 71ms, 1 average
	Brain axial PD	2 dimensional turbo spin echo, 48 slices, slice thickness 3mm, voxel size 0.5x0.5mm, FOV 220x220mm, TR 3000ms, TE 18ms, 1 average
	Brain axial Flair	2 dimensional turbo spin echo 48 slices, slice thickness 3mm, TE 73.0ms, TR 9000ms, voxel size 0.9x0.9. 1 average.
	Spinal sagittal T2	2 dimensional turbo spin echo, 15 slices of 3mm, voxel size 0.6x0.6, TE 67ms TR 4590ms
	Spinal sagittal PD	2 dimensional turbo spin echo, 15 slices of 3mm, voxel size 0.6x0.6, TE 8.3ms TR 4590ms
	Spinal axial T2	Utilised relatively motion insensitive gradient echo sequence (Siemens MEDIC) with 30 consecutive axial slices with a distance factor of 10%. 3mm slice thickness. Voxel size 0.7x0.7mm. TE 17ms, TR 470ms. 2 averages.